nature portfolio

Peer Review File

A multifunctional quasi-solid-state polymer electrolyte with highly selective ion highways for practical zinc ion batteries

Open Access This file is licensed under a Creative Commons Attribution 4.0 International License, which permits use, sharing, adaptation, distribution and reproduction in any medium or format, as long as you give appropriate credit to the original author(s) and the source, provide a link to the Creative Commons license, and indicate if changes were made. In the cases where the authors are anonymous, such as is the case for the reports of anonymous peer reviewers, author attribution should be to 'Anonymous Referee' followed by a clear attribution to the source work. The images or other third party material in this file are included in the article's Creative Commons license, unless indicated otherwise in a credit line to the material. If material is not included in the article's Creative Commons license and your intended use is not permitted by statutory regulation or exceeds the permitted use, you will need to obtain permission directly from the copyright holder. To view a copy of this license, visit http://creativecommons.org/licenses/by/4.0/.

REVIEWER COMMENTS

Reviewer #1 (Remarks to the Author):

The research focuses on developing a quasi-solid-state polymer electrolyte (PLCZ) for aqueous zinc ion batteries (AZIBs). The study addresses the issues of uncontrolled dendrite growth and side reactions in Zn anodes that hinder the large-scale implementation of AZIBs. The authors designed a versatile quasi-solid-state polymer electrolyte with highly selective ion transport channels, achieved through molecular crosslinking of sodium polyacrylate, lithium magnesium silicate, and cellulose nanofiber. Overall, the manuscript is deemed suitable for publication after addressing following concerns.

1. The authors stated that they were inspired by the biological transport phenomena of cell membranes to develop the polymer electrolyte. While this study successfully implemented the characteristics required for polymer electrolytes for ZIBs, the reviewer finds it difficult to see a specific connection between the developed polymer electrolyte and the biological transport phenomena. Therefore, the reviewer advises that the extensive use of terms like 'biomimetic' and 'bioinspired' in the title and content is excessive and should be reconsidered.

2. The current manuscript primarily focuses on the compatibility with Zn and V_2O_5 electrodes. It is necessary to evaluate the compatibility with other electrode materials (e.g., MnO_2, $FePO_4$, etc.) to confirm the versatility of the PLCZ electrolyte.

3. The mechanisms of Zn ion desolvation and transport within the polymer electrolyte remain ambiguous. It is recommended to incorporate simulation (DFT, MD, etc) results to elucidate these mechanisms.

4. It is advisable to evaluate the performance changes by varying the thickness of the electrolyte. While a thinner electrolyte may provide higher ion mobility, it could potentially lower mechanical properties, making it crucial to determine the optimal thickness.

Reviewer #2 (Remarks to the Author):

The manuscript deals with the composite separator for solid state zinc ion battery. It has been well written and presented. It can be accepted after addressing the following concern.

The mechanism of the formation of cell membrane like structure in not clear. It seems the authors have exaggerated the mechanism.

The exact mechanism of the suppression of dendrite growth is missing. From the SEM images (Figure 4C), the random deposition of zinc is visible which can results into the dendrite growth.

Generally the dendrite growth are dominated at high current density. The cycling of the battery in the present study is at very low current density.

Check for the typos.

Reviewer #3 (Remarks to the Author):

The manuscript by Yang et al. describes a method of producing quasi-solid-state polymers for aqueous zinc-ion batteries. The authors claim that these exhibit improved transport properties through biomimetic ion channels and increased cycle stability. Bulk and surface analytical techniques were used to elucidate the structure of the composite material. Compared to reference materials CZ and PCZ, a stabilization of the SEI layer due to MEA formation and reduced dendrite growth was observed. Electrochemical investigations showed an improved cyclability for symmetric Zn||Zn, as well as asymmetric Zn||Cu and Zn||V2O5 cells.

Although this manuscript contains valuable scientific information on the improvement of AZIBs, it contains a few significant weaknesses and room for improvement. The presentation of the data and the structure of the manuscript suffer from a lack of clarity at some points, which repeatedly leaves the reader confused.

1) The comparison of the AZIB structure to the biological membrane tenuous, distracting and confusing for the reader. There is no evidence of the order (i.e. well defined bilayer structures that create distinct compartments with ion channels across the barrier) that is characteristic of a cell membrane. The introduction to the principle and structure of the cell and cell membrane is therefore not relevant in this context and shouldn't be discussed as any more than a sidenote in the introduction. The resulting material is better described as an organic-inorganic composite material, which is what the introduction should focus on as well as the status of AZIBs. Furthermore, the structure and preparation of CZ, PCZ, and PLCZ should be discussed in more detail from the beginning to provide the reader with a better overview of what these acronyms mean.

2) Fig. 1b does not explain the working principle of AZIBs sufficiently. It should be explained in more detail in the text, as it is crucial for understanding this work.

3) In general, the number of subpanels in the Figures makes them difficult to understand. Since a maximum of 10 figures is allowed by the journal, it is suggested to split them up for better clarity (both topic focus and size).

4) QSPE and PLCZ are both used as acronyms for quasi solid-state polymers. This can confuse the reader, they should be accurately explained as the general and specific example studied in this manuscript.

5) In the Section “Electrochemical performance of symmetric cells” can the observations at line 248-251 regarding the discharge be related to the dendrite growth reported at line 262? The authors should comment on whether they believe there is a link.

6) In the Section “Formation and properties of medium-entropy alloy layer,” for the first time in the manuscript, Zn||Cu cells are described without giving context as to why now these systems are used for investigation. It can also be confusing for the reader that the outstanding stability is emphasized before the underlying data is discussed. The order needs to be corrected and the context for the cells that are used added.

7) In Fig. S30, the force-displacement curves are not plotted in the same y-range, which would be beneficial for comparison. In addition, the difference in reversibility during loading and unloading experiments appears to be only marginal between PCZ and PLCZ. Is there any statistical evidence? In Fig. S31 from the images there is no evidence for a more uniform Young’s modulus of PLCZ over PCZ. This is also the case for Fig. 4 m-o where the claims of better uniformity and smoothness cannot be confirmed without further information about roughness and statistics for the images.

However, no further information on AFM experiments is provided in the Experimental section. Therefore, reproducing the results is not possible from the given information, it must be made clear whether these are typical images and statistically whether there is evidence there is uniformity etc. and most importantly the conditions under which the images have been taken.

8) Further, there are no experimental details provided for the nanoindentation measurements.

9) It is stated, that the CV curve in Fig. 6a displays a higher current density compared to CZ and PCZ. However, only the current is plotted on the y-axis and no electrode area is given. Current density must be used to compare different samples.

Minor comments:

1) Figure 1b Field is mis-spelled in the figure annotation.

2) Fig. S4 and S5 weight is not given for strain-stress tests.

3) Fig. S7 displays the nucleation overpotential, not the potential.

4) Why is in Fig 2a PAAs gel given as a reference for the lower wavenumber region but in Fig. 2b CZ for the higher wavenumber region? The reason for the choice of reference should be explained in the text/figure caption. Also 2c is the only one to not have a full frame around the axes.

5) Fig. 2h y-axis label should be current density instead of current. At which current density was the ESW determined? This should be included.

6) Fig. 2i only for electrolyte uptake a value is given on the scale, whether values are used should be applied consistently across all axes.

7) EIS spectra are not plotted using orthonormal scales making visual interpretation meaningless.

8) At line 211 there is no reference to the technique used for activation energy calculation

9) In Fig. 3a parameters are given as 0.5 mA cm-2 0.25 mAh cm-2, whereas in the figure caption it is written 1 mA cm-2 1 mAh cm-2.

10) After how many cycles were the SEM images taken in Fig. 3c-e? Why is the Zn foil in c not colored? The purpose or source of this color should be noted in the caption. Images/photographs are too small.

11) In Fig. 3h it is confusing for the reader to give the x-axis in K-1¬ when temperatures in the text are only described in C.

12) The figure caption in Fig. S24 is wrong. i, j, k instead of a, b, c

13) In Fig. 4 b-d the labelling is not visible very well. Furthermore, it is not explained what the colored regions in the SEM images represent. (Also Fig. S39 and mentioned above in Fig 3)

14) Plotting error in Fig. 4e. The area under the curve shouldn't be filled until the straight line but until the background.

15) How was the nucleation overpotential determined in Fig. S28?

16) In Fig. 5 b-d, the color differences are difficult to see since they are quite small.

17) In Fig. S33, peak assignments (002) and (101) would be good for better understanding.

18) How were RS, RSEI, and RCT determined in Fig. S34.

19) In Fig 6 d and e no clear assignment of the data to the left and right y-axis is visible.

20) Fig 6 g images with digital thermometers are very small, difficult to read.

Reviewer #4 (Remarks to the Author):

I co-reviewed this manuscript with one of the reviewers who provided the listed reports. This is part of the Nature Communications initiative to facilitate training in peer review and to provide appropriate recognition for Early Career Researchers who co-review manuscripts.

REVIEWER COMMENTS

Reviewer #1 (Remarks to the Author):

The research focuses on developing a quasi-solid-state polymer electrolyte (PLCZ) for aqueous zinc ion batteries (AZIBs). The study addresses the issues of uncontrolled dendrite growth and side reactions in Zn anodes that hinder the large-scale implementation of AZIBs. The authors designed a versatile quasi-solid-state polymer electrolyte with highly selective ion transport channels, achieved through molecular crosslinking of sodium polyacrylate, lithium magnesium silicate, and cellulose nanofiber. Overall, the manuscript is deemed suitable for publication after addressing following concerns.

1. The authors stated that they were inspired by the biological transport phenomena of cell membranes to develop the polymer electrolyte. While this study successfully implemented the characteristics required for polymer electrolytes for ZIBs, the reviewer finds it difficult to see a specific connection between the developed polymer electrolyte and the biological transport phenomena. Therefore, the reviewer advises that the extensive use of terms like 'biomimetic' and 'bioinspired' in the title and content is excessive and should be reconsidered.
2. The current manuscript primarily focuses on the compatibility with Zn and V_2O_5 electrodes. It is necessary to evaluate the compatibility with other electrode materials (e.g., MnO_2, $FePO_4$, etc.) to confirm the versatility of the PLCZ electrolyte.
3. The mechanisms of Zn ion desolvation and transport within the polymer electrolyte remain ambiguous. It is recommended to incorporate simulation (DFT, MD, etc) results to elucidate these mechanisms.
4. It is advisable to evaluate the performance changes by varying the thickness of the electrolyte. While a thinner electrolyte may provide higher ion mobility, it could potentially lower mechanical properties, making it crucial to determine the optimal thickness.

Reviewer #2 (Remarks to the Author):

The manuscript deals with the composite separator for solid state zinc ion battery. It has been well written and presented. It can be accepted after addressing the following concern.
The mechanism of the formation of cell membrane like structure in not clear. It seems the authors have exaggerated the mechanism.
The exact mechanism of the suppression of dendrite growth is missing. From the SEM images (Figure 4C), the random deposition of zinc is visible which can result into the dendrite growth.
Generally, the dendrite growth is dominated at high current density. The cycling of the battery in the present study is at very low current density.
Check for the typos.

Reviewer #3 (Remarks to the Author):

The manuscript by Yang et al. describes a method of producing quasi-solid-state polymers for aqueous zinc-ion batteries. The authors claim that these exhibit improved transport properties through biomimetic ion channels and increased cycle stability. Bulk and surface analytical techniques were used to elucidate the structure of the composite material. Compared to reference materials CZ and PCZ, a stabilization of the SEI layer due to MEA formation and reduced dendrite growth was observed. Electrochemical investigations showed an improved cyclability for symmetric Zn||Zn, as well as asymmetric Zn||Cu and Zn||V_2O_5 cells.

Although this manuscript contains valuable scientific information on the improvement of AZIBs, it contains a few significant weaknesses and room for improvement. The presentation of the data and the structure of the manuscript suffer from a lack of clarity at some points, which repeatedly leaves the reader confused.

1) The comparison of the AZIB structure to the biological membrane tenuous, distracting and confusing for the reader. There is no evidence of the order (i.e. well defined bilayer structures that create distinct compartments with ion channels across the barrier) that is characteristic of a cell membrane. The introduction to the principle and structure of the cell and cell membrane is therefore not relevant in this context and shouldn't be discussed as any more than a sidenote in the introduction. The resulting material is better described as an organic-inorganic composite material, which is what the introduction should focus on as well as the status of AZIBs. Furthermore, the structure and preparation of CZ, PCZ, and PLCZ should be discussed in more detail from the beginning to provide the reader with a better overview of what these acronyms mean.
2) Fig. 1b does not explain the working principle of AZIBs sufficiently. It should be explained in more detail in the text, as it is crucial for understanding this work.
3) In general, the number of subpanels in the Figures makes them difficult to understand. Since a maximum of 10 figures is allowed by the journal, it is suggested to split them up for better clarity (both topic focus and size).
4) QSPE and PLCZ are both used as acronyms for quasi solid-state polymers. This can confuse the reader, they should be accurately explained as the general and specific example studied in this manuscript.
5) In the Section "Electrochemical performance of symmetric cells" can the observations at line 248-251 regarding the discharge be related to the dendrite growth reported at line 262? The authors should comment on whether they believe there is a link.
6) In the Section "Formation and properties of medium-entropy alloy layer," for the first time in the manuscript, Zn||Cu cells are described without giving context as to why now these systems are used for investigation. It can also be confusing for the reader that the outstanding stability is emphasized before the underlying data is discussed. The order needs to be corrected and the context for the cells that are used added.
7) In Fig. S30, the force-displacement curves are not plotted in the same y-range, which

would be beneficial for comparison. In addition, the difference in reversibility during loading and unloading experiments appears to be only marginal between PCZ and PLCZ. Is there any statistical evidence? In Fig. S31 from the images there is no evidence for a more uniform Young's modulus of PLCZ over PCZ. This is also the case for Fig. 4 m-o where the claims of better uniformity and smoothness cannot be confirmed without further information about roughness and statistics for the images.
However, no further information on AFM experiments is provided in the Experimental section. Therefore, reproducing the results is not possible from the given information, it must be made clear whether these are typical images and statistically whether there is evidence there is uniformity etc. and most importantly the conditions under which the images have been taken.
8) Further, there are no experimental details provided for the nanoindentation measurements.
9) It is stated, that the CV curve in Fig. 6a displays a higher current density compared to CZ and PCZ. However, only the current is plotted on the y-axis and no electrode area is given. Current density must be used to compare different samples.

Minor comments:
1) Figure 1b Field is mis-spelled in the figure annotation.
2) Fig. S4 and S5 weight is not given for strain-stress tests.
3) Fig. S7 displays the nucleation overpotential, not the potential.
4) Why is in Fig 2a PAAs gel given as a reference for the lower wavenumber region but in Fig. 2b CZ for the higher wavenumber region? The reason for the choice of reference should be explained in the text/figure caption. Also 2c is the only one to not have a full frame around the axes.
5) Fig. 2h y-axis label should be current density instead of current. At which current density was the ESW determined? This should be included.
6) Fig. 2i only for electrolyte uptake a value is given on the scale, whether values are used should be applied consistently across all axes.
7) EIS spectra are not plotted using orthonormal scales making visual interpretation meaningless.
8) At line 211 there is no reference to the technique used for activation energy calculation
9) In Fig. 3a parameters are given as 0.5 mA cm^{-2} 0.25 mAh cm^{-2}, whereas in the figure caption it is written 1 mA cm^{-2} 1 mAh cm^{-2}.
10) After how many cycles were the SEM images taken in Fig. 3c-e? Why is the Zn foil in c not colored? The purpose or source of this color should be noted in the caption. Images/photographs are too small.
11) In Fig. 3h it is confusing for the reader to give the x-axis in K-1¬ when temperatures in the text are only described in C.
12) The figure caption in Fig. S24 is wrong. i, j, k instead of a, b, c
13) In Fig. 4 b-d the labelling is not visible very well. Furthermore, it is not explained what the colored regions in the SEM images represent. (Also Fig. S39 and mentioned above in Fig 3)

14) Plotting error in Fig. 4e. The area under the curve shouldn't be filled until the straight line but until the background.
15) How was the nucleation overpotential determined in Fig. S28?
16) In Fig. 5 b-d, the color differences are difficult to see since they are quite small.
17) In Fig. S33, peak assignments (002) and (101) would be good for better understanding.
18) How were RS, RSEI, and RCT determined in Fig. S34.
19) In Fig 6 d and e no clear assignment of the data to the left and right y-axis is visible.
20) Fig 6 g images with digital thermometers are very small, difficult to read.

Reviewer #4 (Remarks to the Author):

I co-reviewed this manuscript with one of the reviewers who provided the listed reports. This is part of the Nature Communications initiative to facilitate training in peer review and to provide appropriate recognition for Early Career Researchers who co-review manuscripts.

Response letter to reviewers

We are very grateful to the reviewers for their professional and insightful comments. These comments have greatly improved the quality of our manuscript and will be of great help to our future work. We have carefully revised the manuscript according to these comments. A detailed point-by-point response to comments is attached as below and the revised parts in the manuscript are highlighted.

Reviewer #1:

The research focuses on developing a quasi-solid-state polymer electrolyte (PLCZ) for aqueous zinc ion batteries (AZIBs). The study addresses the issues of uncontrolled dendrite growth and side reactions in Zn anodes that hinder the large-scale implementation of AZIBs. The authors designed a versatile quasi-solid-state polymer electrolyte with highly selective ion transport channels, achieved through molecular crosslinking of sodium polyacrylate, lithium magnesium silicate, and cellulose nanofiber. Overall, the manuscript is deemed suitable for publication after addressing following concerns.

Author reply: Thanks for your positive comments and we are glad that you find our work of interest and importance. We have revised the manuscript point-by-point according to your comments.

1. The authors stated that they were inspired by the biological transport phenomena of cell membranes to develop the polymer electrolyte. While this study successfully implemented the characteristics required for polymer electrolytes for ZIBs, the reviewer finds it difficult to see a specific connection between the developed polymer electrolyte and the biological transport phenomena. Therefore, the reviewer advises that the extensive use of terms like 'biomimetic' and 'bioinspired' in the title and content is excessive and should be reconsidered.

Author reply: Thank you very much for your comments. We have deleted the terms like "biomimetic" and "bioinspired" in the revised manuscript and changed the title.

Changes in the manuscript (the highlighted part):

Title

A multifunctional quasi-solid-state polymer electrolyte with highly selective ion highways for practical zinc ion batteries

2. The current manuscript primarily focuses on the compatibility with Zn and V_2O_5 electrodes. It is necessary to evaluate the compatibility with other electrode materials (e.g., MnO_2, $FePO_4$, etc.) to confirm the versatility of the PLCZ electrolyte.

Author reply: Thank you very much for your comments. We have tested the cycling performances of other cathode materials, including MnO_2, $LiFePO_4$ and

$(NH_4)_2V_{10}O_{25}·8H_2O$ (the electrode preparation is shown in the figure caption), and evaluated their compatibility with the PLCZ electrolyte. As shown in Fig. R1, compared with the CZ and PCZ electrolytes, the PLCZ polymer electrolyte improves the discharge capacity and cycling stability of the full cells of MnO_2, $LiFePO_4$ and $(NH_4)_2V_{10}O_{25}·8H_2O$, implying its high adaptability and compatibility with other cathode materials. For the $FePO_4$ material, we used commercial and home-made $FePO_4$ materials to assemble full cells. Both of them generate a negligible discharge capacity of 18 mAh g^{-1} even at a very low current density of 0.05 A g^{-1} when 2 M $ZnSO_4$ liquid aqueous as electrolyte (Fig. R2). The capacity may be come from the conductive carbon rather than $FePO_4$ material. Additionally, $FePO_4$ as the cathode material for aqueous Zn-ion batteries is rarely reported in literature until now. Therefore, we evaluated the compatibility of the PLCZ electrolyte via using MnO_2, $LiFePO_4$ and $(NH_4)_2V_{10}O_{25}·8H_2O$ materials.

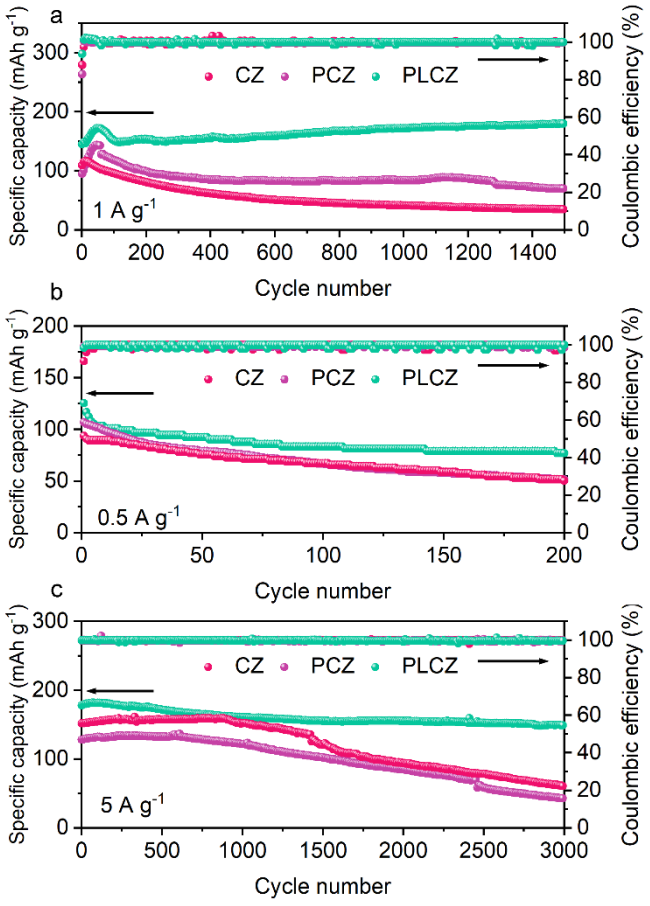

Fig. R1 *The discharge-charge cycling performances of (a) Zn||MnO_2, (b) Zn||$LiFePO_4$ and (c) Zn||$(NH_4)_2V_{10}O_{25}·8H_2O$ full cells with different electrolytes. MnO_2 and $LiFePO_4$ were purchased from commercial sources and used without further purification. For the preparation of $(NH_4)_2V_{10}O_{25}·8H_2O$, 8 mmol NH_4VO_3 was dissolved in 100 ml DI water at 343.15 K and 6 mmol thiourea was pour into the solution with stirring to completely dissolve. Then, dilute sulfuric was added to the above solution to the pH of 2. After that, this solution was stirred another 2.5 h at 363.15 K. After cooling down, the dark green precipitate was filtered, washed with deionized water and finally dried*

in oven. The preparations of MnO_2, $LiFePO_4$ and $(NH_4)_2V_{10}O_{25}·8H_2O$ cathode electrodes were same with that of V_2O_5 cathode electrode, except that the active materials were changed to MnO_2, $LiFePO_4$ and $(NH_4)_2V_{10}O_{25}·8H_2O$.

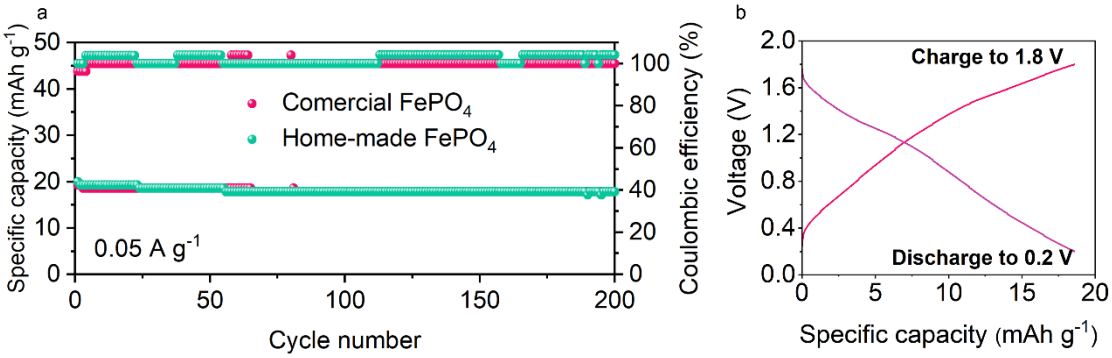

***Fig. R2** (a) The discharge-charge cycling performances of Zn||$FePO_4$ full cells with 2 M $ZnSO_4$ as electrolyte. (b) Voltage profiles of Zn||$FePO_4$ at the 10th cycle.*

Changes in the manuscript (the highlighted part):

The practicability and compatibility of the PLCZ design can be also observed when coupled with other cathode materials, including MnO_2, $LiFePO_4$ and $(NH_4)_2V_{10}O_{25}·8H_2O$ (Supplementary Fig. S53).

Changes in supplementary information:

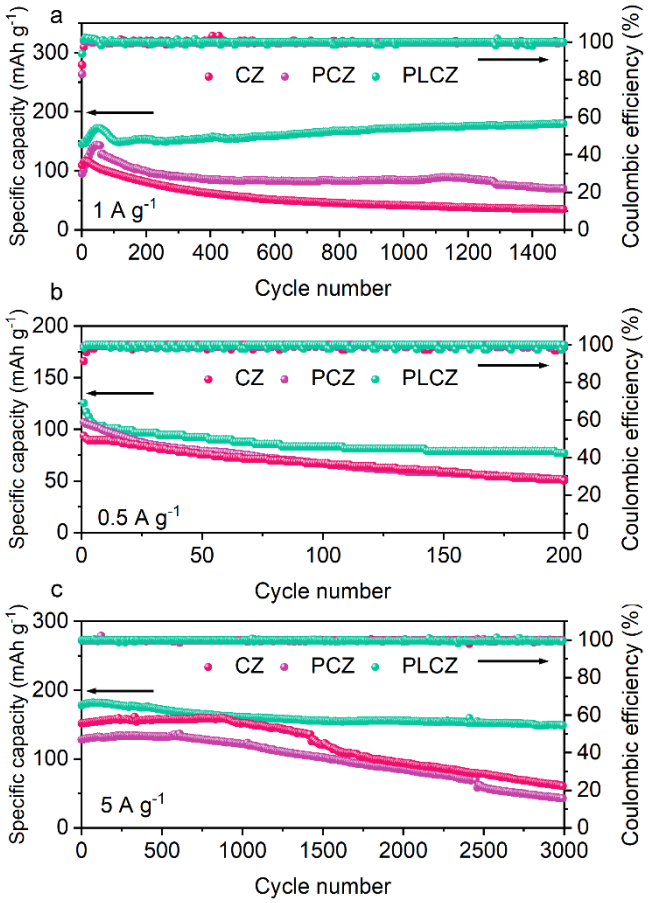

Supplementary Fig. S53 *The discharge-charge cycling performances of (a) Zn||MnO_2, (b) Zn||$LiFePO_4$ and (c) Zn||$(NH_4)_2V_{10}O_{25}·8H_2O$ full cells with different electrolytes. MnO_2 and $LiFePO_4$ were purchased from commercial sources and used without further purification. For the preparation of $(NH_4)_2V_{10}O_{25}·8H_2O$, 8 mmol NH_4VO_3 was dissolved in 100 ml DI water at 343.15 K and 6 mmol thiourea was pour into the solution with stirring to completely dissolve. Then, dilute sulfuric was added to the above solution to the pH of 2. After that, this solution was stirred another 2.5 h at 363.15 K. After cooling down, the dark green precipitate was filtered, washed with deionized water and finally dried in oven. The preparations of MnO_2, $LiFePO_4$ and $(NH_4)_2V_{10}O_{25}·8H_2O$ cathode electrodes were same with that of V_2O_5 cathode electrode, except that the active materials were changed to MnO_2, $LiFePO_4$ and $(NH_4)_2V_{10}O_{25}·8H_2O$.*

3. The mechanisms of Zn ion desolvation and transport within the polymer electrolyte remain ambiguous. It is recommended to incorporate simulation (DFT, MD, etc) results to elucidate these mechanisms.

Author reply: Thank you very much for your comments. We have used the molecular dynamics (MD) simulation to analyze the Zn ion solvation structure and transport within the PLCZ electrolyte. As plotted in Fig. R3, the radial distribution function (RDF) of the CZ liquid electrolyte shows a major peak of Zn^{2+}-O (H_2O) at 2.75 Å with the coordination number (CN) of 6.06, representing the typical Zn^{2+} solvation sheath

structure ($[Zn(H_2O)_6]^{2+}$) in the liquid solution (Nat Commun 2023, 14 (1), 3526). However, for the PCZ and PLCZ electrolytes, the CNs reduce to 4.30 and 3.75, respectively, duo to the electrostatic interactions of -COO^- group and LMS with Zn^{2+} ions, which efficiently replace the coordinated water molecules around Zn^{2+} ions and remodel the solvation structures ($[Zn(H_2O)_4(COO)]^+$ in PCZ and $[Zn(H_2O)_3(COO)LMS]^+$ in PLCZ). Moreover, the PLCZ polymer electrolyte realizes rapid Zn^{2+} ion diffusion and intercalation with a high self-diffusion coefficient (Ds) of 7.55×10^{-11} m^2 s^{-1} (Fig. R4). This enhanced ion mobility is facilitated by the -COO^- groups within the PAAS chain and LMS platelets, which form highly selective transport microchannels functioning as "ion transfer pumps".

We also have analyzed the deposition mechanisms of Zn^{2+} ions in the CZ liquid and PLCZ electrolytes, shown in Fig. R5. Zn^{2+} ions in CZ aqueous electrolyte tend to laterally diffuse along the rough surface and deposit at energetically favorable sites, finally generating the fatal dendrites. Meanwhile, water-induced side reactions aggravate H_2O decomposition and increase local pH value near the Zn electrode. This unfavorable environment promotes the precipitation of $[Zn(H_2O)_6]SO_4$ complex and the generation of ZSH by-product. On the contrary, the PLCZ electrolyte leverages the charged -COO^- groups of polymer chains and LMS platelets to establish high-speed pathways for Zn^{2+} ion transportation through electrostatic interactions. This interaction spontaneously influences solvation structure and expedites desolvation behavior. During subsequent deposition, Si and Mg atoms concurrently deposit with Zn ion to form a robust medium-entropy alloy (MEA) SEI with a strong affinity for Zn. Such unique SEI extends spatial movement of Zn and guides the favorable deposition of Zn(002) planes, ultimately yielding an ultra-stable Zn electrode.

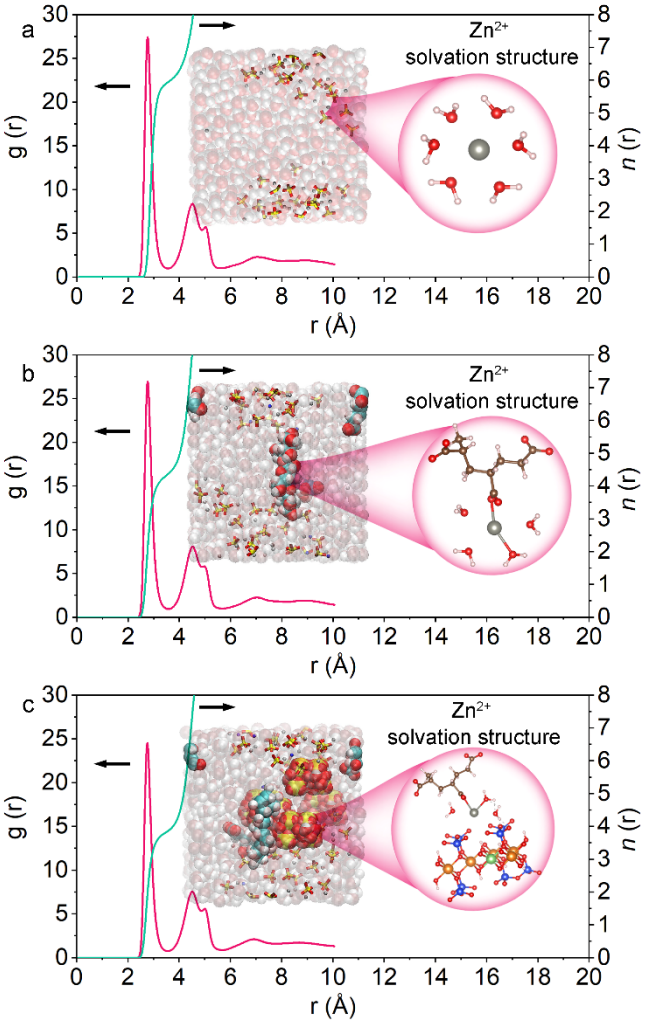

Fig. R3 *The simulated RDF of Zn^{2+}-O (H_2O) and the coordination numbers of Zn^{2+} with water molecules with the corresponding Zn^{2+} solvation structure in the (a) CZ, (b) PCZ and (c) PLCZ electrolytes.*

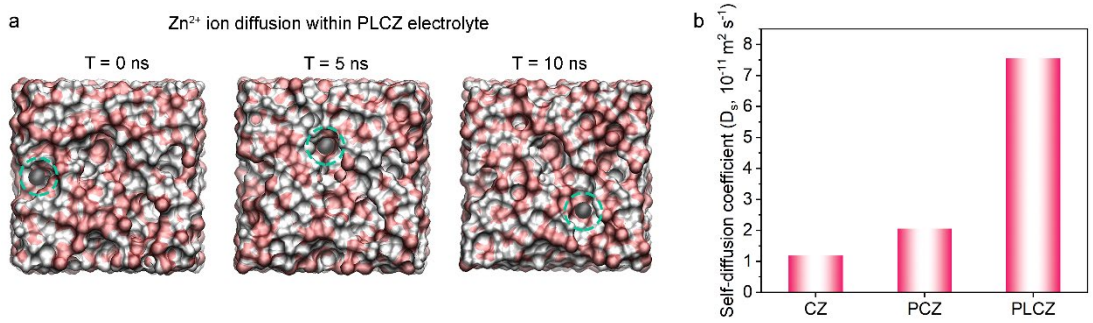

Fig. R4 *(a) The Zn^{2+} diffusion within the PLCZ electrolyte from the 3D snapshots of T =0 ns to 10 ns. (b) The Ds of Zn^{2+} in the CZ, PCZ and PLCZ electrolytes.*

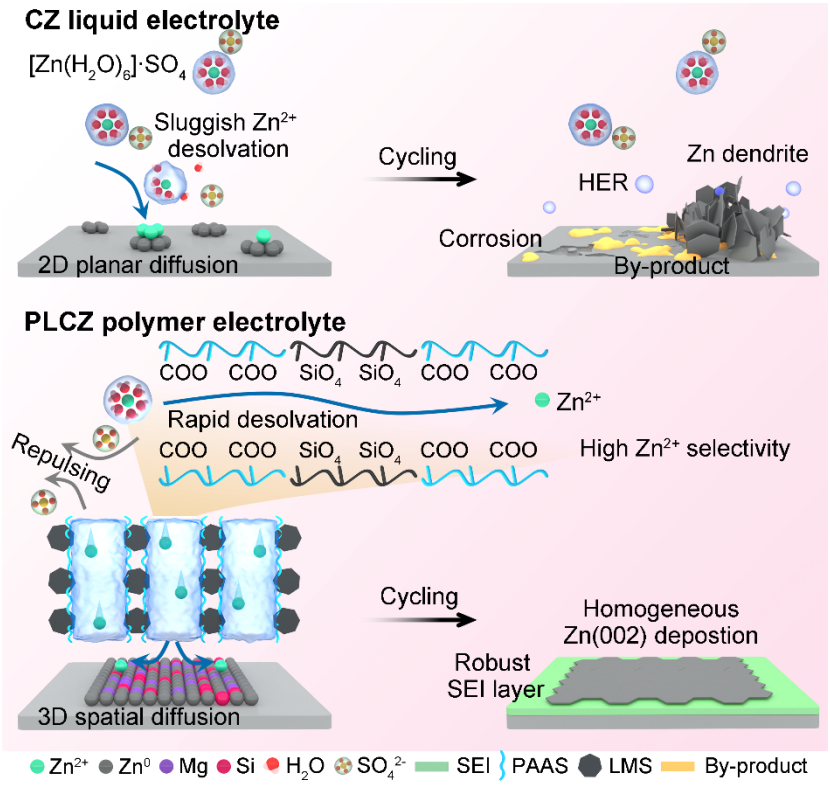

Fig. R5 *Schematically illustrating the Zn deposition in CZ liquid and PLCZ electrolytes.*

Changes in the manuscript (the highlighted part):

Such unique selective aggregation of Zn^{2+} ion confers upon LMS platelets and PAAS chains the ability to work as "ion transfer pumps", which in turn renders a fast ion transportation, even ion nucleation and homogeneous Zn deposition during Zn plating/stripping process[20, 21]. Molecular dynamics (MD) simulations were conducted to validate the above inferences (Fig. 1b and Supplementary Fig. S4). The radial distribution function (RDF) of the CZ liquid electrolyte reveals a prominent peak of Zn^{2+}-O (H_2O) at 2.75 Å, with the coordination number (CN) of 6.06, indicative of the typical Zn^{2+} solvation sheath structure ($[Zn(H_2O)_6]^{2+}$) in the liquid solution[22]. However, the PCZ and PLCZ electrolytes exhibit reduced CN values of 4.30 and 3.75, respectively. This decrease is attributed to the electrostatic interactions of -COO^- group and LMS with Zn^{2+} ions, which efficiently displace the coordinated water molecules around Zn^{2+} ions and alter the solvation structures to $[Zn(H_2O)_4(COO)]^+$ in PCZ and $[Zn(H_2O)_3(COO)LMS]^+$ in PLCZ. Additionally, the PLCZ polymer electrolyte realizes rapid Zn^{2+} ion diffusion and intercalation with high self-diffusion coefficient (Ds) of 7.55×10^{-11} m^2 s^{-1} (Fig. 1c and Supplementary Fig. S5), due to the formed highly selective transportation microchannels by -COO^- within PAAS chain and LMS platelets.

In Supplementary Fig. S46, compared to the CZ and PCZ, the PLCZ obtains smaller and more stable R_{SEI} and R_{CT} values, resulting from the highly conductive MEA SEI and the suppressive by-product. The Zn deposition mechanisms in the CZ liquid

and PLCZ electrolytes were schematically illustrated in Fig. 5e. Zn^{2+} ions in CZ aqueous electrolyte tend to laterally diffuse along the rough surface and deposit at energetically favorable sites, finally generating the fatal dendrites. Meanwhile, water-induced side reactions aggravate H_2O decomposition and increase local pH value near the Zn electrode. This unfavorable environment promotes the precipitation of $[Zn(H_2O)_6]SO_4$ complex and the generation of ZSH by-product. On the contrary, the PLCZ electrolyte leverages the charged -COO^- groups of polymer chains and LMS platelets to establish high-speed pathways for Zn^{2+} ion transportation through electrostatic interactions. This interaction spontaneously influences solvation structure and expedites desolvation behavior. During subsequent deposition, Si and Mg atoms concurrently deposit with Zn ion to form a robust MEA SEI with a strong affinity for Zn. Such unique SEI extends spatial movement of Zn and guides the favorable deposition of Zn(002) planes, ultimately yielding an ultra-stable Zn electrode.

Theoretical calculations

Zn ion desolvation and transport within the polymer electrolyte were investigated by using the classical MD simulations for three systems i.e. (1) The 36 $ZnSO_4$ and 1000 water molecules; (2) The 2 PAAS, 1 cellulose, 36 $ZnSO_4$ and 1000 water molecules were randomly added into simulation system; (3) The 5 LMS, 2 PAAS, 1 cellulose, 36 $ZnSO_4$ and 1000 water molecules were randomly added into simulation system. The all molecules were randomly added into each simulation system. The DLPOLY 4.10 package[63] was used for this study. The starting box size was 40 × 40 × 40 $Å^3$ and the simulations were performed under the Nose-Hoover ensemble[64] at the temperature of 298 K. The periodic boundary conditions and the minimum image convention were applied. The cutoff radius for short-ranged interaction is 12 Å and the long-ranged interaction was treated by the Ewald summation method[65]. In order to equilibrate the simulation box size, the simulations were first carried out under NPT ensemble for about 2 ns with the time step of 1 fs. The production runs were then carried out under NVT ensemble for 20 ns. The trajectories were collected from the last 10 ns and the RDFs were computed.

The DREIDING force-field[66] was used for interactions of other atom types. The Lennard-Jones (LJ) parameters for different types of atom (σ_{ij}, ε_{ij}) are taken from pure types (σ_{ii}, ε_{jj}) following the Lorentz-Berthelot mixing rule[67], which is written as

$$\sigma_{ij} = \frac{\sigma_{ii}+\sigma_{jj}}{2};\ \varepsilon_{ij} = \sqrt{\varepsilon_{ii}\varepsilon_{jj}} \qquad (2)$$

All partial atomic charges except for water molecules, were extracted from the calculations by using the ORCA program. The HF/6-31G(d) theory and the electrostatic potential fitting (ESP) of CHELPG[68] have been used.

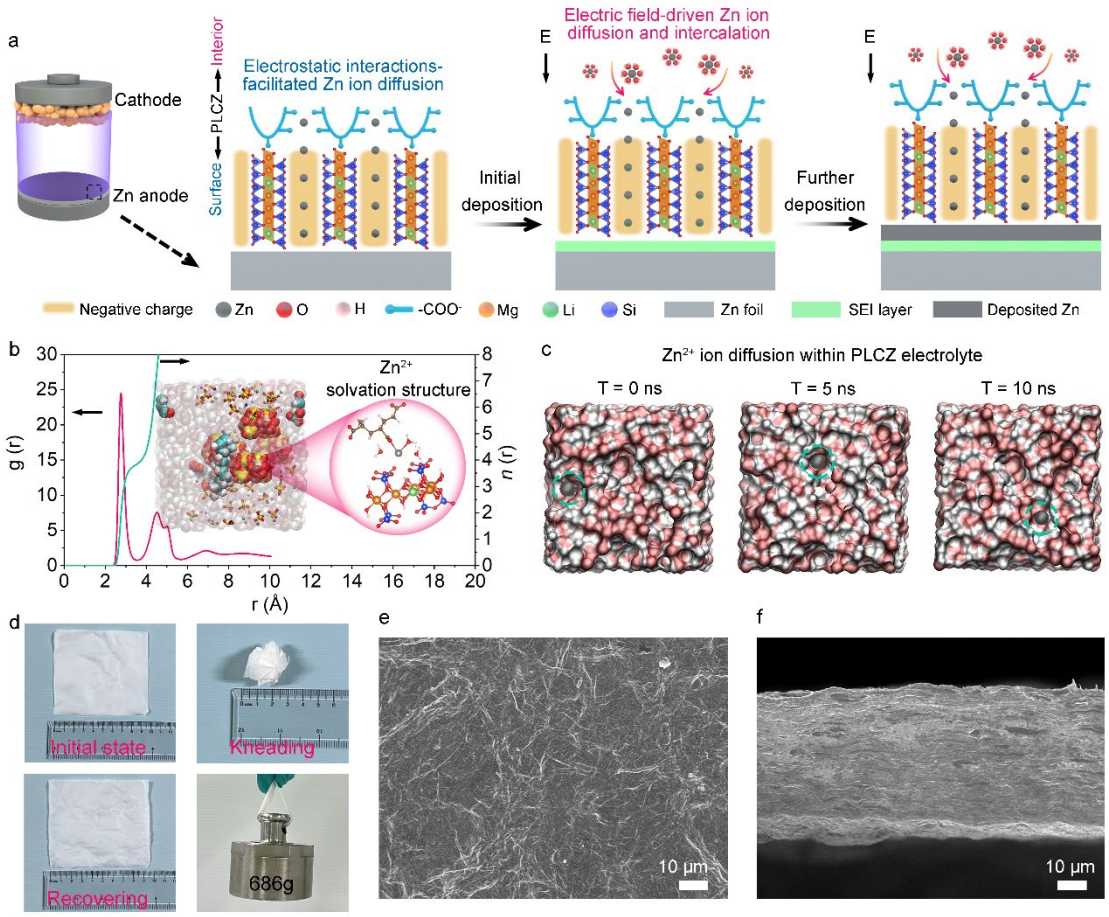

Fig. 1 *(a) Schematically illustrating the Zn^{2+} ion diffusion and transport cross the PLCZ polymer electrolyte. (b) The simulated RDF of Zn^{2+}-O (H_2O) and the coordination numbers of Zn^{2+} with water molecules with the corresponding Zn^{2+} solvation structure in the PLCZ electrolytes. (c) The Zn^{2+} diffusion within the PLCZ electrolyte from the 3D snapshots of T =0 ns to 10 ns. (d) The digital photographs of the designed PLCZ electrolyte under initial state, kneading and recovering and the corresponding strain-stress test. SEM images of the PLCZ electrolyte on (e) the top view and (f) cross-sectional view.*

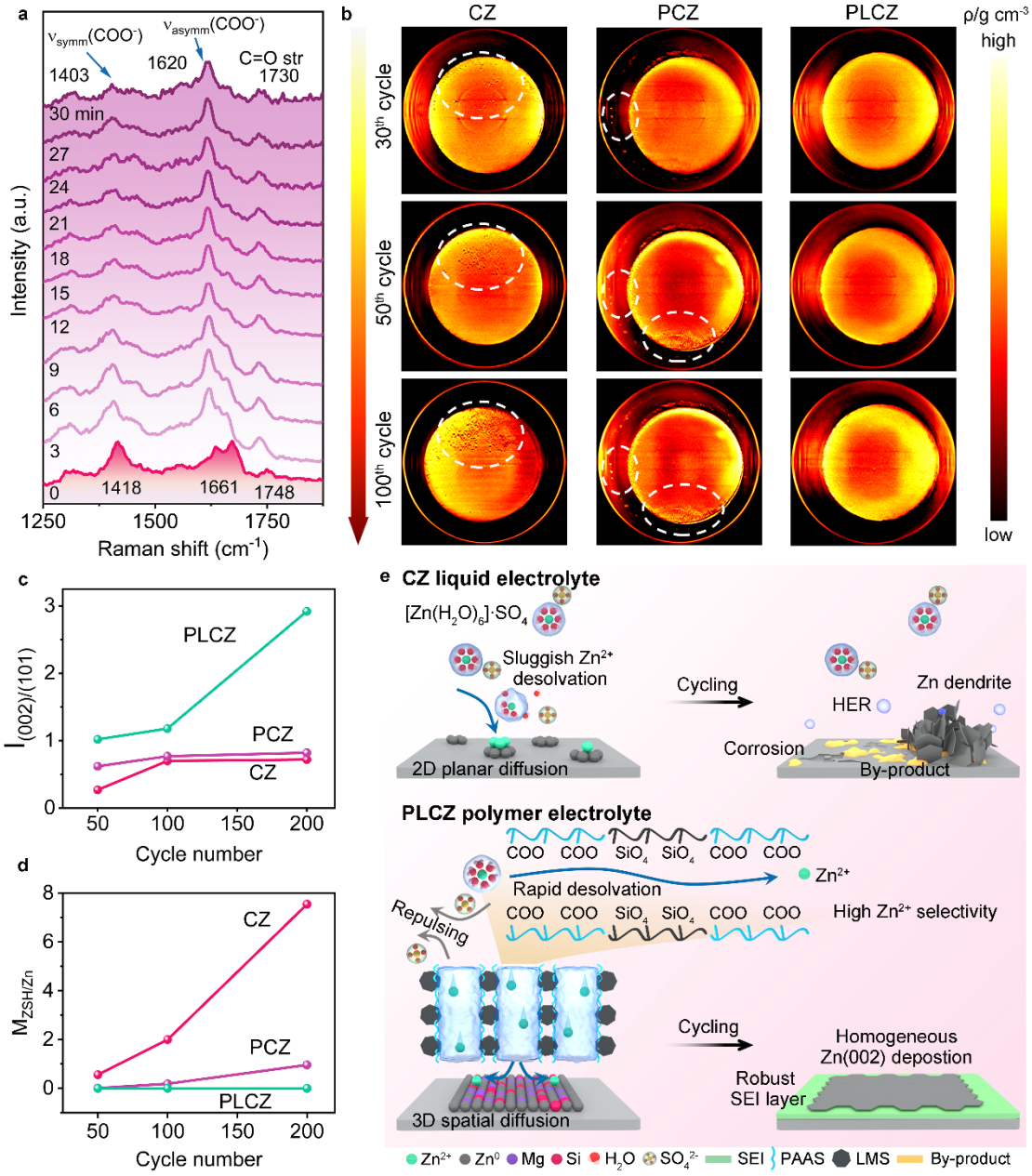

Fig. 5 *(a) The in-situ Raman spectra of Zn||Ag cell during deposition. (b) The micro-CT images of Zn||Zn cells at different cycles CZ, PCZ and PLCZ electrolytes. Color representation: orange/yellow circle for cathode case, orange/yellow circle wafer for Zn electrode, orange/yellow dot for Zn dendrite, black/wine red dot for corrosion pit. The calculated (c) $I_{(002)/(101)}$ and (d) $M_{ZSH/Zn}$ on Zn anodes based on XRD patterns. (e) Schematically illustrating the Zn deposition in CZ liquid and PLCZ electrolytes.*

Changes in supplementary information:

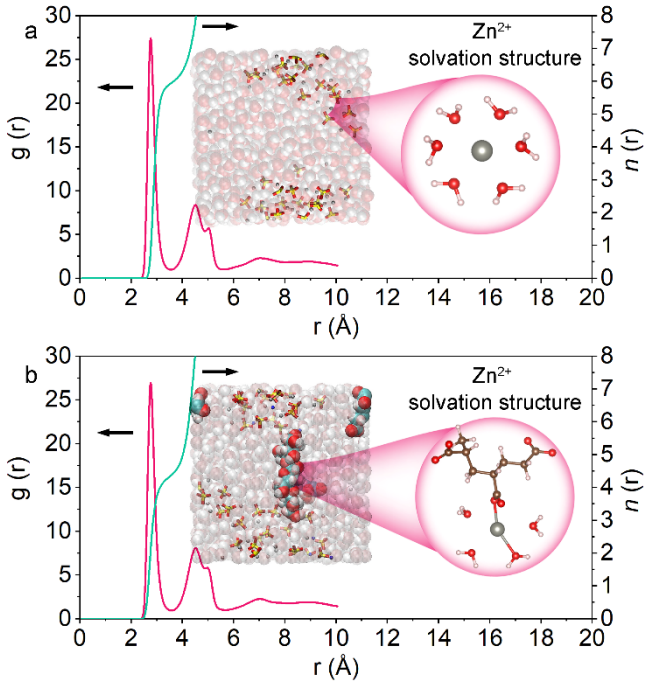

Supplementary Fig. S4 *The simulated RDF of Zn^{2+}-O (H_2O) and the coordination numbers of Zn^{2+} with water molecules with the corresponding Zn^{2+} solvation structure in the (a) CZ and (b) PCZ electrolytes.*

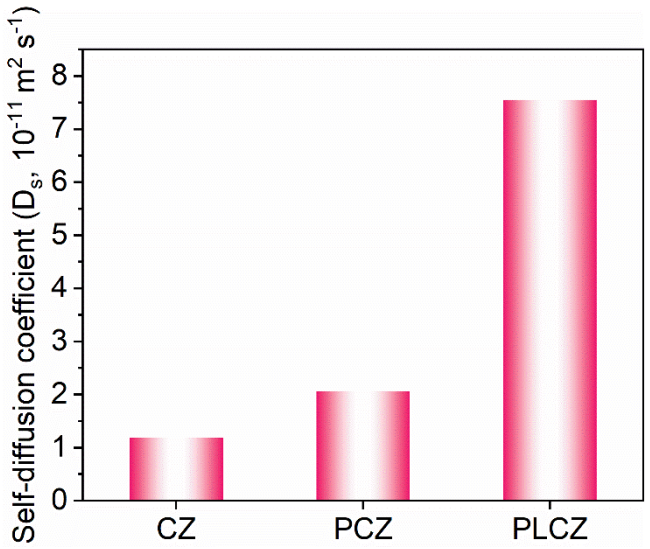

Supplementary Fig. S5 *The D_s of Zn^{2+} in the CZ, PCZ and PLCZ electrolytes.*

4. It is advisable to evaluate the performance changes by varying the thickness of the electrolyte. While a thinner electrolyte may provide higher ion mobility, it could potentially lower mechanical properties, making it crucial to determine the optimal thickness.

Author reply: Thank you very much for your comments. In the synthetic process of polymer electrolytes, when the used amounts of CNF dispersion solution, PAAS and LMS are 30, 0.1 and 0.1 g, respectively, the PLCZ electrolyte shows the best cycling

performance under various current densities and areal capacities (the polymer electrolyte with this mass ratio is denoted as $P_{0.1}L_{0.1}CZ$ in the manuscript). Therefore, based on this mass ratio of CNF, PAAS and LMS, we have prepared another two PLCZ electrolytes. The electrolyte thickness is regulated by controlling the used volume of the PAAS-LMS-CNF solution. The resultant PAAS-LMS-CNF solutions for the three PLCZ electrolytes are shown in Fig. R6 and the volumes are 70, 140 and 280 ml, respectively (the volume of PAAS-LMS-CNF solution for $P_{0.1}L_{0.1}CZ$ is 140 ml). We measured the corresponding electrolyte thicknesses, as shown in Fig. R7a. We also did the strain-stress tests. When the electrolyte thickness is 73 μm, the polymer electrolyte is failed to support the weight of ingot (Fig. R7b). When the electrolyte thickness is 128 or 219 μm, the electrolytes can hang the ingot (Fig. 1d and Fig. R7c). We tested the cycling performances of the polymer electrolytes with different thicknesses at the current densities of 0.5 mA cm^{-2}/0.25 mAh cm^{-2} and 5 mA cm^{-2}/2.5 mAh cm^{-2}. As shown in Figs. 3a, b and Fig. R8, the cycling lifespans of Zn||Zn symmetric cells with the various electrolytes exhibit a trend of first increasing and then decreasing with the increasing electrolyte thickness, and among all the electrolytes, the PLCZ with optimal electrolyte thickness (128 μm) obtains the better cycling performance at the current densities of 0.5 mA cm^{-2}/0.25 mAh cm^{-2} and 5 mA cm^{-2}/2.5 mAh cm^{-2}.

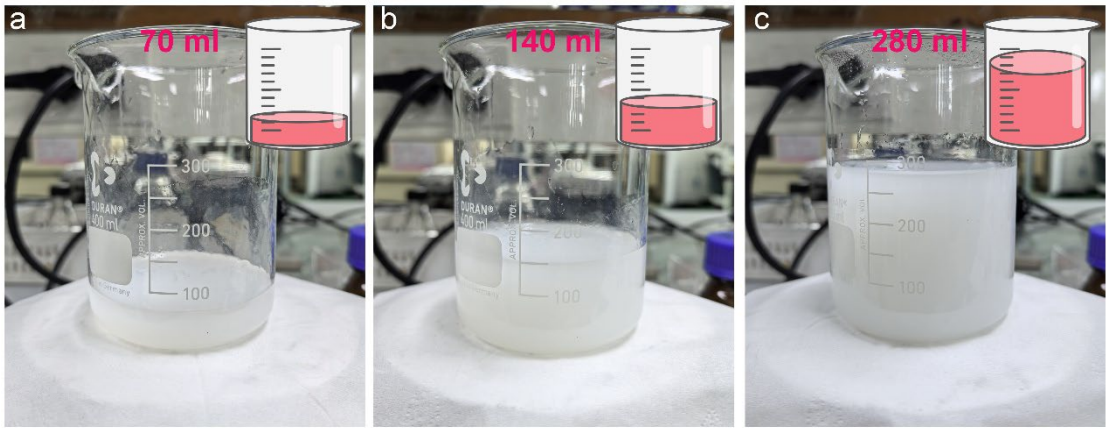

Fig. R6 *The PAAS-LMS-CNF solutions with the volume of (a) 70, (b) 140 and (c) 280 ml.*

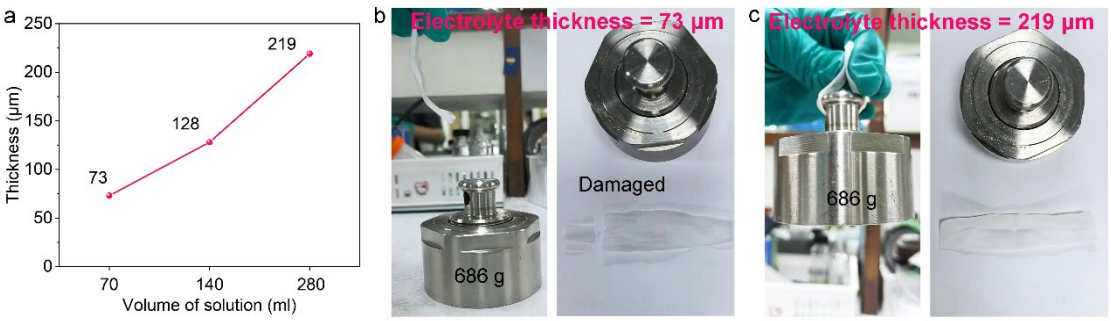

Fig. R7 *(a) The thickness of the polymer electrolytes. The strain-stress tests of when the electrolyte thickness is (b) 73 and (c) 219 μm. After strain-stress test, the electrolyte with the thickness of 73 μm is damaged, but when with 219 μm, it keeps unwounded,*

indicating a good mechanical property.

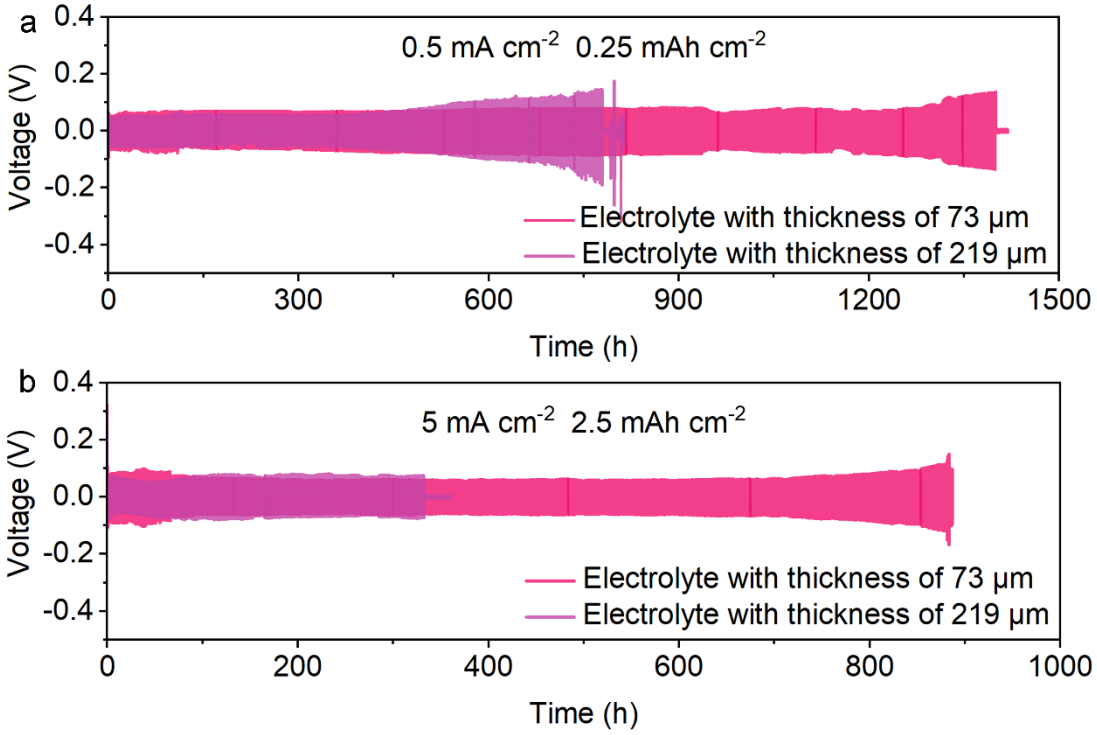

Fig. R8 *Galvanostatic cycling of the PLCZ cells with the electrolyte thicknesses of 73 and 219 μm at (a) 0.5 mA cm^{-2}, 0.25 mAh cm^{-2} and (b) 5 mA cm^{-2}, 2.5 mAh cm^{-2}.*

Changes in the manuscript (the highlighted part):

The PLCZ symmetric cell with the electrolyte thickness of 128 μm demonstrates an exceptionally prolonged lifespan exceeding 4400 h at 0.5 mA cm^{-2} and 0.25 mAh cm^{-2}, nearly 22 and 10 times greater than those of CZ (203 h) and PCZ (443 h) respectively, as illustrated in Fig. 3a and Supplementary Fig. S21a. The amplified voltage profiles provide the further affirmation of the consistent and minimal voltage hysteresis throughout the entire cycling process. The PLCZ symmetric cell also exhibits an excellent duration of 1200 h at 5 mA cm^{-2} and 2.5 mAh cm^{-2} (Supplementary Figs. S21b and S22).

Fig. 3 *Cycling performances of Zn||Zn symmetric cells with the CZ, PCZ and PLCZ at (a) 0.5 mA cm^{-2}, 0.25 mAh cm^{-2} and (b) 2 mA cm^{-2}, 10 mAh cm^{-2}. The electrolyte thickness of PLCZ here is 128 μm. SEM images of the Zn anodes on the top view and side view of (c) CZ, (d) PCZ and (e) PLCZ after 200 cycles. For easy of result comparison and analysis, the Zn dendrite, Zn foil, PCZ electrolyte and PLCZ electrolyte are colored with red, blue, pink and green, respectively. (f) CA tests and (g) Tafel plots of the CZ, PCZ and PLCZ.*

Changes in supplementary information:

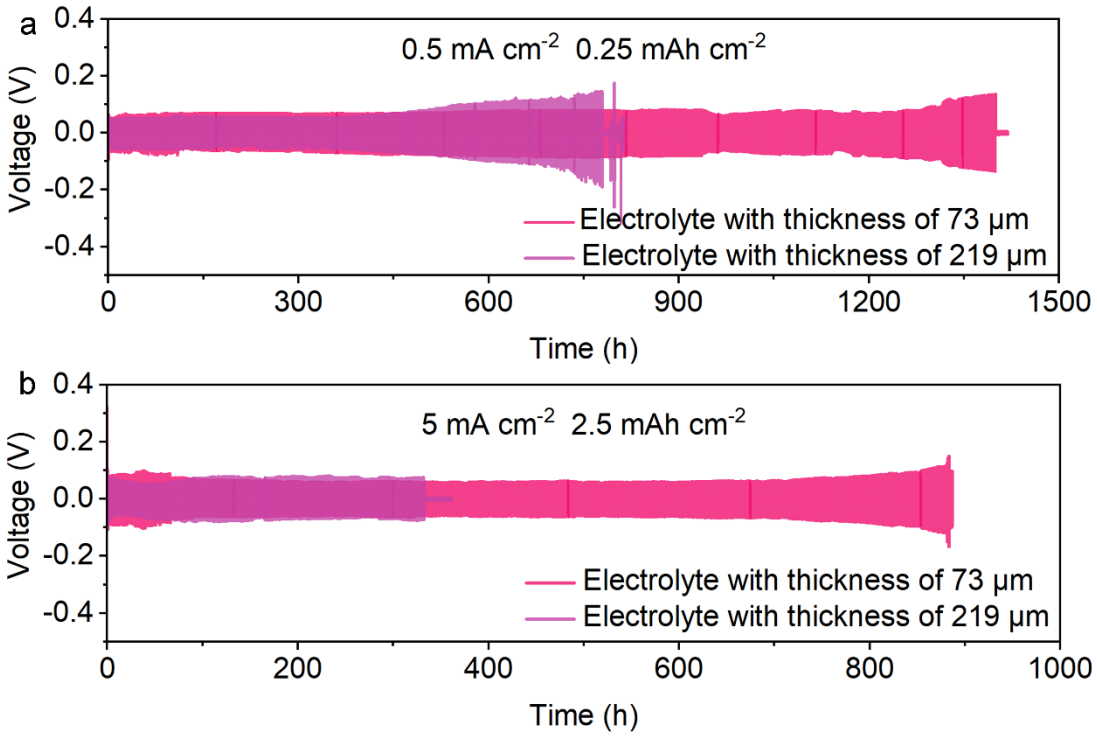

Supplementary Fig. S21 *Galvanostatic cycling of the PLCZ cells with the electrolyte thicknesses of 73 and 219 μm at (a) 0.5 mA cm^{-2}, 0.25 mAh cm^{-2} and (b) 5 mA cm^{-2}, 2.5 mAh cm^{-2}. The electrolyte thickness is regulated by controlling the used volume of the PAAS-LMS-CNF solution in which the mass ratio between PAAS, LMS and CNF is 0.1:0.1:30. When the volume of the PAAS-LMS-CNF solution is 70, 140, 280 ml, the electrolyte thickness is 73, 128 and 219 μm, respectively.*

Reviewer #2:

The manuscript deals with the composite separator for solid state zinc ion battery. It has been well written and presented. It can be accepted after addressing the following concern.

Author reply: Thanks for your positive comments and we are glad that you find our work of interest and importance. We have revised the manuscript point-by-point according to your comments.

1. The mechanism of the formation of cell membrane like structure in not clear. It seems the authors have exaggerated the mechanism.

Author reply: Thank you very much for your comments. We have removed the description of the cell membrane like structure about the designed polymer electrolyte in the revised manuscript, because all the reviewers comment that the relationship between cell membrane and the polymer electrolyte in our work is not clear and suitable. We also deleted the terms of "biomimetic" and "bioinspired" in the revised manuscript and changed the manuscript title.

We further used the molecular dynamics (MD) simulation to analyze the Zn ion solvation structure and transport within the PLCZ electrolyte. As plotted in Fig. R3, the radial distribution function (RDF) of the CZ liquid electrolyte shows a major peak of

Zn^{2+}-O (H_2O) at 2.75 Å with the coordination number (CN) of 6.06, representing the typical Zn^{2+} solvation sheath structure ($[Zn(H_2O)_6]^{2+}$) in the liquid solution (Nat Commun 2023, 14 (1), 3526). However, for the PCZ and PLCZ electrolytes, the CNs reduce to 4.30 and 3.75, respectively, duo to the electrostatic interactions of -COO^- group and LMS with Zn^{2+} ions, which efficiently replace the coordinated water molecules around Zn^{2+} ions and remodel the solvation structures ($[Zn(H_2O)_4(COO)]^+$ in PCZ and $[Zn(H_2O)_3(COO)LMS]^+$ in PLCZ). Moreover, the PLCZ polymer electrolyte realizes rapid Zn^{2+} ion diffusion and intercalation with a high self-diffusion coefficient (Ds) of 7.55 × 10^{-11} m^2 s^{-1} (Fig. R4). This enhanced ion mobility is facilitated by the -COO^- groups within the PAAS chain and LMS platelets, which form highly selective transport microchannels functioning as "ion transfer pumps".

We also analyzed the deposition mechanism of Zn in the PLCZ electrolyte, please see the answer of the ***comment 2****.*

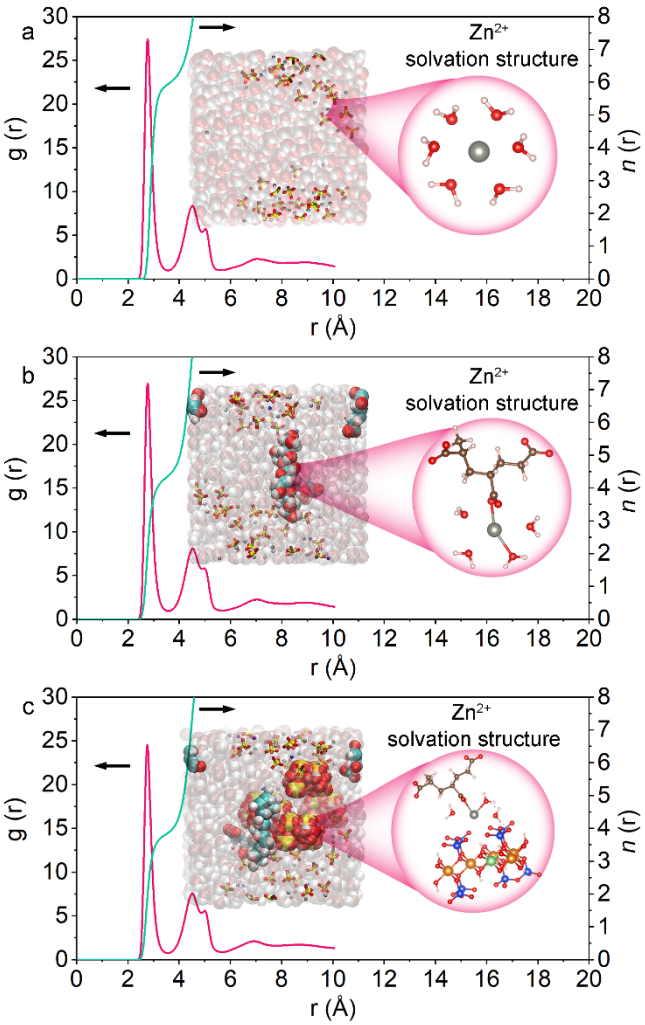

Fig. R3 *The simulated RDF of Zn^{2+}-O (H_2O) and the coordination numbers of Zn^{2+} with water molecules with the corresponding Zn^{2+} solvation structure in the (a) CZ, (b) PCZ and (c) PLCZ electrolytes.*

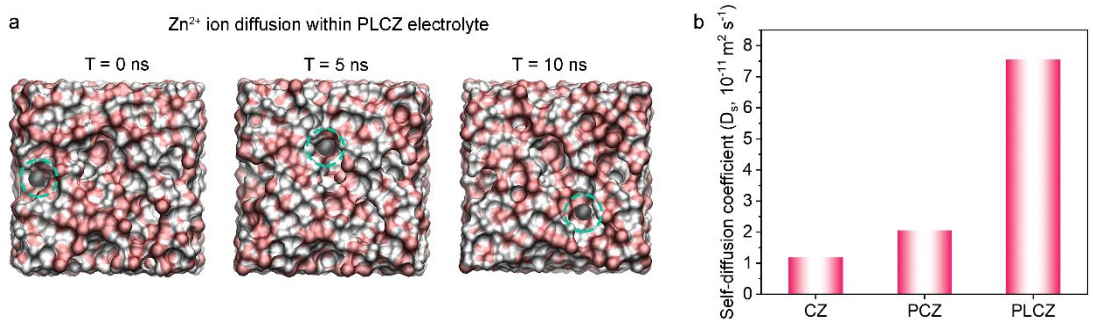

Fig. R4 *(a) The Zn^{2+} diffusion within the PLCZ electrolyte from the 3D snapshots of T =0 ns to 10 ns. (b) The Ds of Zn^{2+} in the CZ, PCZ and PLCZ electrolytes.*

Changes in the manuscript (the highlighted part):

Title

A multifunctional quasi-solid-state polymer electrolyte with highly selective ion highways for practical zinc ion batteries

Such unique selective aggregation of Zn^{2+} ion confers upon LMS platelets and PAAS chains the ability to work as "ion transfer pumps", which in turn renders a fast ion transportation, even ion nucleation and homogeneous Zn deposition during Zn plating/stripping process[20, 21]. Molecular dynamics (MD) simulations were conducted to validate the above inferences (Fig. 1b and Supplementary Fig. S4). The radial distribution function (RDF) of the CZ liquid electrolyte reveals a prominent peak of Zn^{2+}-O (H_2O) at 2.75 Å, with the coordination number (CN) of 6.06, indicative of the typical Zn^{2+} solvation sheath structure ($[Zn(H_2O)_6]^{2+}$) in the liquid solution[22]. However, the PCZ and PLCZ electrolytes exhibit reduced CN values of 4.30 and 3.75, respectively. This decrease is attributed to the electrostatic interactions of -COO^- group and LMS with Zn^{2+} ions, which efficiently displace the coordinated water molecules around Zn^{2+} ions and alter the solvation structures to $[Zn(H_2O)_4(COO)]^+$ in PCZ and $[Zn(H_2O)_3(COO)LMS]^+$ in PLCZ. Additionally, the PLCZ polymer electrolyte realizes rapid Zn^{2+} ion diffusion and intercalation with high self-diffusion coefficient (Ds) of 7.55×10^{-11} m^2 s^{-1} (Fig. 1c and Supplementary Fig. S5), due to the formed highly selective transportation microchannels by -COO^- within PAAS chain and LMS platelets.

Theoretical calculations

Zn ion desolvation and transport within the polymer electrolyte were investigated by using the classical MD simulations for three systems i.e. (1) The 36 $ZnSO_4$ and 1000 water molecules; (2) The 2 PAAS, 1 cellulose, 36 $ZnSO_4$ and 1000 water molecules were randomly added into simulation system; (3) The 5 LMS, 2 PAAS, 1 cellulose, 36 $ZnSO_4$ and 1000 water molecules were randomly added into simulation system. The all

molecules were randomly added into each simulation system. The DLPOLY 4.10 package[63] was used for this study. The starting box size was 40 × 40 × 40 Å^3 and the simulations were performed under the Nose-Hoover ensemble[64] at the temperature of 298 K. The periodic boundary conditions and the minimum image convention were applied. The cutoff radius for short-ranged interaction is 12 Å and the long-ranged interaction was treated by the Ewald summation method[65]. In order to equilibrate the simulation box size, the simulations were first carried out under NPT ensemble for about 2 ns with the time step of 1 fs. The production runs were then carried out under NVT ensemble for 20 ns. The trajectories were collected from the last 10 ns and the RDFs were computed.

The DREIDING force-field[66] was used for interactions of other atom types. The Lennard-Jones (LJ) parameters for different types of atom (σ_{ij}, ε_{ij}) are taken from pure types (σ_{ii}, ε_{jj}) following the Lorentz-Berthelot mixing rule[67], which is written as

$$\sigma_{ij} = \frac{\sigma_{ii}+\sigma_{jj}}{2};\ \varepsilon_{ij} = \sqrt{\varepsilon_{ii}\varepsilon_{jj}} \qquad (2)$$

All partial atomic charges except for water molecules, were extracted from the calculations by using the ORCA program. The HF/6-31G(d) theory and the electrostatic potential fitting (ESP) of CHELPG[68] have been used.

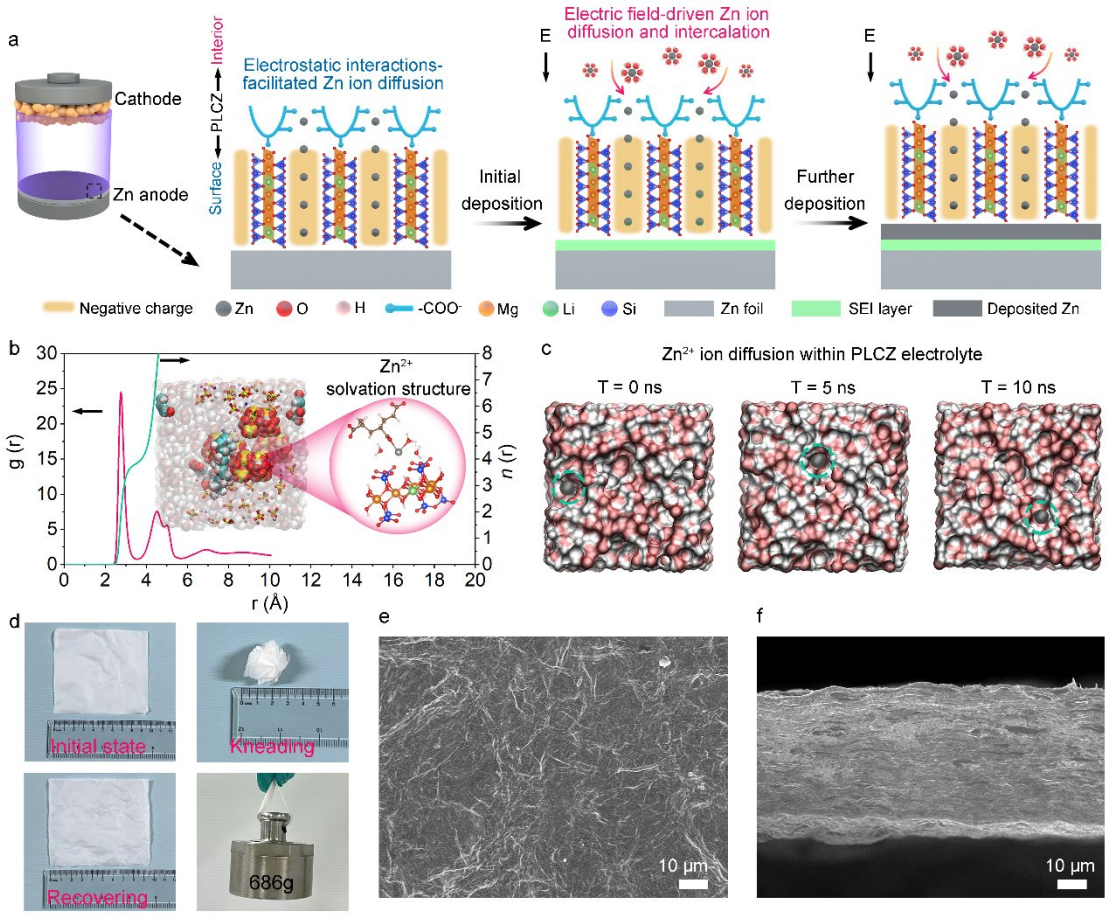

Fig. 1 *(a) Schematically illustrating the Zn^{2+} ion diffusion and transport cross the PLCZ polymer electrolyte. (b) The simulated RDF of Zn^{2+}-O (H_2O) and the coordination*

numbers of Zn^{2+} with water molecules with the corresponding Zn^{2+} solvation structure in the PLCZ electrolytes. (c) The Zn^{2+} diffusion within the PLCZ electrolyte from the 3D snapshots of T =0 ns to 10 ns. (d) The digital photographs of the designed PLCZ electrolyte under initial state, kneading and recovering and the corresponding strain-stress test. SEM images of the PLCZ electrolyte on (e) the top view and (f) cross-sectional view.

Changes in supplementary information:

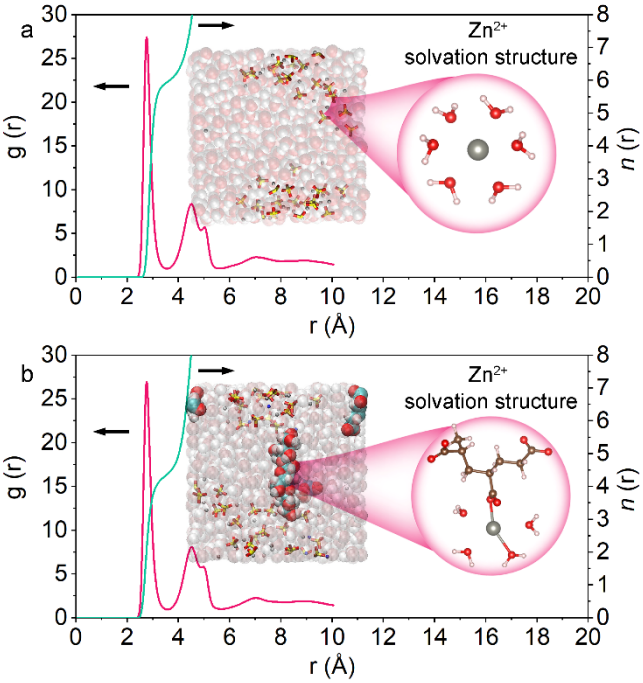

Supplementary Fig. S4 *The simulated RDF of Zn^{2+}-O (H_2O) and the coordination numbers of Zn^{2+} with water molecules with the corresponding Zn^{2+} solvation structure in the (a) CZ and (b) PCZ electrolytes.*

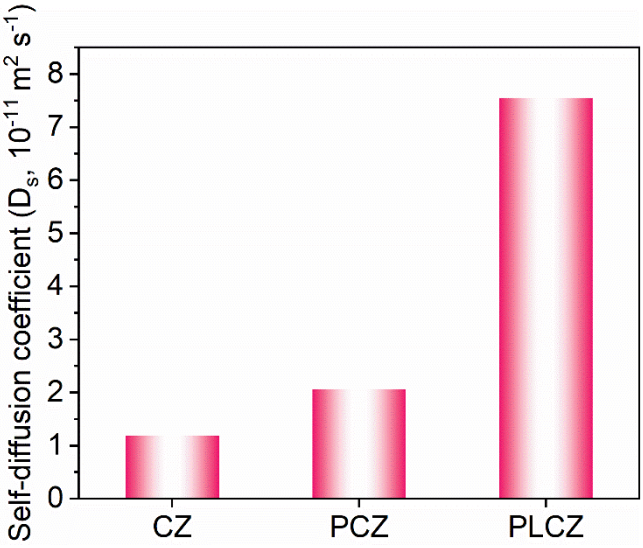

Supplementary Fig. S5 *The D_s of Zn^{2+} in the CZ, PCZ and PLCZ electrolytes.*

2. The exact mechanism of the suppression of dendrite growth is missing. From the SEM images (Figure 4C), the random deposition of zinc is visible which can result into the dendrite growth.

Author reply: Thank you very much for your comments.

For the Question 1: *The exact mechanism of the suppression of dendrite growth is missing.*

We have drawn the deposition mechanisms of Zn^{2+} ions in the CZ liquid and PLCZ electrolytes, shown in Fig. R5. Zn^{2+} ions in CZ aqueous electrolyte tend to laterally diffuse along the rough surface and deposit at energetically favorable sites, finally generating the fatal dendrites. Meanwhile, water-induced side reactions aggravate H_2O decomposition and increase local pH value near the Zn electrode. This unfavorable environment promotes the precipitation of $[Zn(H_2O)_6]SO_4$ complex and the generation of ZSH by-product. On the contrary, the PLCZ electrolyte leverages the charged $-COO^-$ groups of polymer chains and LMS platelets to establish high-speed pathways for Zn^{2+} ion transportation through electrostatic interactions. This interaction spontaneously influences solvation structure and expedites desolvation behavior. During subsequent deposition, Si and Mg atoms concurrently deposit with Zn ion to form a robust medium-entropy alloy (MEA) SEI with a strong affinity for Zn. Such unique SEI extends spatial movement of Zn and guides the favorable deposition of Zn(002) planes, ultimately yielding an ultra-stable Zn electrode.

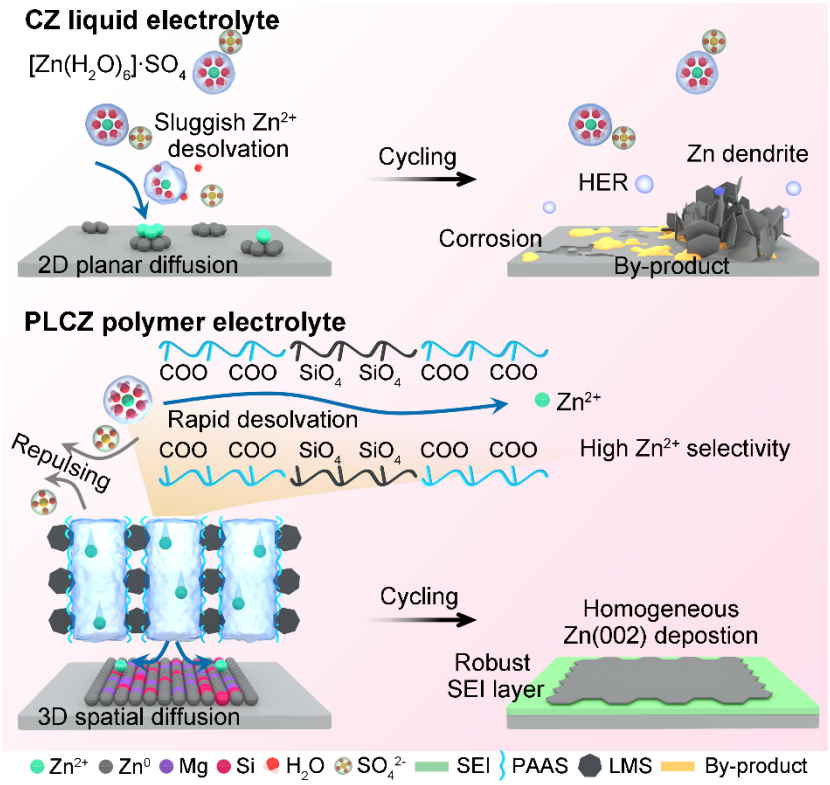

Fig. R5 *Schematically illustrating the Zn deposition in CZ liquid and PLCZ electrolytes.*

For the Question 2: *From the SEM images (Figure 4C), the random deposition of zinc is visible which can result into the dendrite growth.*

The SEM images of Cu cathode of the CZ and PCZ electrolytes after cycling are shown in Figure 4b and 4c, respectively. The SEM image in Figure 4d is belonged to the PLCZ electrolyte. Yes, from the SEM images (Figure 4b and 4c), the random deposition of Zn is indeed visible which can result into the dendrite growth. However, for the PLCZ (Figure 4d), the SEM image of Cu cathode exhibits smooth surface without evident Zn dendrite formation, indicating high reversibility of Zn deposition/dissolution behavior. For easy of understanding, we have labeled the sample names at the top of the SEM images in the revised manuscript (Fig. R9).

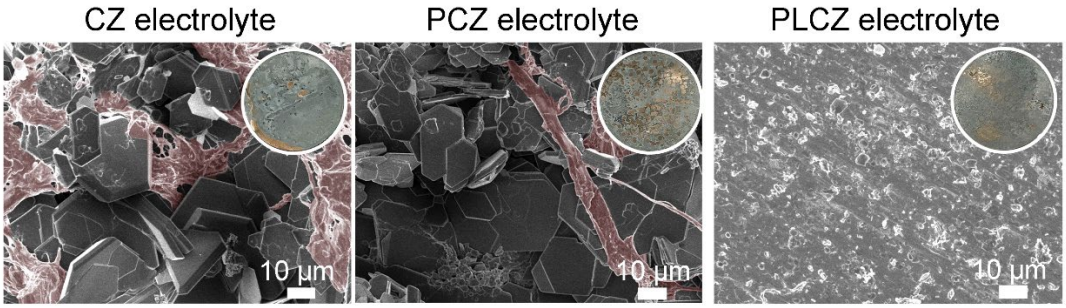

Fig. R9 *SEM images of Cu cathode of CZ, PCZ and PLCZ (insets: digital photographs of Cu electrodes). The red color in the SEM images represent the CNF fiber.*

Changes in the manuscript (the highlighted part):

In Supplementary Fig. S46, compared to the CZ and PCZ, the PLCZ obtains smaller and more stable R_{SEI} and R_{CT} values, resulting from the highly conductive MEA SEI and the suppressive by-product. The Zn deposition mechanisms in the CZ liquid and PLCZ electrolytes were schematically illustrated in Fig. 5e. Zn^{2+} ions in CZ aqueous electrolyte tend to laterally diffuse along the rough surface and deposit at energetically favorable sites, finally generating the fatal dendrites. Meanwhile, water-induced side reactions aggravate H_2O decomposition and increase local pH value near the Zn electrode. This unfavorable environment promotes the precipitation of $[Zn(H_2O)_6]SO_4$ complex and the generation of ZSH by-product. On the contrary, the PLCZ electrolyte leverages the charged -COO^- groups of polymer chains and LMS platelets to establish high-speed pathways for Zn^{2+} ion transportation through electrostatic interactions. This interaction spontaneously influences solvation structure and expedites desolvation behavior. During subsequent deposition, Si and Mg atoms concurrently deposit with Zn ion to form a robust MEA SEI with a strong affinity for Zn. Such unique SEI extends spatial movement of Zn and guides the favorable deposition of Zn(002) planes, ultimately yielding an ultra-stable Zn electrode.

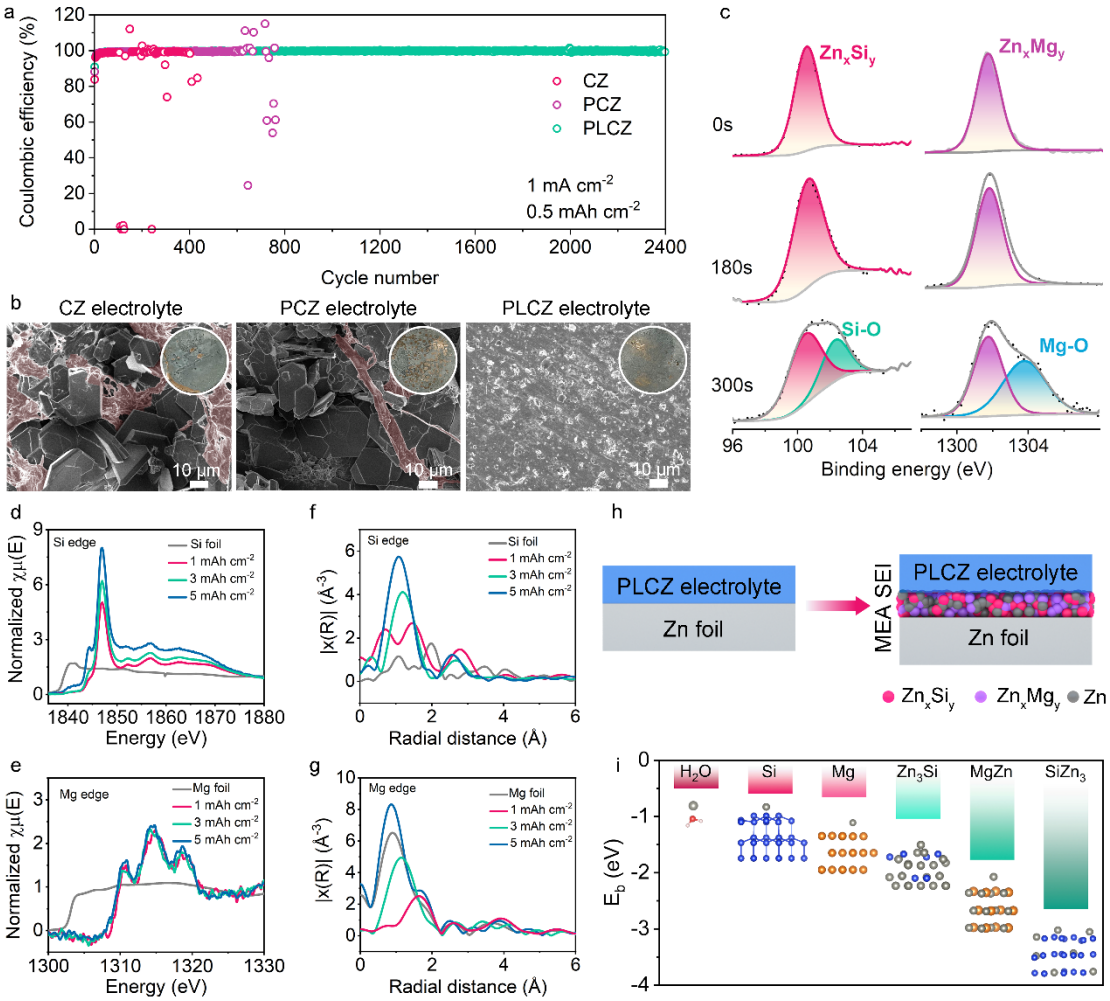

Fig. 4 *(a) Cycling performance of Zn||Cu asymmetric cells as well the corresponding (b) SEM images of Cu cathode of the CZ, PCZ and PLCZ (insets: digital photographs of Cu electrodes). The red color in the SEM images represent the CNF fiber. (c) Si 2p and Mg 1s XPS spectra of the cycled Zn anodes of PLCZ electrolyte. XANES spectra and the corresponding r-space date of (d, f) Si K-edge and (e, g) Mg K-edge of Zn anodes after deposited different Zn capacities with PLCZ electrolyte. (h) Schematically illustrating the formation of MEA SEI layer on Zn anode. (i) The calculated E_b of Zn on the alloy ingredients.*

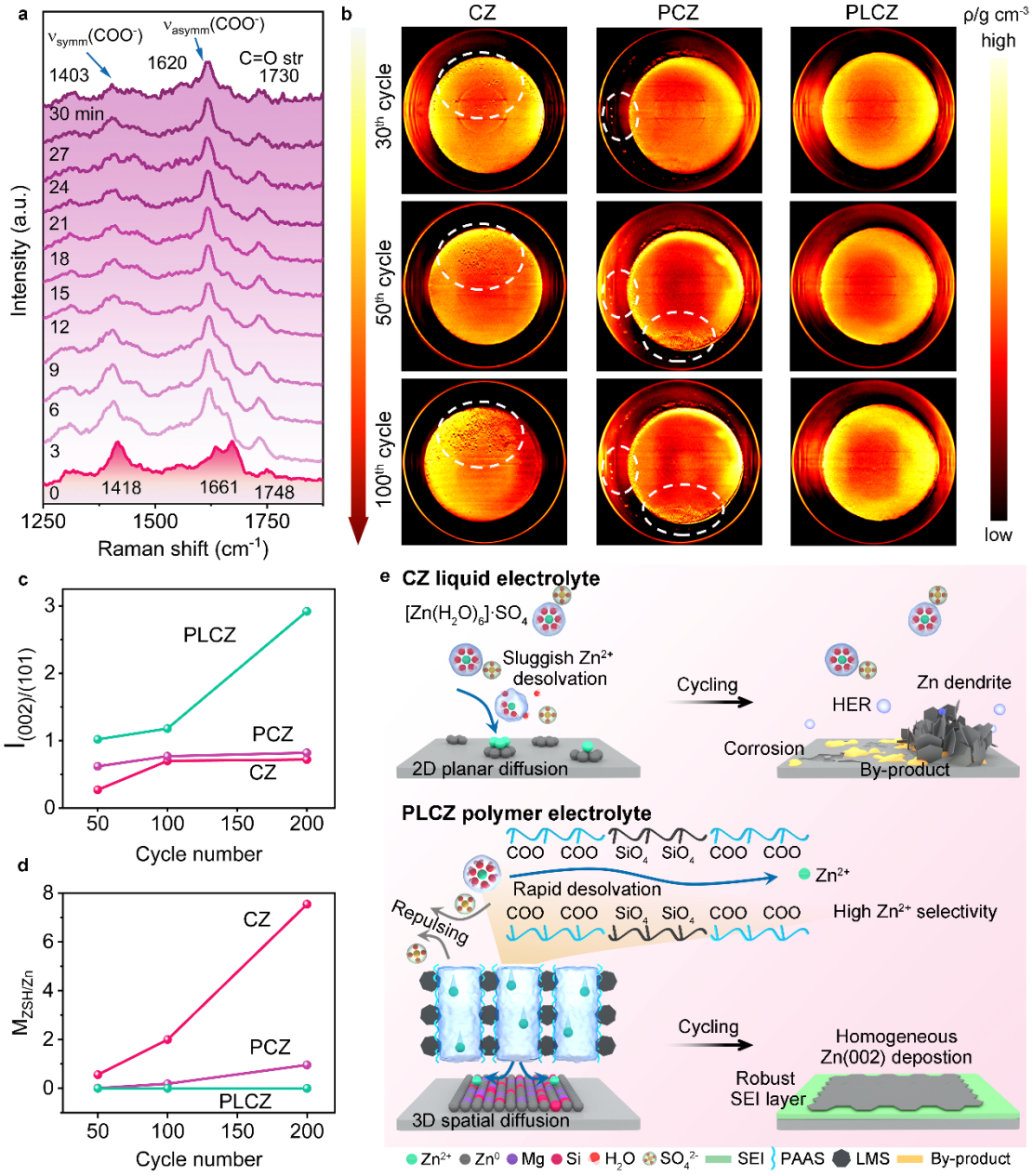

Fig. 5 *(a) The in-situ Raman spectra of Zn||Ag cell during deposition. (b) The micro-CT images of Zn||Zn cells at different cycles CZ, PCZ and PLCZ electrolytes. Color representation: orange/yellow circle for cathode case, orange/yellow circle wafer for Zn electrode, orange/yellow dot for Zn dendrite, black/wine red dot for corrosion pit. The calculated (c) $I_{(002)/(101)}$ and (d) $M_{ZSH/Zn}$ on Zn anodes based on XRD patterns. (e) Schematically illustrating the Zn deposition in CZ liquid and PLCZ electrolytes.*

3. Generally, the dendrite growth is dominated at high current density. The cycling of the battery in the present study is at very low current density.

Author reply: Thank you very much for your comments. Yes, the high current density is easier to cause the dendrite formation and growth. In our work, the Zn||Zn symmetric cells with the CZ, PCZ and PLCZ electrolytes have been tested at the current densities

of 0.5 mA cm^{-2}/0.25 mAh cm^{-2}, 2 mA cm^{-2}/10 mAh cm^{-2}, 5 mA cm^{-2}/2.5 mAh cm^{-2} and 10 mA cm^{-2}/1 mAh cm^{-2}. We also supplemented the cycling performance of Zn||Zn cells at the current densities of 20 mA cm^{-2}/5 mAh cm^{-2} (Fig. R10) and 40 mA cm^{-2}/1 mAh cm^{-2} (Fig. R11). At these high current densities, the Zn||Zn cells with the PLCZ electrolyte still maintain better cycling lifespan and stability than that with the CZ and PCZ electrolytes.

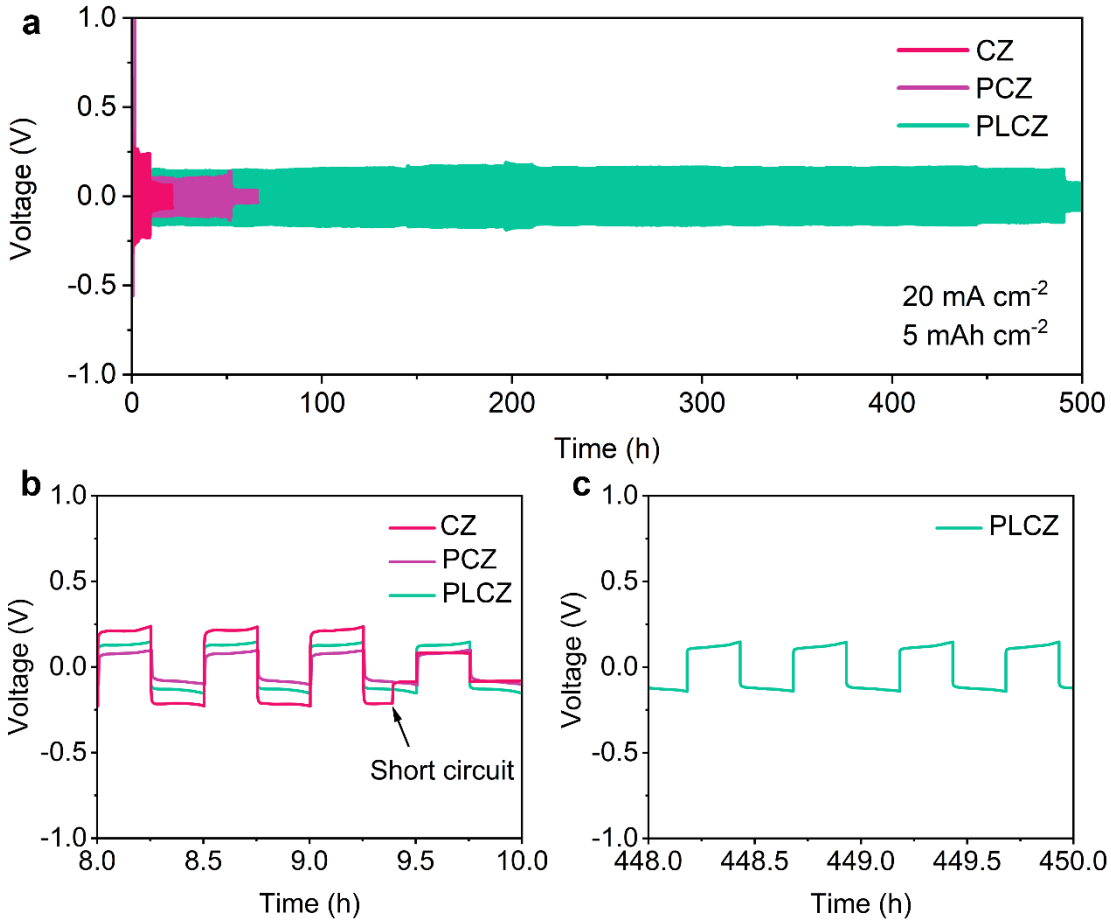

Fig. R10 *(a) Galvanostatic cycling of Zn||Zn cells with CZ, PCZ and PLCZ at 20 mA cm^{-2}/5 mAh cm^{-2}. The voltage-time profile of Zn||Zn cells at (b) 17-20 cycles and (c) 897-900 cycles.*

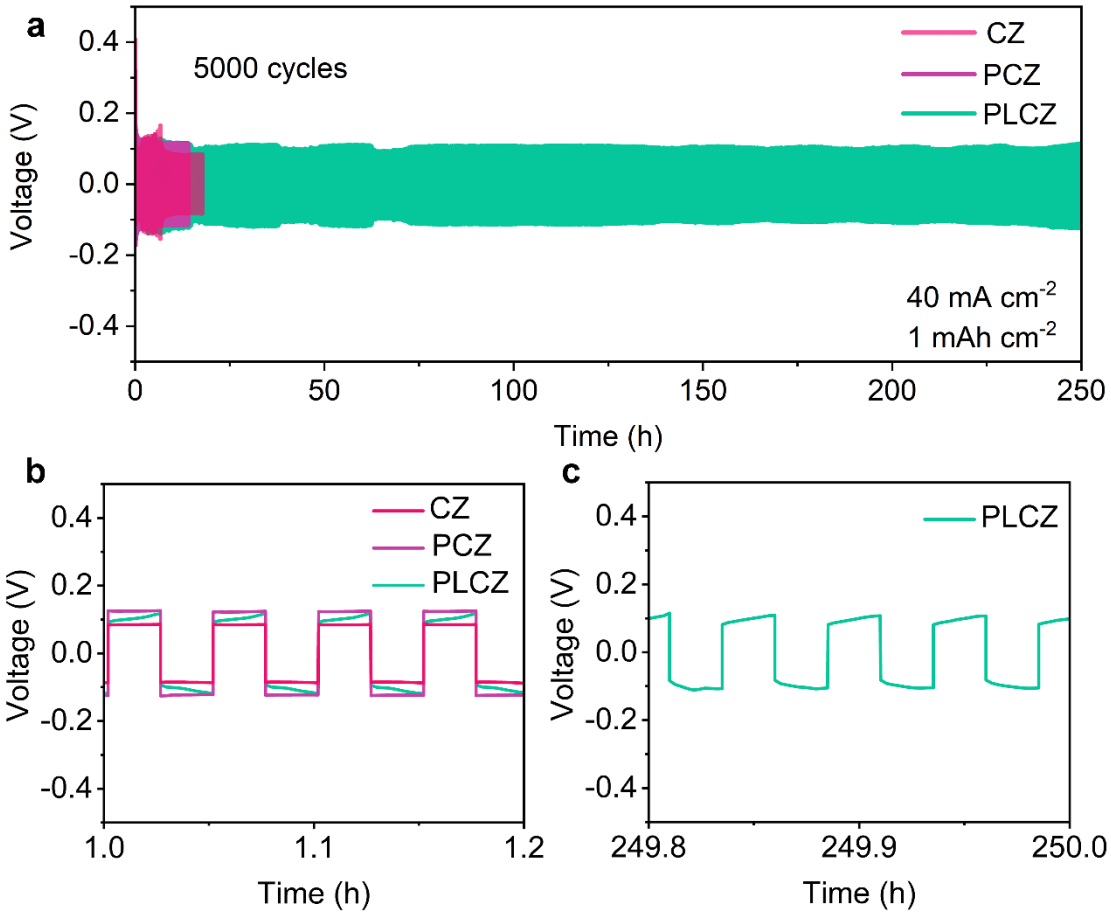

Fig. R11 *(a) Galvanostatic cycling of Zn||Zn cells with CZ, PCZ and PLCZ at 40 mA cm^{-2}/1 mAh cm^{-2}. The voltage-time profile of Zn||Zn cells at (b) 21-24 cycles and (c) 4997-5000 cycles.*

Changes in the manuscript (the highlighted part):

When under the current density of 10 mA cm^{-2} and 1 mAh cm^{-2}, it sustains an impressive cycle lifespan of 1400 h (7000 cycles) without discernible voltage fluctuation (Supplementary Fig. S23). Even under higher current densities (20 mA cm^{-2}, 5 mAh cm^{-2} and 40 mA cm^{-2}, 1 mAh cm^{-2}), the PLCZ symmetric cells still maintain better cycling lifespans and stabilities than that of the CZ and PCZ electrolytes (Supplementary Figs. S24 and S25).

Changes in supplementary information:

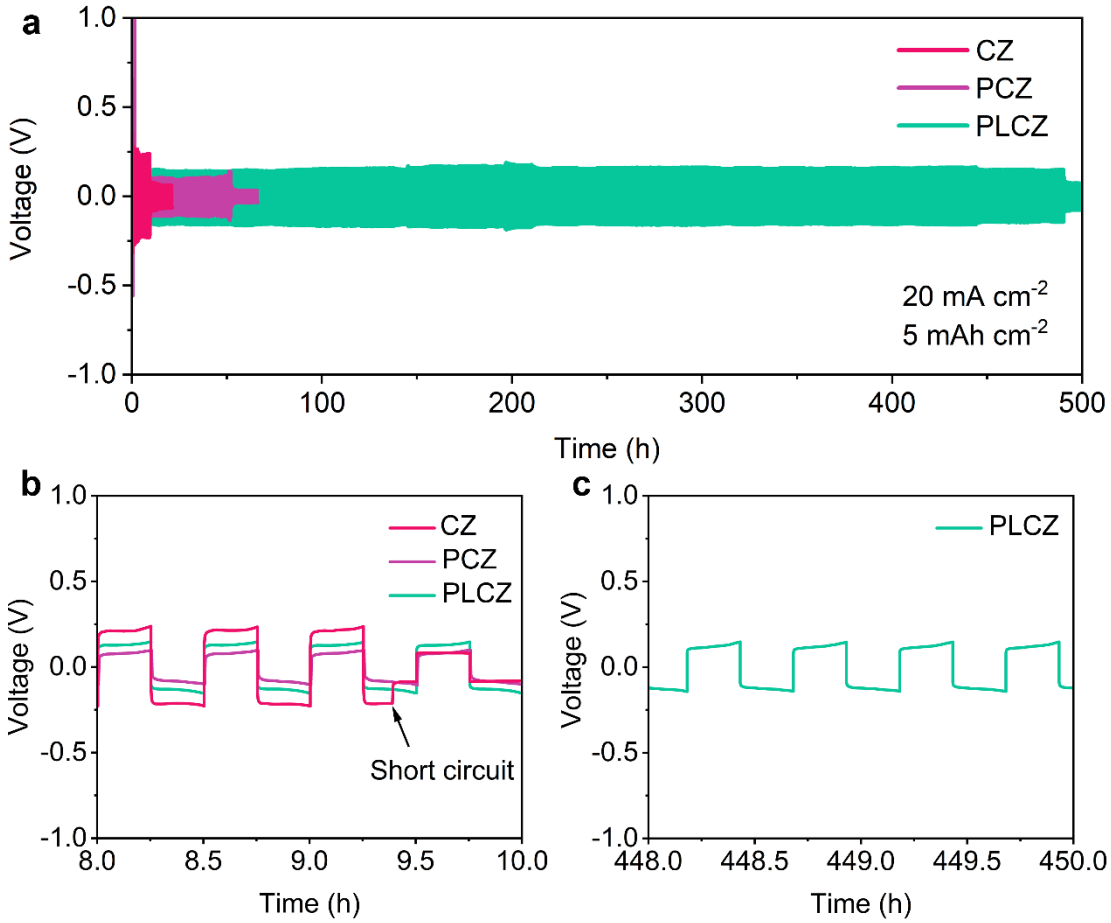

Supplementary Fig. S24 *(a) Galvanostatic cycling of Zn||Zn cells with CZ, PCZ and PLCZ at 20 mA cm^{-2}/5 mAh cm^{-2}. The voltage-time profile of Zn||Zn cells at (b) 17-20 cycles and (c) 897-900 cycles.*

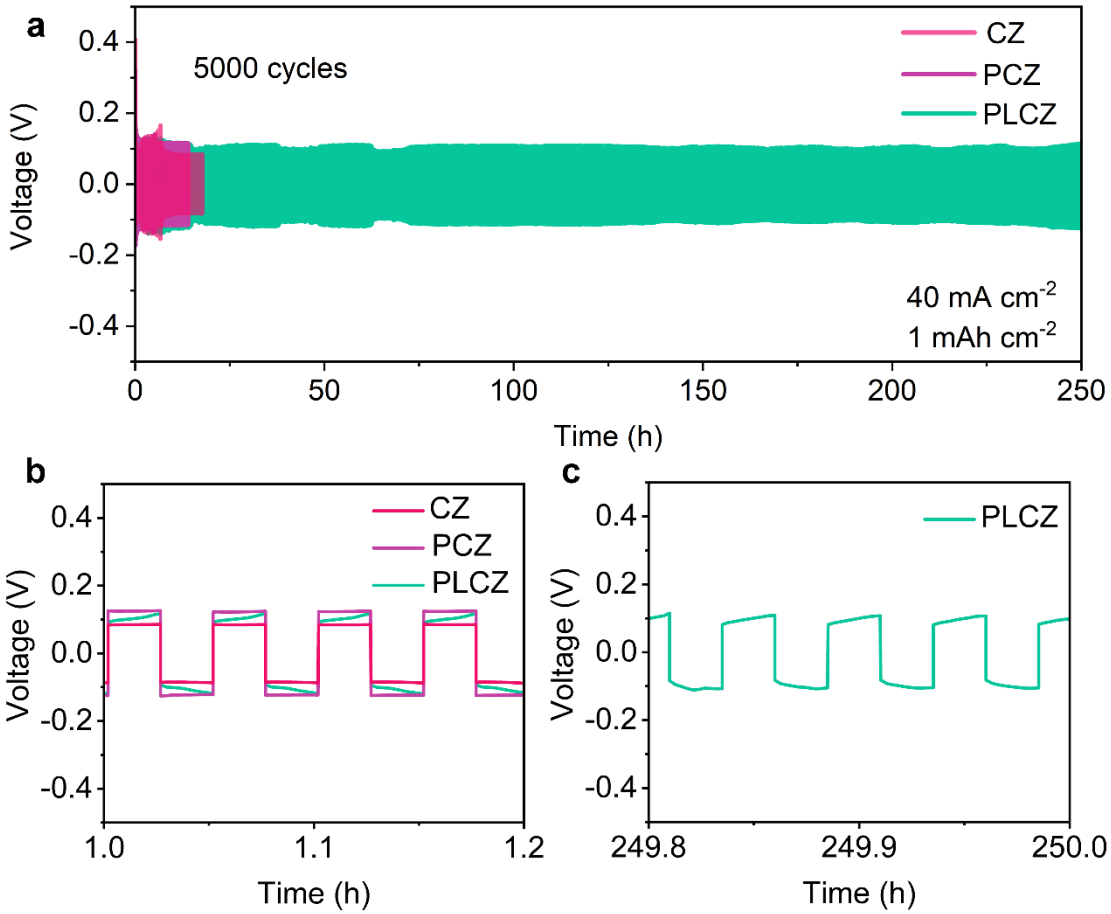

Supplementary Fig. S25 *(a) Galvanostatic cycling of Zn||Zn cells with CZ, PCZ and PLCZ at 40 mA cm^{-2}/1 mAh cm^{-2}. The voltage-time profile of Zn||Zn cells at (b) 21-24 cycles and (c) 4997-5000 cycles.*

4. Check for the typos.

Author reply: Thank you very much for your comments. We sincerely apologize for any typos made. Here is the revised version with careful attention to detail:

Changes in the manuscript (the highlighted part):

1. *We designed a versatile quasi-solid-state polymer electrolyte with highly selective ion transport channels via molecular crosslinking of sodium polyacrylate, lithium magnesium silicate and cellulose nanofiber.*
2. *In addition, the charged groups (e.g., carboxyl, sulfonate, phosphate and hydroxyl groups) inherently contribute to a firm adherence between substrate and polymer electrolyte, which in turn restrains interfacial dislocation and maintains stable electrode reactions.*
3. *Fig. 1d shows the digital photographs of the PLCZ electrolyte, which exhibits a complete structure and no visible damages even after kneading, highlighting its excellent flexibility and restorability.*
4. *The PLCZ electrolyte features a sleek and consistent surface (Fig. 1e) and a dense*

texture in its cross-section (Fig. 1f and Supplementary Fig. S10), contributing to reinforce interfacial stability between the electrolyte and Zn anode and to set up an effective bridge for fast Zn ion transportation.

5. *Compared with the pristine PAAS aqueous gel, symmetric and asymmetric -COO^- stretching vibrations after ion exchange of the PCZ experience a notable blue shift, due to the metal coordination with Zn^{2+} ions with electrostatic forces, highly advantageous for the confinement and control of Zn^{2+} ion migration along the polymer chain.*
6. *Besides, FTIR spectra of the CZ show the stretching vibration of the O-H bonds at 3245 cm^{-1} (Fig. 2b).*
7. *The high-resolution XPS spectra of Zn 2p in electrolytes are shown in Fig. 2e.*
8. *Unwanted dendrite agglutination and penetration are generated on the surface of the CZ and PCZ at the 100^{th} and 200^{th} cycles.*
9. *X-ray absorption spectra (XAS) of Zn anode after depositing different Zn capacities (1, 3 and 5 mAh cm^{-2}) were used to investigate the local structure and chemical environment of Si and Mg atoms.*
10. *These results indicate that the Zn-containing MEA layer has higher chemical affinity towards Zn^{2+} ions, conducive to the homogeneous nucleation and Zn^{2+} deposition with a lower Zn nucleation barrier.*
11. *This striking disparity in cycling performance can be primarily attributed to the distinctive properties of the PLCZ electrolyte, which effectively creates a swift ionic transportation path and eliminates the adverse effects caused by Zn dendrite and by-product.*
12. *After cooling down, the synthetic V_2O_5 powder was fully ground.*
13. *In-situ micro CT (Bruker skyscan 1173) was employed to observe Zn dendrite growth and by-product distribution on the surface of Zn anode.*
14. *For V_2O_5 cathode electrode, the slurry of V_2O_5, conductive carbon and PVDF in a 7:2:1 ratio was coated on carbon paper and dried in oven overnight.*
15. *where A, R and L are the resistance, surface area and thickness of the CNF separator and solid-state electrolytes, respectively.*

Reviewer #3:

The manuscript by Yang et al. describes a method of producing quasi-solid-state polymers for aqueous zinc-ion batteries. The authors claim that these exhibit improved transport properties through biomimetic ion channels and increased cycle stability. Bulk and surface analytical techniques were used to elucidate the structure of the composite material. Compared to reference materials CZ and PCZ, a stabilization of the SEI layer due to MEA formation and reduced dendrite growth was observed. Electrochemical investigations showed an improved cyclability for symmetric Zn||Zn, as well as asymmetric Zn||Cu and Zn||V_2O_5 cells.

Although this manuscript contains valuable scientific information on the improvement of AZIBs, it contains a few significant weaknesses and room for improvement. The

presentation of the data and the structure of the manuscript suffer from a lack of clarity at some points, which repeatedly leaves the reader confused.

Author reply: Thanks for your positive comments and we are glad that you find our work of interest and importance. We have revised the manuscript point-by-point according to your comments.

1) The comparison of the AZIB structure to the biological membrane tenuous, distracting and confusing for the reader. There is no evidence of the order (i.e. well defined bilayer structures that create distinct compartments with ion channels across the barrier) that is characteristic of a cell membrane. The introduction to the principle and structure of the cell and cell membrane is therefore not relevant in this context and shouldn't be discussed as any more than a sidenote in the introduction. The resulting material is better described as an organic-inorganic composite material, which is what the introduction should focus on as well as the status of AZIBs. Furthermore, the structure and preparation of CZ, PCZ, and PLCZ should be discussed in more detail from the beginning to provide the reader with a better overview of what these acronyms mean.

Author reply: Thank you very much for your comments. We have removed the introduction of the principle and structure of the cell and cell membrane. We also deleted the terms of "biomimetic" and "bioinspired" in the revised manuscript and changed the manuscript title. Additionally, we discussed the structure and preparation of the CZ, PCZ and PLCZ electrolytes in the Introduction Section (the third paragraph).

Changes in the manuscript (the highlighted part):

Here, to cope with these above-mentioned challenges, we designed a versatile QSPE with rapid Zn-ion diffusion, high selectivity and strong mechanical properties through the cross-linking of sodium polyacrylate (PAAS), lithium magnesium silicate (LMS) and cellulose nanofiber (CNF). PAAS and LMS were first dissolved in CNF solution to establish physical entanglement and after dried, followed by complete Zn^{2+} ion exchange in $ZnSO_4$ solution. The prepared polymer electrolyte is designated as PLCZ. For comparative purposes, we also prepared a polymer electrolyte without the LMS additive (PCZ) and an aqueous $ZnSO_4$ electrolyte equipped with a CNF separator (CZ). The LMS platelets, consisting of silicate tetrahedrons and intermediate octahedrons of Li and Mg ions coordinated with oxygen atoms and hydroxyl groups, create an anisotropic charge distribution where the silicate tetrahedron layers induce a negative charge and Mg-O octahedrons in the platelet edge have positive charge (Supplementary Fig. S1)[14, 15].

2) Fig. 1b does not explain the working principle of AZIBs sufficiently. It should be explained in more detail in the text, as it is crucial for understanding this work.

Author reply: Thank you very much for your comments. The lithium magnesium silicate (LMS) platelets are composed of silicate tetrahedrons and intermediate octahedrons of Li and Mg ions coordinated with oxygen atoms and hydroxyl groups (Fig. R12a). The LMS platelets have anisotropic charge distribution where the silicate tetrahedron

layers have negative charge and Mg-O octahedrons in the platelet edge have positive charge (Fig. R12b). Thus, the Mg-O octahedrons promote the bonding with the carboxylate anions (-COO^-) in PAAS polymer chains to construct microchannels that are composed of -COO^- groups and silicate tetrahedrons (Fig. R13). The -COO^- groups in PAAS chains can accelerate the permeation of Zn^{2+} in the PLCZ electrolyte by metal coordination bonds and concentration gradients. The silicate tetrahedron layers with negative charge on the LMS surface cause the selective adsorption of Zn^{2+} ions into the interparticle nanogaps of LMS platelets. Therefore, the constructed microchannels not only can improve the Zn^{2+} transportation and remodel the Zn^{2+} solvation structure by substituting partial water molecules, but also uniformize ion nucleation and Zn deposition. We also used the molecular dynamics (MD) simulations to analyze the Zn ion solvation structure and transport within the PLCZ electrolyte. As plotted in Fig. R3, the radial distribution function (RDF) of the CZ liquid electrolyte shows a major peak of Zn^{2+}-O (H_2O) at 2.75 Å with the coordination number (CN) of 6.06, representing the typical Zn^{2+} solvation sheath structure ($[Zn(H_2O)_6]^{2+}$) in the liquid solution (Nat Commun 2023, 14 (1), 3526). However, for the PCZ and PLCZ electrolytes, the CNs reduce to 4.30 and 3.75, respectively, duo to the electrostatic interactions of -COO^- group and LMS with Zn^{2+} ions, which efficiently replace the coordinated water molecules around Zn^{2+} ions and remodel the solvation structures ($[Zn(H_2O)_4(COO)]^+$ in PCZ and $[Zn(H_2O)_3(COO)LMS]^+$ in PLCZ). Moreover, the PLCZ polymer electrolyte realizes rapid Zn^{2+} ion diffusion and intercalation with a high self-diffusion coefficient (Ds) of 7.55×10^{-11} m^2 s^{-1} (Fig. R4). This enhanced ion mobility is facilitated by the -COO^- groups within the PAAS chain and LMS platelets, which form highly selective transport microchannels functioning as "ion transfer pumps".

We also have analyzed the deposition mechanisms of Zn^{2+} ions in the CZ liquid and PLCZ electrolytes, shown in Fig. R5. Zn^{2+} ions in CZ aqueous electrolyte tend to laterally diffuse along the rough surface and deposit at energetically favorable sites, finally generating the fatal dendrites. Meanwhile, water-induced side reactions aggravate H_2O decomposition and increase local pH value near the Zn electrode. This unfavorable environment promotes the precipitation of $[Zn(H_2O)_6]SO_4$ complex and the generation of ZSH by-product. On the contrary, the PLCZ electrolyte leverages the charged -COO^- groups of polymer chains and LMS platelets to establish high-speed pathways for Zn^{2+} ion transportation through electrostatic interactions. This interaction spontaneously influences solvation structure and expedites desolvation behavior. During subsequent deposition, Si and Mg atoms concurrently deposit with Zn ion to form a robust medium-entropy alloy (MEA) SEI with a strong affinity for Zn. Such unique SEI extends spatial movement of Zn and guides the favorable deposition of Zn(002) planes, ultimately yielding an ultra-stable Zn electrode.

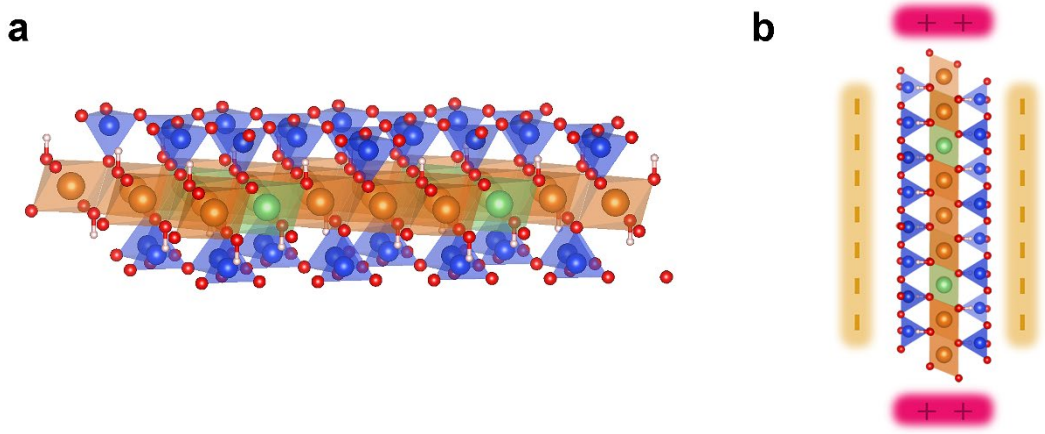

Fig. R12 *(a) The structure of LMS platelet, in which the red, blue, pink, yellow and green balls represent O, Si, H, Mg, and Li atoms. (b) The charge distribution in LMS.*

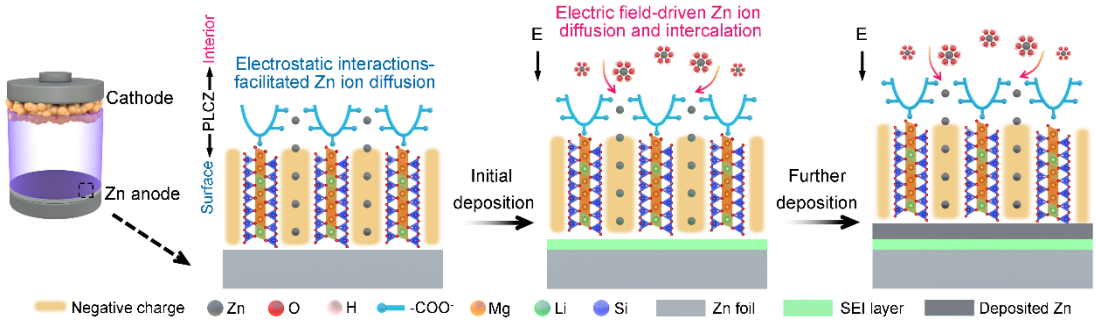

Fig. R13 *Schematically illustrating the Zn^{2+} ion diffusion and transport cross the PLCZ polymer electrolyte.*

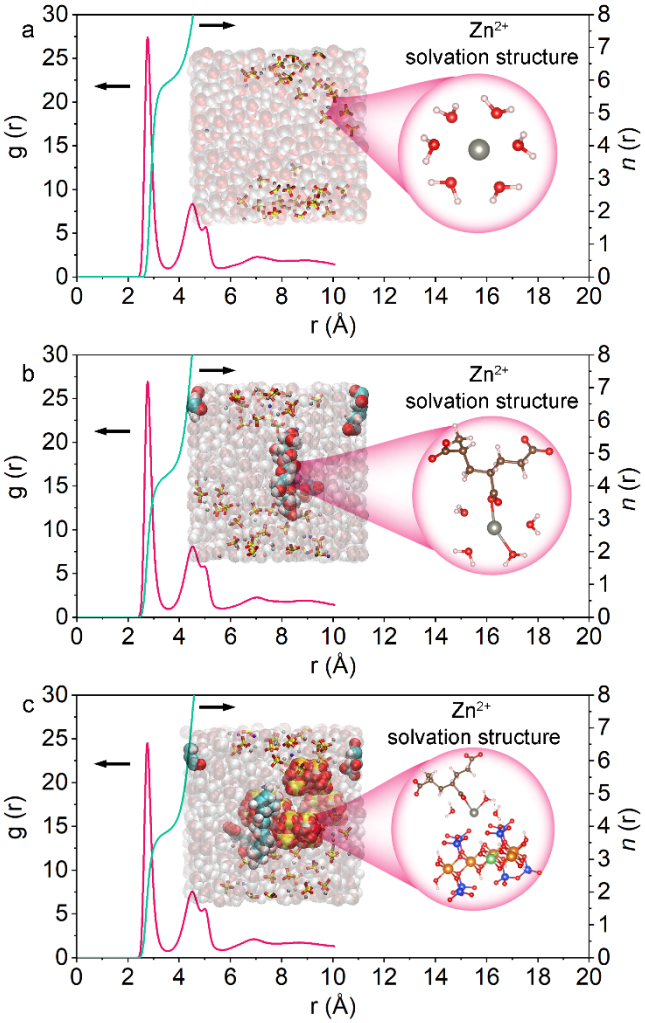

Fig. R3 *The simulated RDF of Zn^{2+}-O (H_2O) and the coordination numbers of Zn^{2+} with water molecules with the corresponding Zn^{2+} solvation structure in the (a) CZ, (b) PCZ and (c) PLCZ electrolytes.*

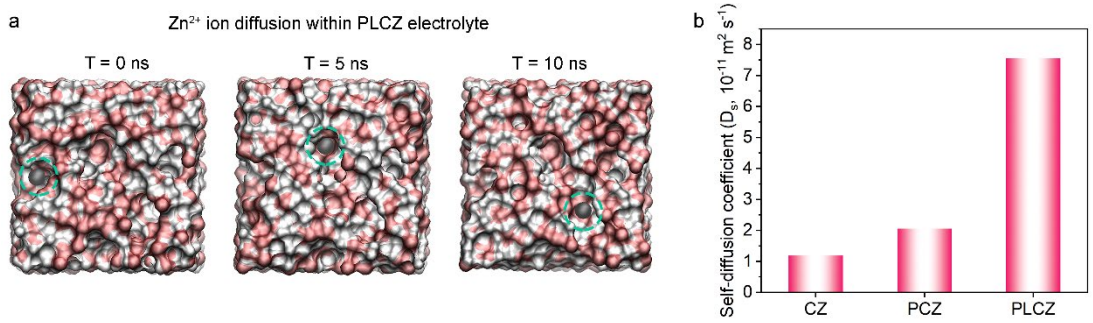

Fig. R4 *(a) The Zn^{2+} diffusion within the PLCZ electrolyte from the 3D snapshots of T =0 ns to 10 ns. (b) The Ds of Zn^{2+} in the CZ, PCZ and PLCZ electrolytes.*

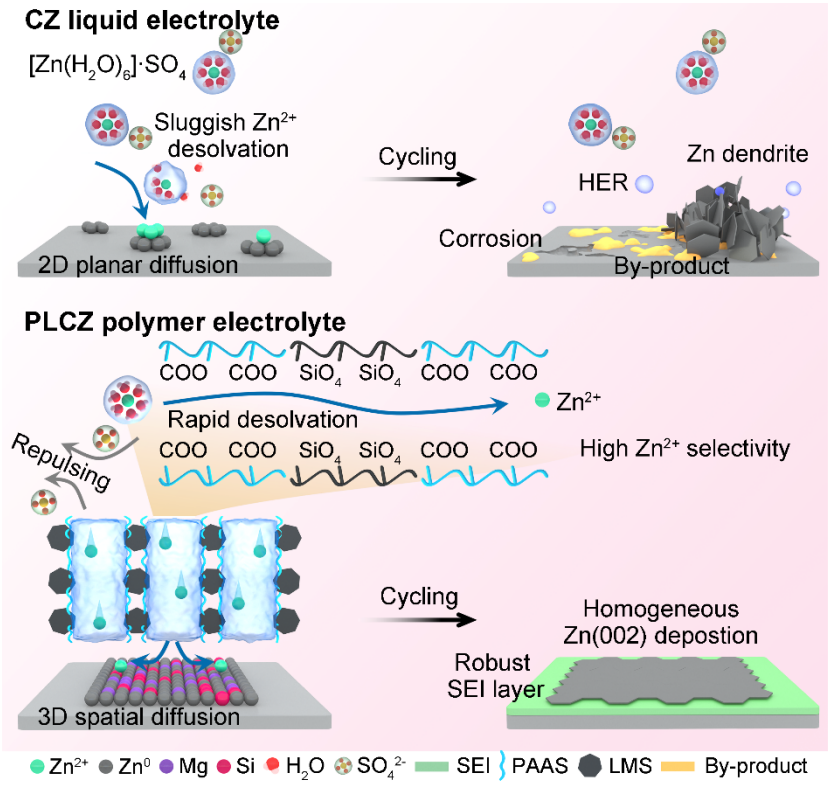

Fig. R5 *Schematically illustrating the Zn deposition in CZ liquid and PLCZ electrolytes.*

Changes in the manuscript (the highlighted part):

The LMS platelets, consisting of silicate tetrahedrons and intermediate octahedrons of Li and Mg ions coordinated with oxygen atoms and hydroxyl groups, create an anisotropic charge distribution where the silicate tetrahedron layers induce a negative charge and Mg-O octahedrons in the platelet edge have positive charge (Supplementary Fig. S1)[14, 15]. Therefore, the Mg-O octahedrons allow for easy bonding with the carboxylate (-COO^-) groups in polymer chain via electrostatic interaction, orchestrating the assembly of microchannels constituted by -COO^- groups and silicate tetrahedrons (Fig. 1a). Then, by selectively gathering Zn^{2+} ions in the created microchannels through LMS and PAAS, ion migration in and out of the PLCZ electrolyte can be rapidly forced by concentration gradients and electric fields. The constructed ion migration channels effectively modulate Zn^{2+} solvation structure and repel SO_4^{2-} anions, thus relieving by-product generation.

Afterwards, the resulting PAAS-LMS-CNF membrane (Supplementary Fig. S3) was immersed in $ZnSO_4$ solution to ensure sufficient ion exchange. The negative charge of -COO^- can facilitate the permeation of Zn^{2+} ion by metal coordination bonds and concentration gradients, which thus speeds up Zn^{2+} diffusion in the PLCZ electrolyte and more importantly, restructure the solvation structure of hydrated Zn^{2+} by substituting partial water molecules (Fig. 1a and Supplementary Fig. S2d)[17]. On the other hand, the outer negative charges on the LMS platelet surface result in the selective

adsorption of Zn^{2+} ion into the interparticle nanogaps of LMS platelets[18, 19]. Such unique selective aggregation of Zn^{2+} ion confers upon LMS platelets and PAAS chains the ability to work as "ion transfer pumps", which in turn renders a fast ion transportation, even ion nucleation and homogeneous Zn deposition during Zn plating/stripping process[20, 21]. Molecular dynamics (MD) simulations were conducted to validate the above inferences (Fig. 1b and Supplementary Fig. S4). The radial distribution function (RDF) of the CZ liquid electrolyte reveals a prominent peak of Zn^{2+}-O (H_2O) at 2.75 Å, with the coordination number (CN) of 6.06, indicative of the typical Zn^{2+} solvation sheath structure ($[Zn(H_2O)_6]^{2+}$) in the liquid solution[22]. However, the PCZ and PLCZ electrolytes exhibit reduced CN values of 4.30 and 3.75, respectively. This decrease is attributed to the electrostatic interactions of -COO^- group and LMS with Zn^{2+} ions, which efficiently displace the coordinated water molecules around Zn^{2+} ions and alter the solvation structures to $[Zn(H_2O)_4(COO)]^+$ in PCZ and $[Zn(H_2O)_3(COO)LMS]^+$ in PLCZ. Additionally, the PLCZ polymer electrolyte realizes rapid Zn^{2+} ion diffusion and intercalation with high self-diffusion coefficient (Ds) of 7.55×10^{-11} m^2 s^{-1} (Fig. 1c and Supplementary Fig. S5), due to the formed highly selective transportation microchannels by -COO^- within PAAS chain and LMS platelets. Fig. 1d shows the digital photographs of the PLCZ electrolyte, which exhibits a complete structure and no visible damages even after kneading, highlighting its excellent flexibility and restorability.

In Supplementary Fig. S46, compared to the CZ and PCZ, the PLCZ obtains smaller and more stable R_{SEI} and R_{CT} values, resulting from the highly conductive MEA SEI and the suppressive by-product. The Zn deposition mechanisms in the CZ liquid and PLCZ electrolytes were schematically illustrated in Fig. 5e. Zn^{2+} ions in CZ aqueous electrolyte tend to laterally diffuse along the rough surface and deposit at energetically favorable sites, finally generating the fatal dendrites. Meanwhile, water-induced side reactions aggravate H_2O decomposition and increase local pH value near the Zn electrode. This unfavorable environment promotes the precipitation of $[Zn(H_2O)_6]SO_4$ complex and the generation of ZSH by-product. On the contrary, the PLCZ electrolyte leverages the charged -COO^- groups of polymer chains and LMS platelets to establish high-speed pathways for Zn^{2+} ion transportation through electrostatic interactions. This interaction spontaneously influences solvation structure and expedites desolvation behavior. During subsequent deposition, Si and Mg atoms concurrently deposit with Zn ion to form a robust MEA SEI with a strong affinity for Zn. Such unique SEI extends spatial movement of Zn and guides the favorable deposition of Zn(002) planes, ultimately yielding an ultra-stable Zn electrode.

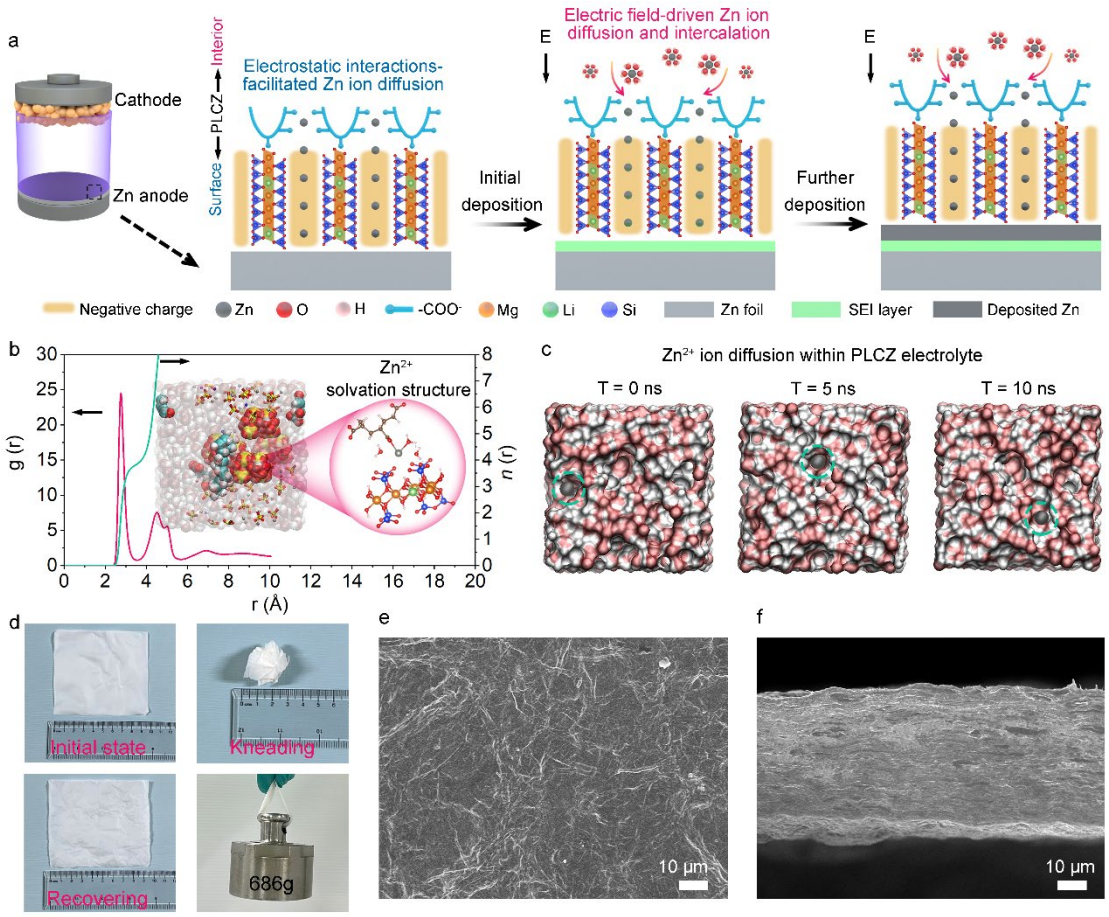

Fig. 1 *(a) Schematically illustrating the Zn^{2+} ion diffusion and transport cross the PLCZ polymer electrolyte. (b) The simulated RDF of Zn^{2+}-O (H_2O) and the coordination numbers of Zn^{2+} with water molecules with the corresponding Zn^{2+} solvation structure in the PLCZ electrolytes. (c) The Zn^{2+} diffusion within the PLCZ electrolyte from the 3D snapshots of T =0 ns to 10 ns. (d) The digital photographs of the designed PLCZ electrolyte under initial state, kneading and recovering and the corresponding strain-stress test. SEM images of the PLCZ electrolyte on (e) the top view and (f) cross-sectional view.*

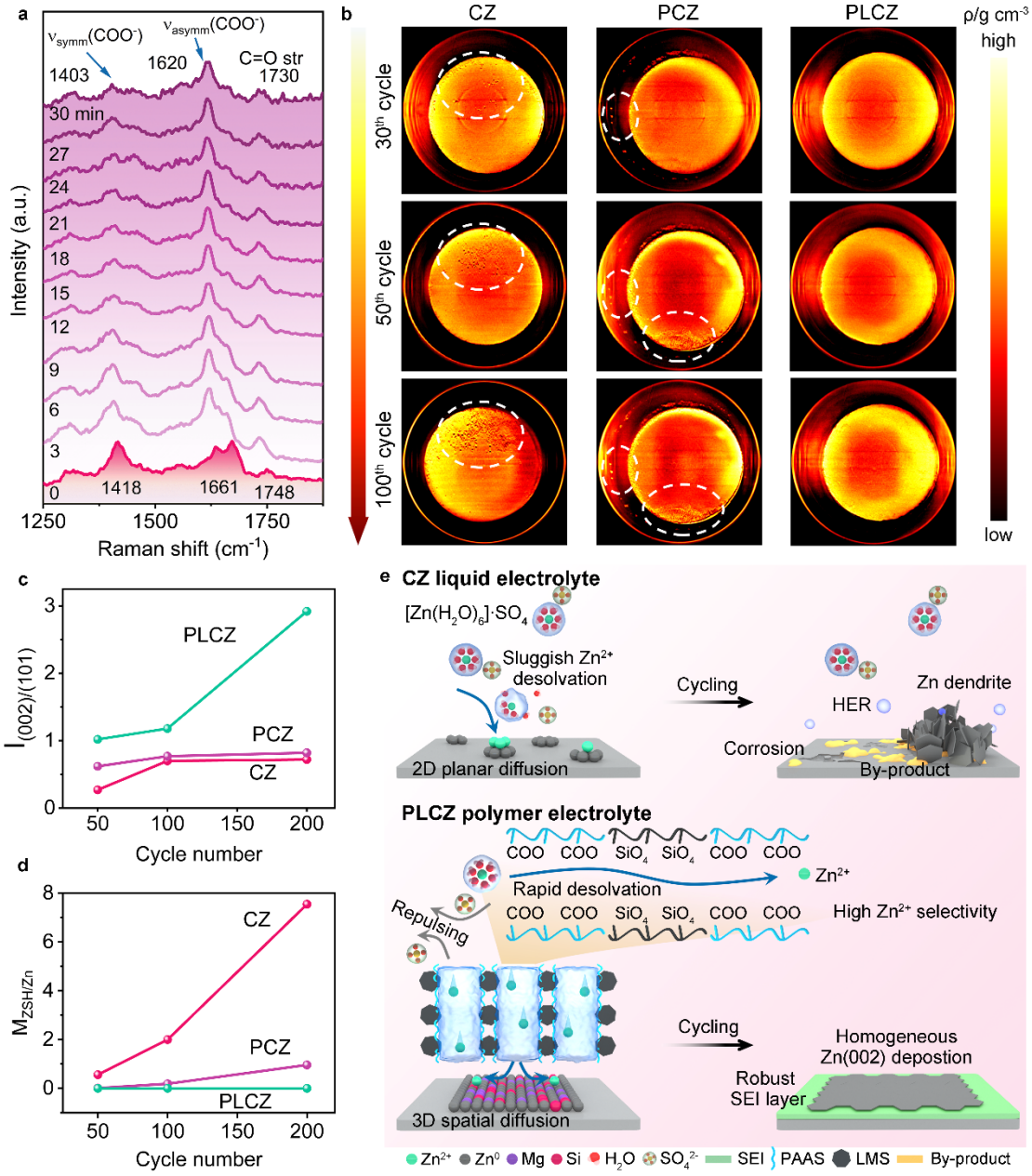

Fig. 5 *(a) The in-situ Raman spectra of Zn||Ag cell during deposition. (b) The micro-CT images of Zn||Zn cells at different cycles CZ, PCZ and PLCZ electrolytes. Color representation: orange/yellow circle for cathode case, orange/yellow circle wafer for Zn electrode, orange/yellow dot for Zn dendrite, black/wine red dot for corrosion pit. The calculated (c) $I_{(002)/(101)}$ and (d) $M_{ZSH/Zn}$ on Zn anodes based on XRD patterns. (e) Schematically illustrating the Zn deposition in CZ liquid and PLCZ electrolytes.*

3) In general, the number of subpanels in the Figures makes them difficult to understand. Since a maximum of 10 figures is allowed by the journal, it is suggested to split them up for better clarity (both topic focus and size).

Author reply: Thank you very much for your comments. In response to your suggestion, we have re-evaluated the structure of Figs. 4 and 5 that have more than 10 figures and

made the following modifications:

Changes in the manuscript (the highlighted part):

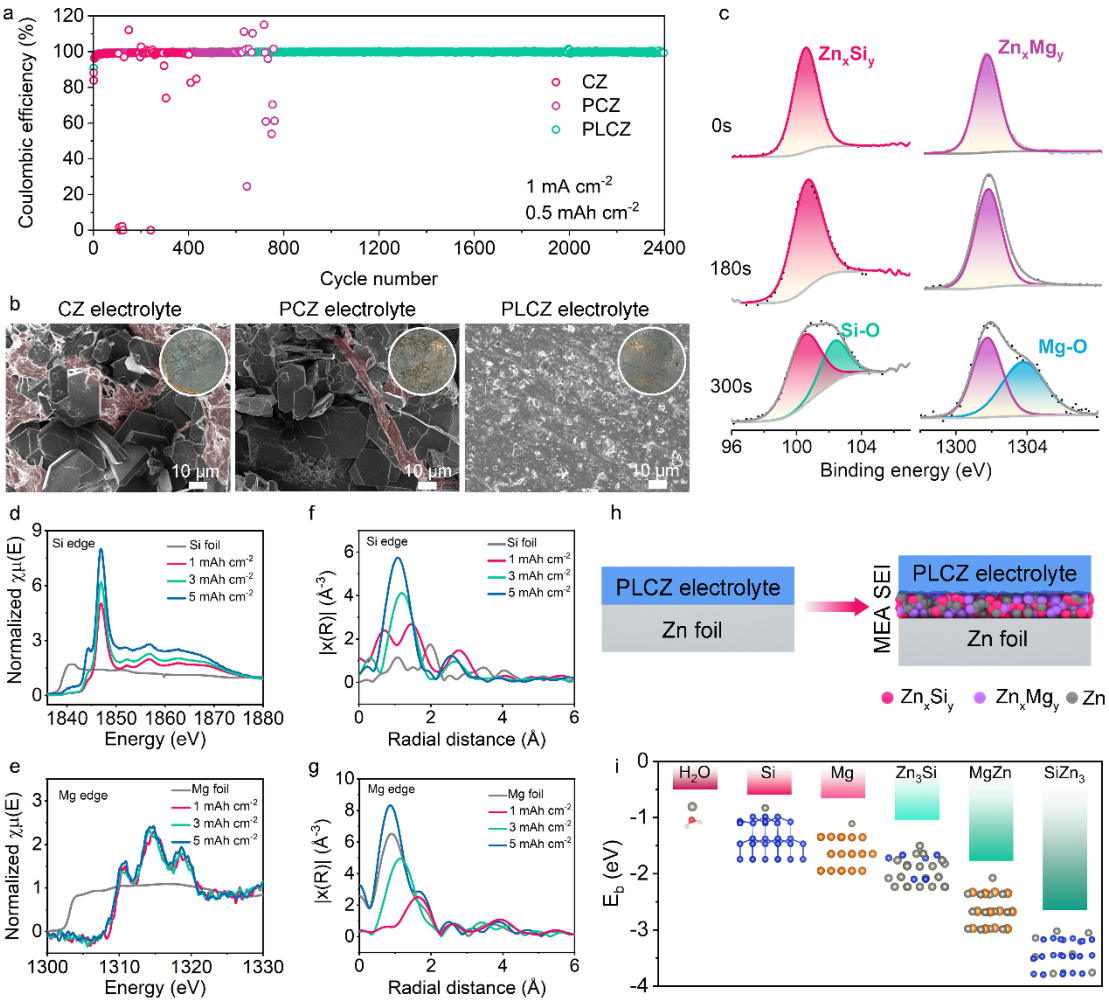

Fig. 4 *(a) Cycling performance of Zn||Cu asymmetric cells as well the corresponding (b) SEM images of Cu cathode of the CZ, PCZ and PLCZ (insets: digital photographs of Cu electrodes). The red color in the SEM images represent the CNF fiber. (c) Si 2p and Mg 1s XPS spectra of the cycled Zn anodes of PLCZ electrolyte. XANES spectra and the corresponding r-space date of (d, f) Si K-edge and (e, g) Mg K-edge of Zn anodes after deposited different Zn capacities with PLCZ electrolyte. (h) Schematically illustrating the formation of MEA SEI layer on Zn anode. (i) The calculated E_b of Zn on the alloy ingredients.*

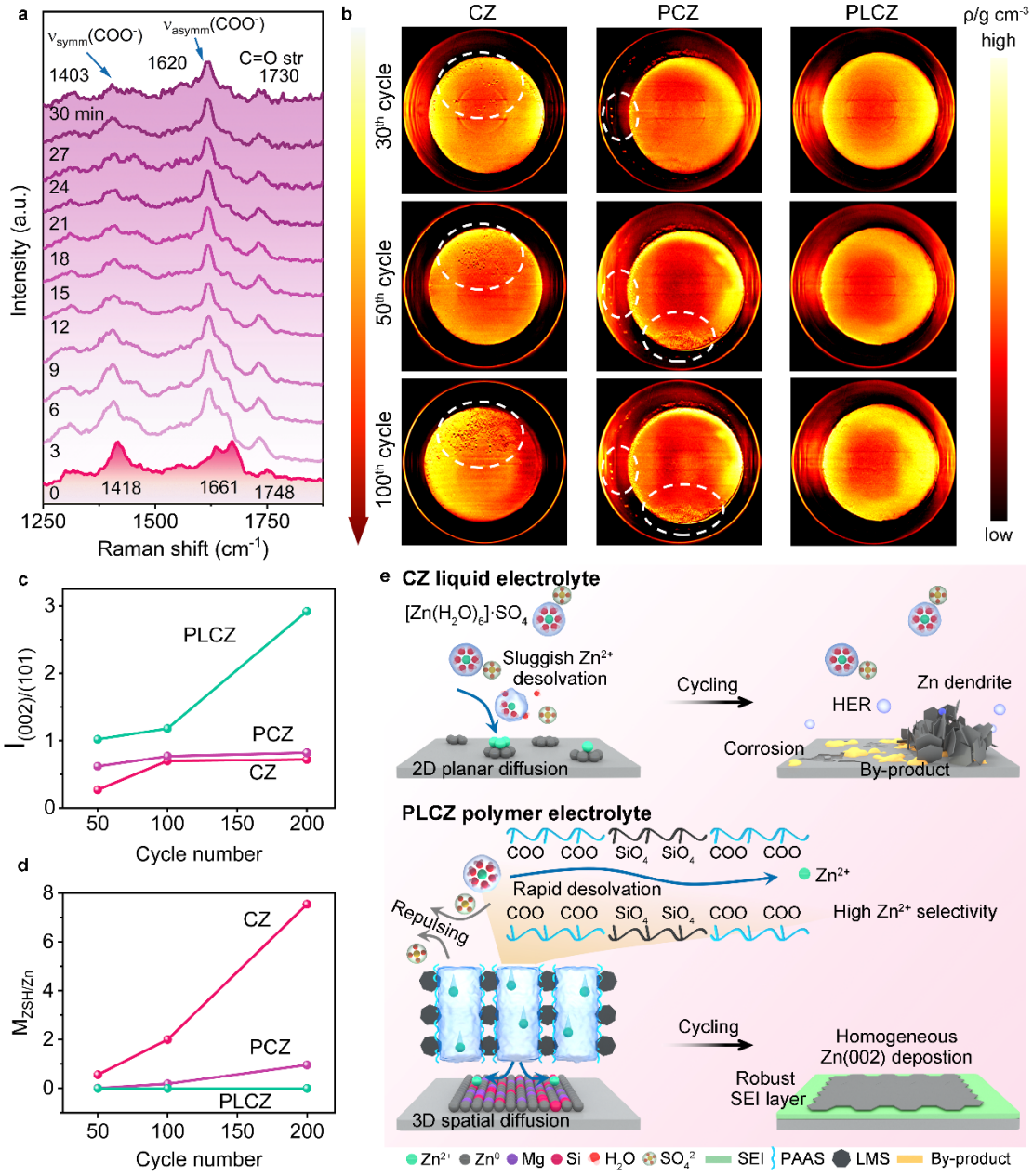

Fig. 5 *(a) The in-situ Raman spectra of Zn||Ag cell during deposition. (b) The micro-CT images of Zn||Zn cells at different cycles CZ, PCZ and PLCZ electrolytes. Color representation: orange/yellow circle for cathode case, orange/yellow circle wafer for Zn electrode, orange/yellow dot for Zn dendrite, black/wine red dot for corrosion pit. The calculated (c) $I_{(002)/(101)}$ and (d) $M_{ZSH/Zn}$ on Zn anodes based on XRD patterns. (e) Schematically illustrating the Zn deposition in CZ liquid and PLCZ electrolytes.*

4) QSPE and PLCZ are both used as acronyms for quasi solid-state polymers. This can confuse the reader, they should be accurately explained as the general and specific example studied in this manuscript.

Author reply: Thank you very much for your comments. We appreciate your comment regarding the potential confusion between the acronyms QSPE and PLCZ. To enhance

clarity, we have amended the manuscript to accurately explain that QSPE is the acronym of quasi solid-state polymer electrolytes, while PLCZ is a specific example prepared and studied in our work. The revised sections of the manuscript are detailed below.

Changes in the manuscript (the highlighted part):

Here, we designed a versatile quasi-solid-state polymer electrolyte with highly-selective ion transport channels via molecular crosslinking of sodium polyacrylate, lithium magnesium silicate and cellulose nanofiber.

Quasi-solid-state polymer electrolytes (QSPEs) as a promising kind of "beyond aqueous" electrolytes that reconcile mechanical properties of solid electrolytes and ionic diffusion behaviors of liquid electrolytes are triggered to break through the aforesaid obstacles in AZIBs.

Here, to cope with these above-mentioned challenges, we designed a versatile QSPE with rapid Zn-ion diffusion, high selectivity and strong mechanical properties through the cross-linking of sodium polyacrylate (PAAS), lithium magnesium silicate (LMS) and cellulose nanofiber (CNF). PAAS and LMS were first dissolved in CNF solution to establish physical entanglement and after dried, followed by complete Zn^{2+} ion exchange in $ZnSO_4$ solution. The prepared polymer electrolyte is designated as PLCZ. For comparative purposes, we also prepared a polymer electrolyte without the LMS additive (PCZ) and an aqueous $ZnSO_4$ electrolyte equipped with a CNF separator (CZ).

5) In the Section "Electrochemical performance of symmetric cells" can the observations at line 248-251 regarding the discharge be related to the dendrite growth reported at line 262? The authors should comment on whether they believe there is a link.

Author reply: Thank you very much for your comments.

The text of line 248-251: *The performance of the PLCZ cell remains remarkable even when subjected to a large depth of discharge (DOD) of Zn anode (85.6 %), by a sustained lifespan of 600 h, whereas cells utilizing CZ and PCZ cease operation after just a few cycles (Fig. 3b). This underscores the commendable Zn utilization rate and energy density facilitated by the PLCZ.*

The text of line 262: *The cross-sectional view reveals intimate adhesion between the PLCZ polymer electrolyte and Zn electrode, while significant cavity and ravine are clear between the PCZ and electrode due to pronounced Zn dendrite growth.*

Yes, the observation at line 248-251 regarding the discharge is related to the dendrite growth reported at line 262. The discrepancy in cycling performance between three kinds of electrolytes in our work can be ascribed to the different dendrite growth behaviors. Commonly, high DOD can exacerbate Zn dendrite formation and growth duo the increased Zn accumulation at high current density and areal capacity (Adv.

Mater. 2021, 33, 2101649; Energy Storage Materials 2022, 50, 580). This will result in the fast growth of Zn dendrites, which can impale the electrolyte and induce interior short circuits, ultimately impair battery lifetime. Our experiments and analyses reveal that the PLCZ electrolyte exhibits intimate adhesion to Zn electrode, which plays a critical role in relieving dendrite growth. The stable and robust electrode-electrolyte interfacial adhesion helps to uniformize the Zn^{2+} ion flux near Zn anode and Zn deposition (Nanomicro Lett 2023, 15, 171; Angew Chem Int Ed Engl 2023, e202302701), thus reducing the possibility of Zn dendrite initiation and propagation. Additionally, significant cavities and ravines observed in the PCZ cell indicate the severe dendrite formation and growth, which align with their rapid battery failure at high DOD.

6) In the Section "Formation and properties of medium-entropy alloy layer," for the first time in the manuscript, Zn||Cu cells are described without giving context as to why now these systems are used for investigation. It can also be confusing for the reader that the outstanding stability is emphasized before the underlying data is discussed. The order needs to be corrected and the context for the cells that are used added.
Author reply: Thank you very much for your comments. The Zn||Cu asymmetric cells were used to evaluate the Zn deposition/dissolution behavior, assess the Coulombic efficiency and analyze the zinc electrode's reversibility. We have added a sentence at the beginning of the paragraph to explain the relevance and significance of using Zn||Cu cells in our investigation. We also have corrected the order of the text for the Zn||Cu cells, namely, first discussing the underlying data and then emphasizing the outstanding stability. The revised parts with highlighted mark are shown below. We apologize for your and reader's confusion.

Changes in the manuscript (the highlighted part):

The CE of Zn deposition/dissolution, a pivotal parameter evaluating reversibility, was examined in Zn||Cu asymmetric cells[12]. The high stability and reversibility of Zn deposition/dissolution by the PLCZ are evident through a steady CE of 99.7% over 2400 cycles (Fig. 4a and Supplementary Fig. S32). In contrast, the CZ and PCZ systems experience rapid cycling deterioration after only 110 and 580 cycles, respectively. The remarkable stability of the PLCZ cell is also demonstrated at harsher cycling condition (Supplementary Fig. S33). The PLCZ polymer electrolyte enhances key aspects of the electrochemical performance of Zn anode by facilitating rapid Zn^{2+} transport, promoting uniform Zn nucleation and delaying surface corrosion and side reactions. These improvements contribute to the outstanding cycling performance in Zn||Cu cells.

7) In Fig. S30, the force-displacement curves are not plotted in the same y-range, which would be beneficial for comparison. In addition, the difference in reversibility during loading and unloading experiments appears to be only marginal between PCZ and PLCZ. Is there any statistical evidence? In Fig. S31 from the images there is no evidence for a more uniform Young's modulus of PLCZ over PCZ. This is also the case

for Fig. 4 m-o where the claims of better uniformity and smoothness cannot be confirmed without further information about roughness and statistics for the images. However, no further information on AFM experiments is provided in the Experimental section. Therefore, reproducing the results is not possible from the given information, it must be made clear whether these are typical images and statistically whether there is evidence there is uniformity etc. and most importantly the conditions under which the images have been taken.

Author reply: Thank you very much for your comments.

For the Question 1: *In Fig. S30, the force-displacement curves are not plotted in the same y-range, which would be beneficial for comparison. In addition, the difference in reversibility during loading and unloading experiments appears to be only marginal between PCZ and PLCZ. Is there any statistical evidence?*

We really acknowledge the importance of plotting force-displacement curves in the same y-range allows for better comparison. We have revised Fig. S30 to ensure that all force-displacement curves are plotted within the same y-range. Maybe because the different y-range between the force-displacement curves of PCZ and PLCZ, the difference in reversibility during loading and unloading experiments looks like be marginal. Actually, the different between PCZ and PLCZ is not marginal after using same y-range (Fig. R14). Additionally, we have performed a statistical evidence to quantify the differences in reversibility between PCZ and PLCZ (Fig. R15). For each sample, we all provide six force displacement curves. The revised figure is included in the file of supplementary information. Generally, analyzing whether the loading and unloading curves coincide can help us understand the elastic, plastic and other deformation behaviors of the material (Acta Materialia 49, 3539-3551 (2001); Materials Characterization ***110****, 86-93 (2015)). There are two types: (1) Elastic deformation. If the loading and unloading curves coincide exactly, it means that the deformation experienced by the material during loading is completely elastic. This shows that the material is able to fully return to its original shape after the removal of the load, with no residual deformation. (2) Elastic-plastic deformation. Most materials in the process of loading and unloading, loading and unloading curves will not completely coincide, usually there will be a hysteresis phenomenon, which indicates that the material has undergone elastic-plastic deformation. After unloading, the material will retain a certain permanent deformation, this part of the deformation is called plastic deformation. Therefore, compared with CZ and PCZ, the force-displacement curve of PLCZ during loading and unloading process are more reversible, meaning that the formed MEA SEI layer by the PLCZ has better reversibility and elastic deformation.*

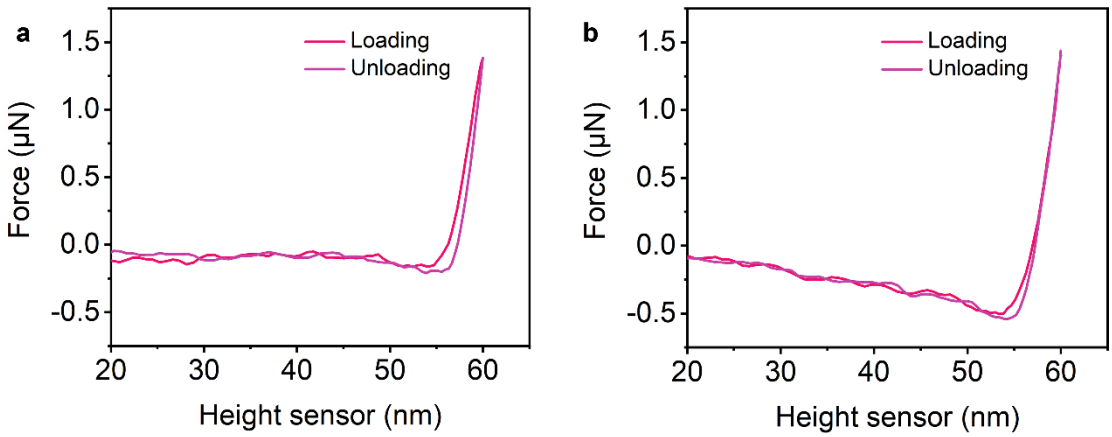

Fig. R14 *The force-displacement curves of PCZ and PLCZ after plotted in the same y-range.*

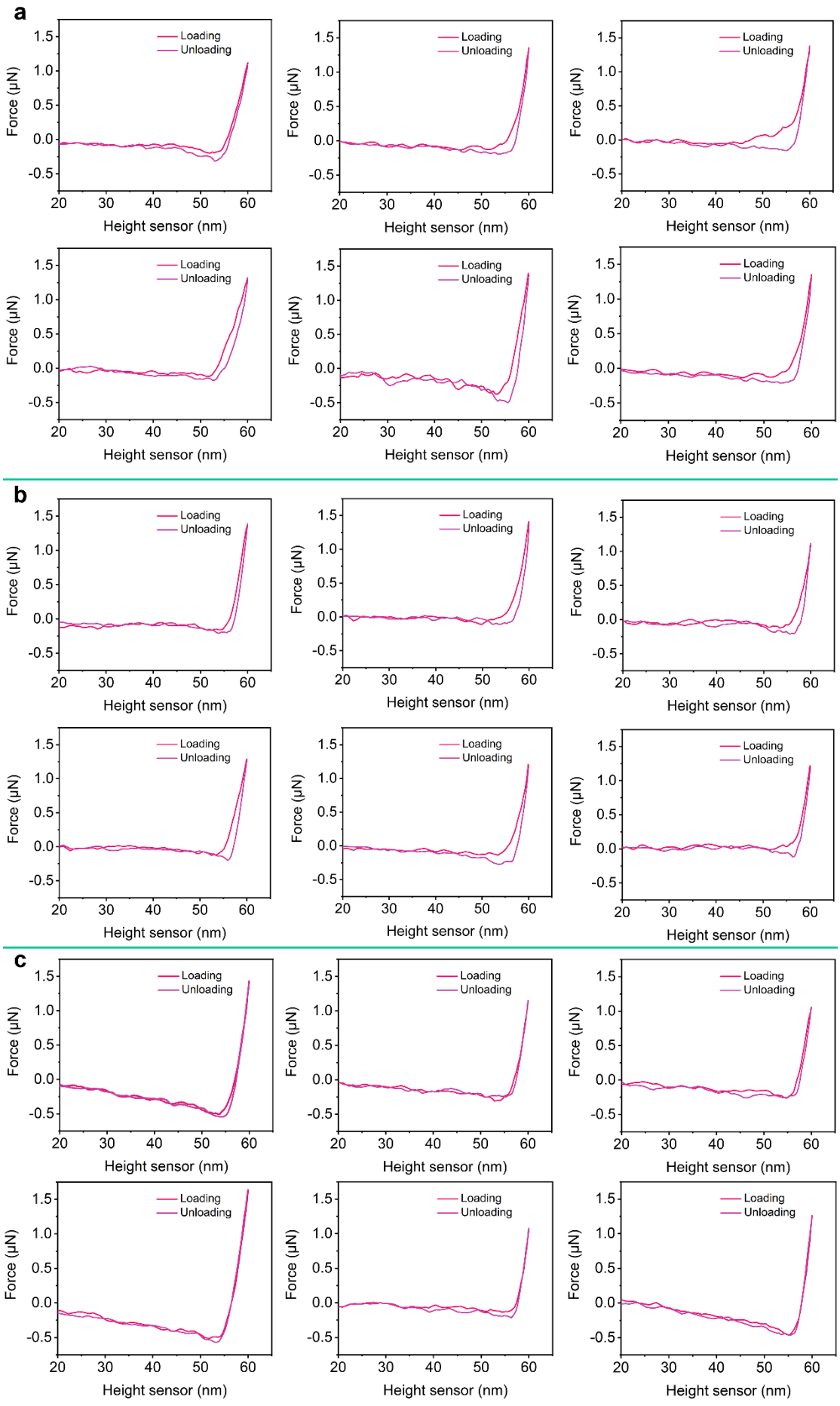
a
b
c
Loading
Unloading
Force (μN)
Height sensor (nm)
1.5
1.0
0.5
0.0
-0.5
20
30
40
50
60

Fig. R15 *The force-displacement curves for nanoindentation measurements of (a) CZ, (b) PCZ and (c) PLCZ. Each Zn anode sample was tested 6 times for nanoindentation measurements.*

For the Question 2: *In Fig. S31 from the images there is no evidence for a more uniform Young's modulus of PLCZ over PCZ.*

Actually, we measured 64 values of Young's modulus for each sample, according to the wireframe (Fig. R16), to calculate the average Young's modulus. In the plotted wireframe, the intersection of horizontal and vertical lines represents a Young's modulus measurement point (total 64 points). The measured Youngs' moduli of CZ, PCZ and PLCZ are listed in Tables R1-3 and shown in Fig. R17. Therefore, from the statistical analysis, the PLCZ has more uniform Young's modulus than CZ and PCZ. The revised figure of Youngs' moduli is attached in the file of supplementary information.

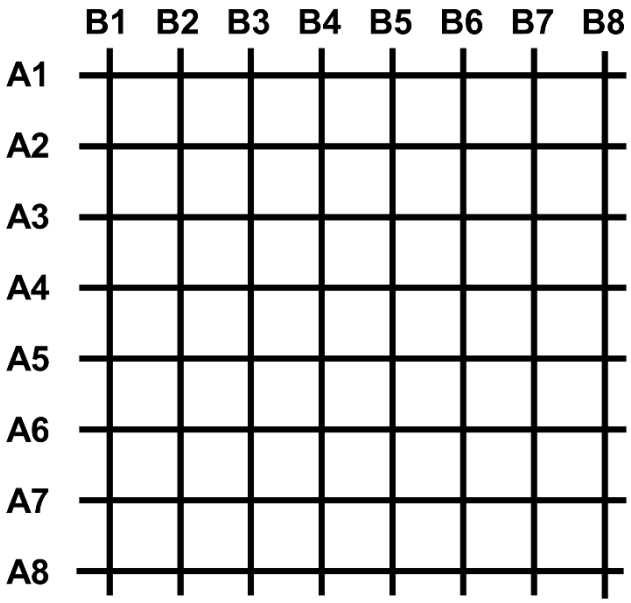

Fig. R16 *The wireframe figure for the measurement point of Young's modulus.*

Table R1 *Young's modulus of CZ (unit: GPa).*

A1B1	A1B2	A1B3	A1B4	A1B5	A1B6	A1B7	A1B8	A2B1	A2B2	A2B3
0.77	3.53	5.34	2.99	3.80	2.53	4.47	2.237	3.70	1.63	2.18
A2B4	A2B5	A2B6	A2B7	A2B8	A3B1	A3B2	A3B3	A3B4	A3B5	A3B6
6.39	5.66	0.81	1.27	1.14	0.36	5.83	1.10	1.41	0.22	0.91
A3B7	A3B8	A4B1	A4B2	A4B3	A4B4	A4B5	A4B6	A4B7	A4B8	A5B1
1.00	2.62	1.63	8.27	0.60	2.17	0.32	0.76	0.42	0.85	0.91
A5B2	A5B3	A5B4	A5B5	A5B6	A5B7	A5B8	A6B1	A6B2	A6B3	A6B4
0.48	0.97	1.16	9.16	1.01	0.17	0.42	0.63	0.31	0.64	0.22
A6B5	A6B6	A6B7	A6B8	A7B1	A7B2	A7B3	A7B4	A7B5	A7B6	A7B7
0.5	0.19	0.95	3.51	4.89	4.57	0.25	1.58	1.61	3.12	0.36
A7B8	A8B1	A8B2	A8B3	A8B4	A8B5	A8B6	A8B7	A8B8		

1.56	6.63	0.49	1.38	1.49	1.58	1.35	1.67	0.64		

Table R2 *Young's modulus of PCZ (unit: GPa).*

A1B1	A1B2	A1B3	A1B4	A1B5	A1B6	A1B7	A1B8	A2B1	A2B2	A2B3
6.97	0.55	0.39	4.51	7.59	1.31	0.99	8.12	4.69	2.66	6.01
A2B4	A2B5	A2B6	A2B7	A2B8	A3B1	A3B2	A3B3	A3B4	A3B5	A3B6
5.87	3.12	0.18	0.50	1.86	1.58	4.56	2.47	1.39	0.63	3.36
A3B7	A3B8	A4B1	A4B2	A4B3	A4B4	A4B5	A4B6	A4B7	A4B8	A5B1
2.07	5.70	5.80	0.85	1.59	1.10	0.86	2.48	0.13	0.58	1.26
A5B2	A5B3	A5B4	A5B5	A5B6	A5B7	A5B8	A6B1	A6B2	A6B3	A6B4
1.01	2.07	1.52	0.98	0.1	4.72	2.08	1.63	0.93	3.51	5.54
A6B5	A6B6	A6B7	A6B8	A7B1	A7B2	A7B3	A7B4	A7B5	A7B6	A7B7
4.39	2.02	3.84	2.15	4.41	6.52	4.83	8.12	4.03	3.01	5.69
A7B8	A8B1	A8B2	A8B3	A8B4	A8B5	A8B6	A8B7	A8B8		
0.80	1.97	0.32	1.64	8.22	3.76	2.86	0.31	1.05		

Table R3 *Young's modulus of PLCZ (unit: GPa).*

A1B1	A1B2	A1B3	A1B4	A1B5	A1B6	A1B7	A1B8	A2B1	A2B2
10.19	11.02	8.94	14.58	11.65	12.46	11.73	8.00	13.19	6.65
A2B3	A2B4	A2B5	A2B6	A2B7	A2B8	A3B1	A3B2	A3B3	A3B4
9.56	7.52	8.05	9.21	13.60	10.27	9.87	12.02	10.47	12.15
A3B5	A3B6	A3B7	A3B8	A4B1	A4B2	A4B3	A4B4	A4B5	A4B6
11.79	10.89	12.48	12.88	13.84	11.37	13.42	12.41	14.53	13.76
A4B7	A4B8	A5B1	A5B2	A5B3	A5B4	A5B5	A5B6	A5B7	A5B8
13.09	11.44	10.73	9.99	14.52	9.04	11.19	13.04	11.99	10.64
A6B1	A6B2	A6B3	A6B4	A6B5	A6B6	A6B7	A6B8	A7B1	A7B2
10.52	10.93	14.27	13.10	10.70	13.73	10.61	12.48	14.67	8.69
A7B3	A7B4	A7B5	A7B6	A7B7	A7B8	A8B1	A8B2	A8B3	A8B4
13.33	10.97	6.88	11.81	9.82	7.09	7.00	10.71	7.64	12.20
A8B5	A8B6	A8B7	A8B8						
6.80	10.59	8.54	11.30						

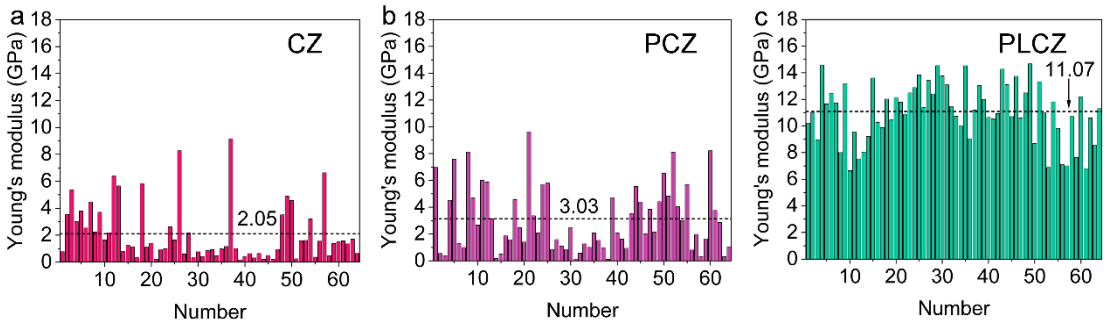

Fig. R17 *The Young's modulus of (a) CZ, (b) PCZ and (c) PLCZ.*

For the Question 3: *This is also the case for Fig. 4 m-o where the claims of better*

uniformity and smoothness cannot be confirmed without further information about roughness and statistics for the images.

We now provide two-dimension (2D) and three-dimensional (3D) AFM images of CZ, PCZ and PLCZ (Fig. R18). We also tested the roughness five times along the white line in the 2D AFM images and the roughness results are also shown in the figure. Compared with the CZ (72.7 nm) and PCZ (56.0 nm), the PLCZ exhibits a reduced average roughness (36.0 nm), indicating that the MEA SEI layer surface has a better uniformity and smoothness than $Zn(OH)_2$-based SEIs. The revised Figure is shown as below.

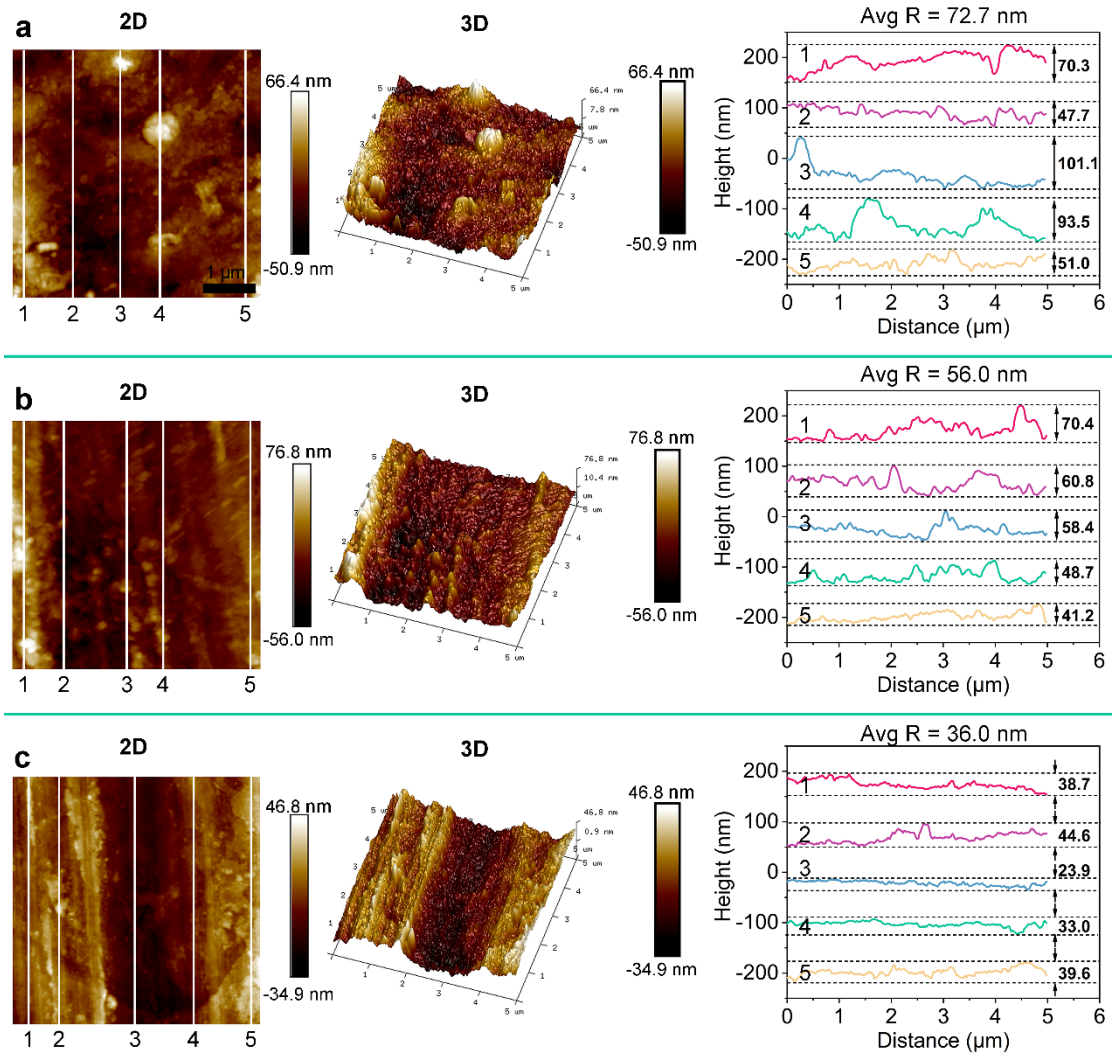

Fig. R18 *2D and 3D AFM images of Zn anodes of (a) CZ, (b) PCZ and (c) PLCZ with the corresponding roughness lines. The average roughness of the CZ, PCZ and PLCZ are 72.7, 56.0 and 36.0 nm, respectively. From AFM images and average roughness, the MEA SEI layer surface shows a better uniformity and smoothness than $Zn(OH)_2$-based SEIs.*

For the Question 4: *However, no further information on AFM experiments is provided in the Experimental section. Therefore, reproducing the results is not possible from the given information, it must be made clear whether these are typical images and*

statistically whether there is evidence there is uniformity etc. and most importantly the conditions under which the images have been taken.

We apologize for the oversight in the Experimental section. We have now added details regarding the AFM experiments and nanoindentation measurements, including the following:

All AFM measurements and nanoindentation measurements were conducted using Bruker Dimension Icon with a Hysitron TI 950 TriboIndenter with a diamond indenter tip (radius of 50 nm). The instrument was used a standard fused silica sample to calibrate for load and displacement. Indentation depths were controlled to be within 30 nm to avoid substrate effects. The loading and unloading rates were set to 0.2 mN s^{-1} to ensure consistent and repeatable measurements and the holding time for loading/unloading segments was 5 s. Before AFM experiment, the Zn foils with the diameter of 1.4 cm were cleaned by ethanol and deionized water, respectively, and then dried by nitrogen gas. The experimental details have been added to the Methods section of our manuscript.

Changes in the manuscript (the highlighted part):

All AFM measurements and Nanoindentation measurements were conducted using a Hysitron TI 950 TriboIndenter with a diamond indenter tip (radius of 50 nm). Zn foils with the diameter of 1.4 cm were cleaned by ethanol and deionized water, respectively, and dried by nitrogen gas before test. Indentation depths were controlled within 30 nm and the loading/unloading rates were set as 0.2 mN s^{-1} with a holding time of 5 s for each segment.

Changes in supplementary information:

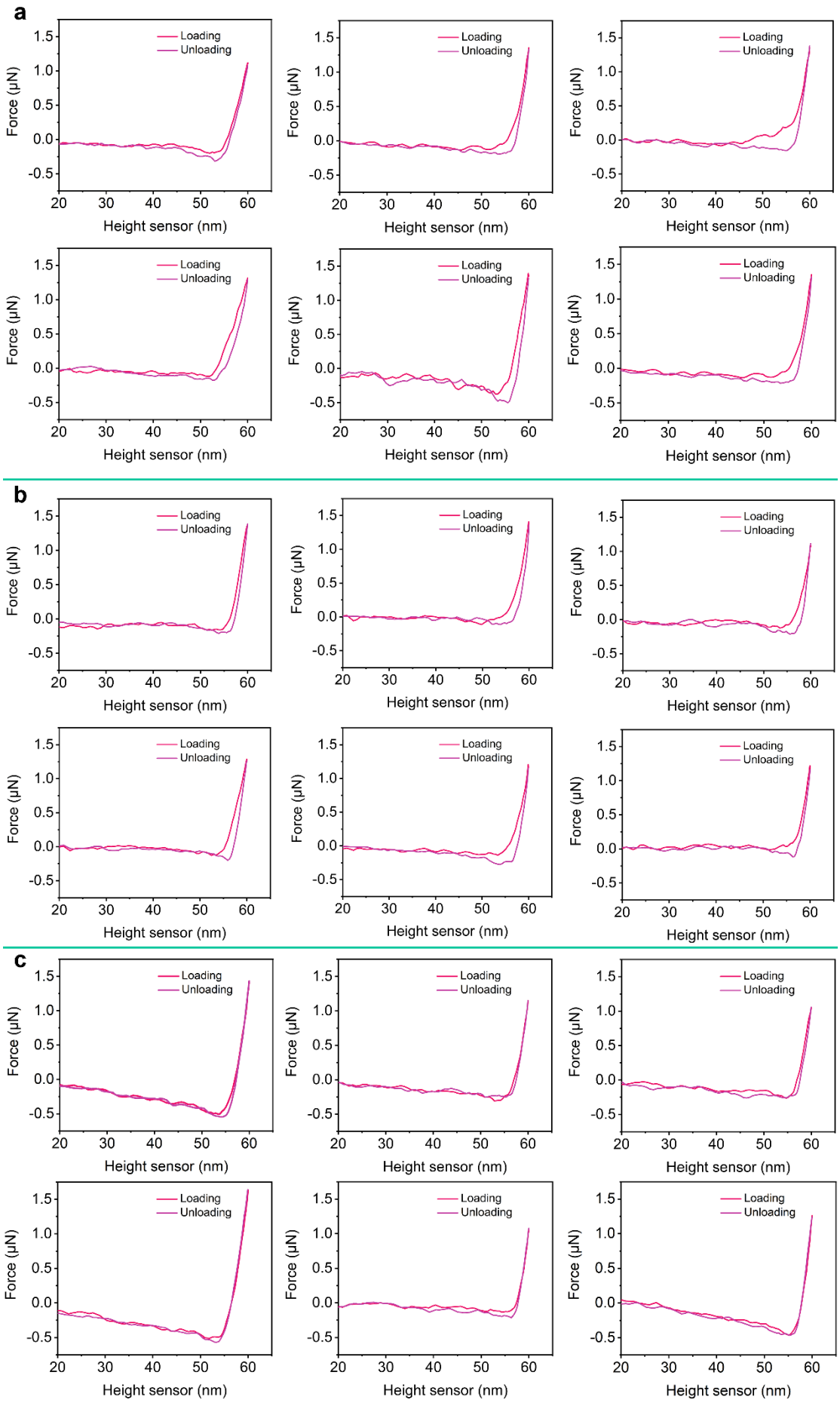
a
b
c
Loading
Unloading
Force (μN)
Height sensor (nm)
1.5
1.0
0.5
0.0
-0.5
20
30
40
50
60

Supplementary Fig. S36 *The force-displacement curves for nanoindentation experiments on the Zn anodes with (a) CZ, (b) PCZ and (c) PLCZ electrolytes. Each Zn anode sample was tested 6 times for nanoindentation measurements.*

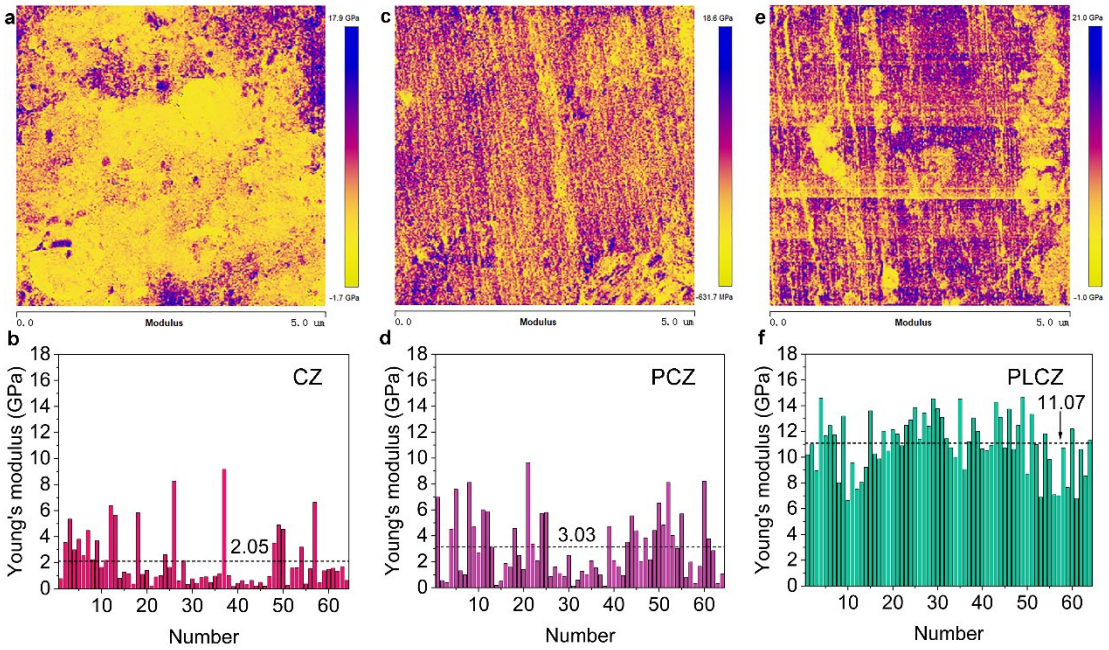

Supplementary Fig. S38 *The distributions of Young' modulus with the measured values on the Zn electrodes with (a, b) CZ, (c, d) PCZ and (e, f) PLCZ.*

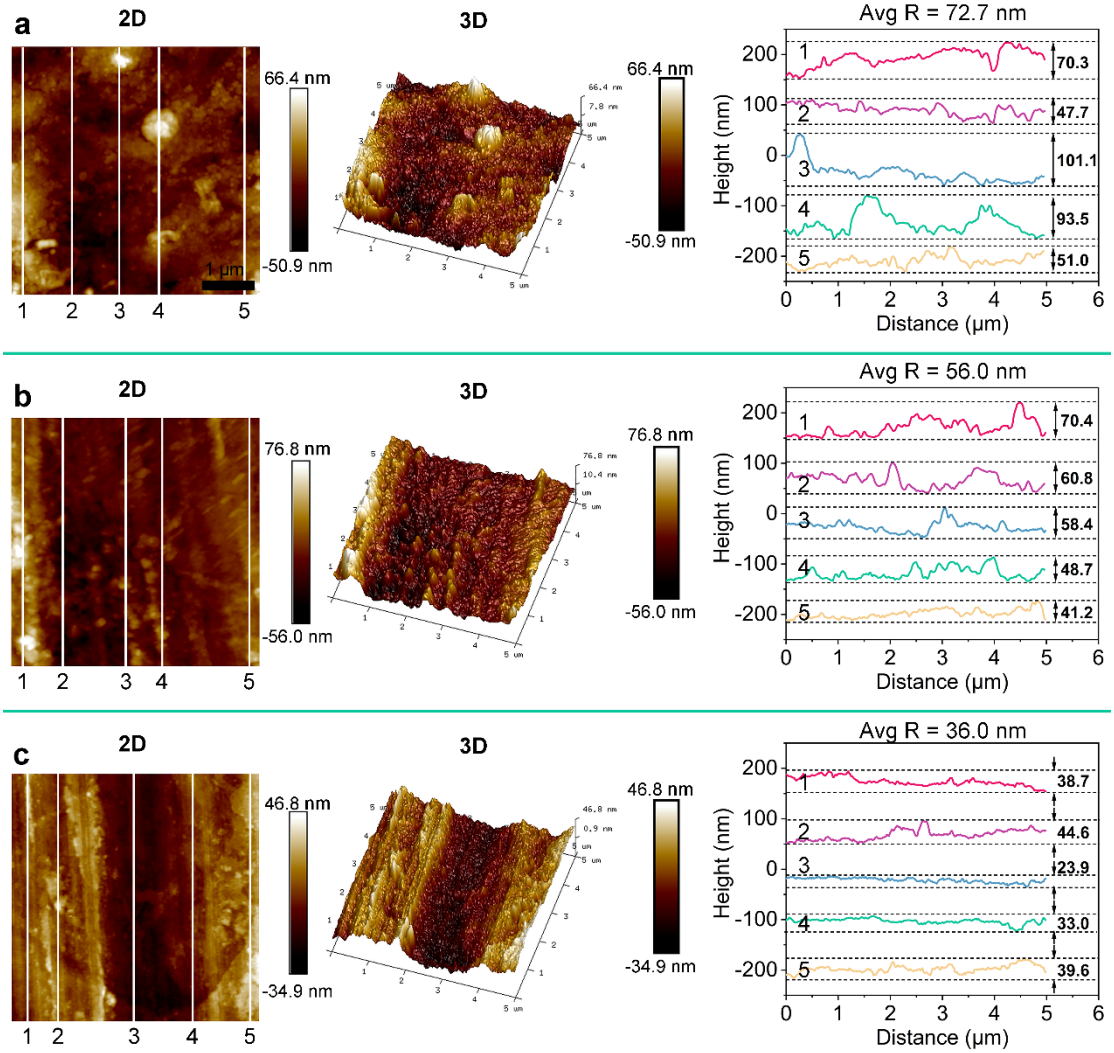

Supplementary Fig. S39 *2D and 3D AFM images of Zn anodes of (a) CZ, (b) PCZ and (c) PLCZ with the corresponding roughness lines. The average roughness of the CZ, PCZ and PLCZ are 72.7, 56.0 and 36.0 nm, respectively. From AFM images and average roughness, the MEA SEI layer surface shows a better uniformity and smoothness than $Zn(OH)_2$-based SEIs.*

8) Further, there are no experimental details provided for the nanoindentation measurements.

Author reply: Thank you very much for your comments. We are very sorry for our oversight. Nanoindentation experiments were conducted on Bruker Dimension Icon with a Hysitron TI 950 TriboIndenter with a diamond indenter tip (radius of 50 nm). The instrument was used a standard fused silica sample to calibrate for load and displacement. Indentation depths were controlled to be within 30 nm to avoid substrate effects. The loading and unloading rates were set to 0.2 mN s^{-1} to ensure consistent and repeatable measurements and the holding time for loading/unloading segments was 5 s. Before AFM experiment, the Zn foils with the diameter of 1.4 cm were cleaned by ethanol and deionized water, respectively, and then dried by nitrogen gas. The

experimental details have been added to the Methods section of our manuscript.

Changes in the manuscript (the highlighted part):

All AFM measurements and Nanoindentation measurements were conducted using a Hysitron TI 950 TriboIndenter with a diamond indenter tip (radius of 50 nm). Zn foils with the diameter of 1.4 cm were cleaned by ethanol and deionized water, respectively, and dried by nitrogen gas before test. Indentation depths were controlled within 30 nm and the loading/unloading rates were set as 0.2 mN s^{-1} with a holding time of 5 s for each segment.

9) It is stated, that the CV curve in Fig. 6a displays a higher current density compared to CZ and PCZ. However, only the current is plotted on the y-axis and no electrode area is given. Current density must be used to compare different samples.

Author reply: Thank you very much for your comments. CV curves of Zn||V_2O_5 cells were measured in CR2032-type coin cell with the electrode (anode and cathode) area of 1.54 cm^{-2}. In response to your feedback, we have recalculated the data to include the current density and updated Figure 6a accordingly., as shown in Fig. R19. We provided the electrode area in figure caption and the section of Battery assembly with highlighted mark in the revised manuscript. We also updated the CV data in the file of Source data.

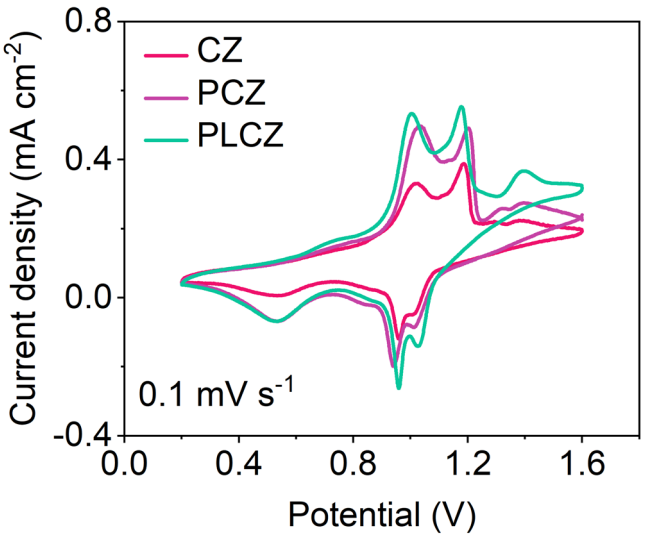

Fig. R19 *CV curves of Zn||V_2O_5 cells with CZ, PCZ and PLCZ. The electrode area is 1.54 cm^{-2}.*

Changes in the manuscript (the highlighted part):

Battery assembly

Symmetric cells (Zn||Zn), asymmetric cells (Zn||Cu) and full cells (Zn||V_2O_5) were tested in CR2032-type coin cells. The diameter of anode and cathode electrodes was 14 mm and the corresponding electrode area was 1.54 cm^{-2}. The diameter of CNF separator and polymer electrolyte was 19 mm.

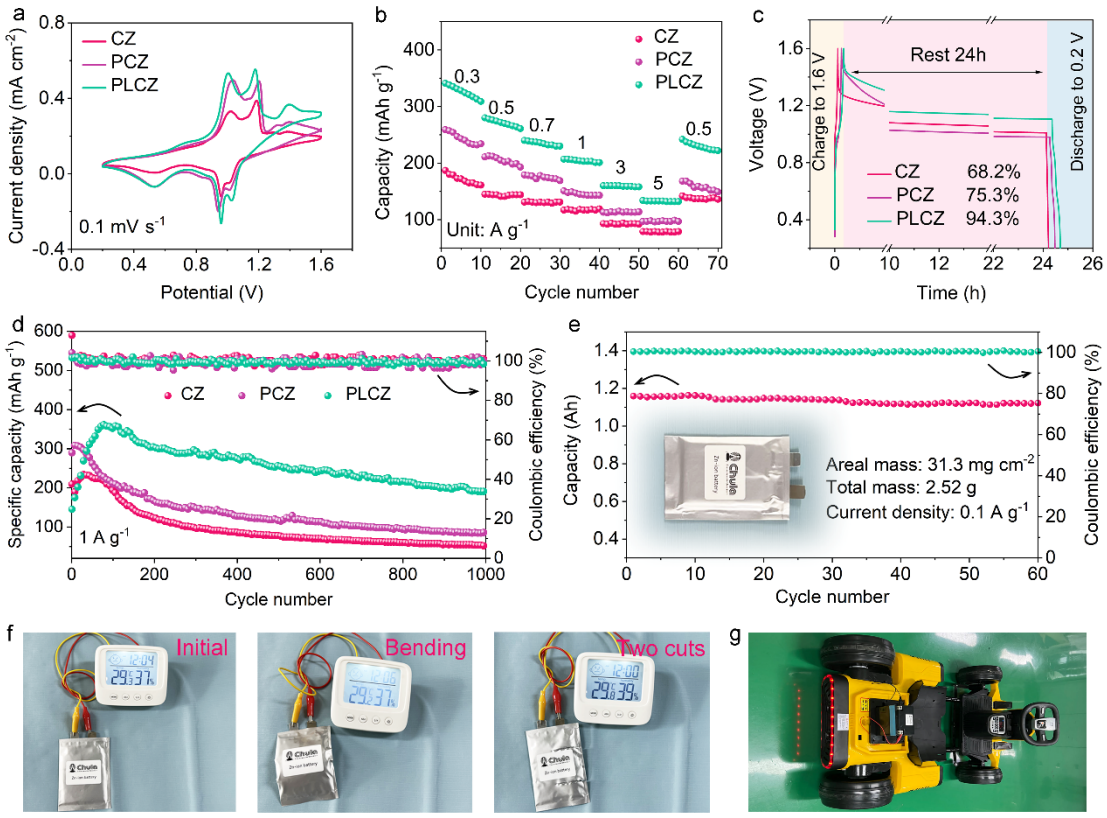

Fig. 6 *(a) CV curves Zn||V_2O_5 cells with CZ, PCZ and PLCZ. The electrode area is 1.54 cm^{-2}. (b) rate performances of Zn||V_2O_5 cells with CZ, PCZ and PLCZ. (c) Capacity retention test after charging to1.6 V, resting 24 h and discharging to 0.2 V. (d) Long-term cycling performances of full cells. (e) Cycling performance of pouch cell with PLCZ. The digital photographs of pouch cell (f) supporting electronic device under initial state, bending and cutting and (g) running a toy car.*

Minor comments:

1) Figure 1b Field is mis-spelled in the figure annotation.

Author reply: Thank you very much for your reminding and comments. We have corrected the spelling mistake. The word "Field" is now correctly spelled in the figure annotation., as shown in Fig. R13.

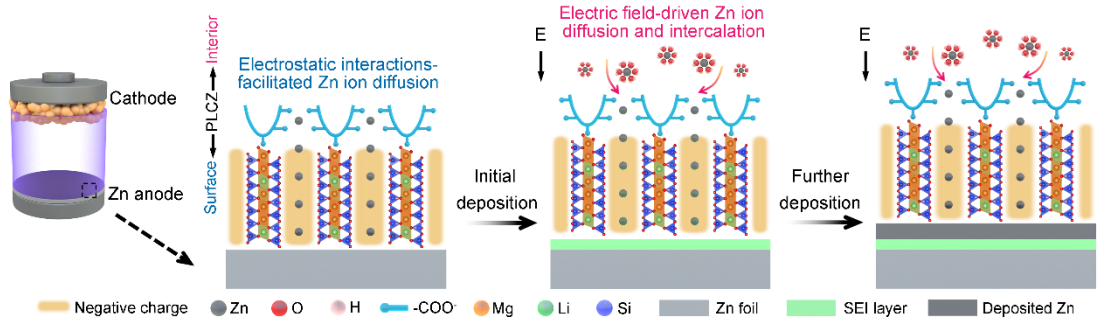

Fig. R13 *Schematically illustrating the Zn^{2+} ion diffusion and transport cross the PLCZ polymer electrolyte.*

Changes in the manuscript (the highlighted part):

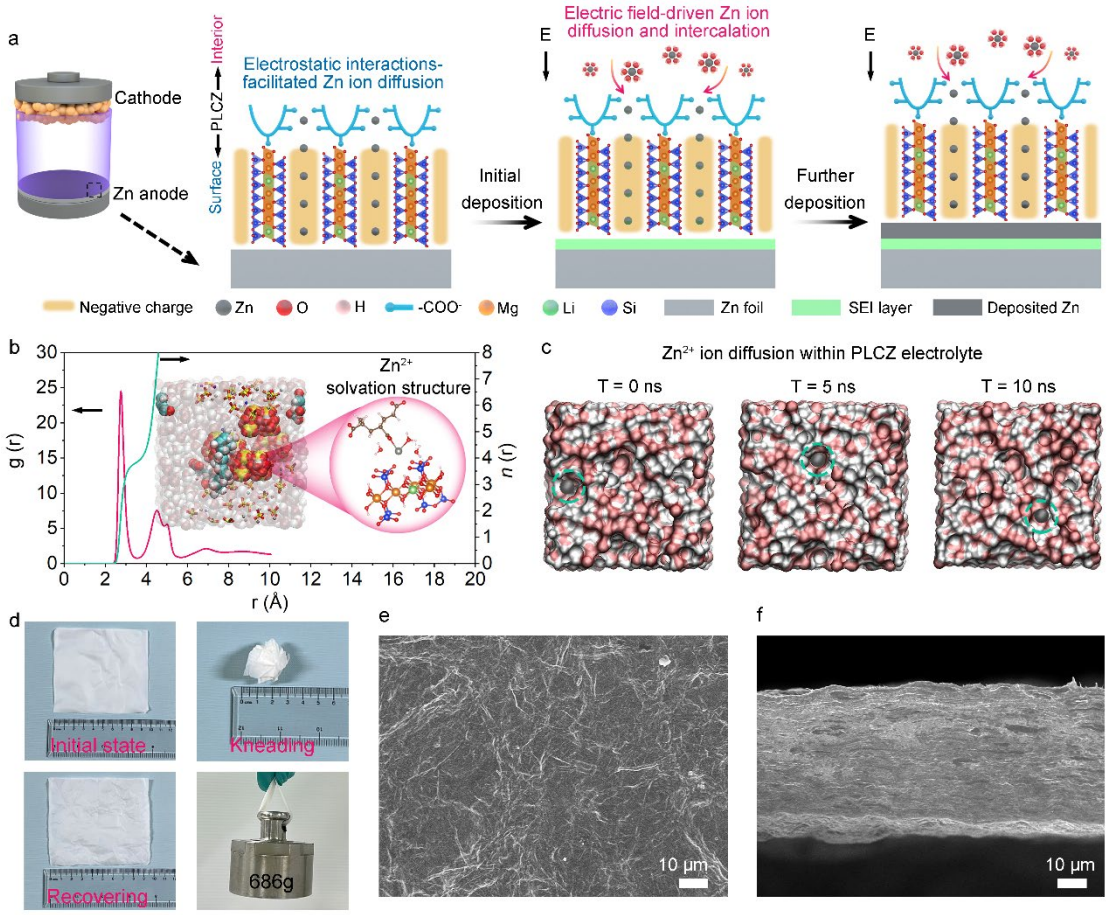

Fig. 1 *(a) Schematically illustrating the Zn^{2+} ion diffusion and transport cross the PLCZ polymer electrolyte. (b) The simulated RDF of Zn^{2+}-O (H_2O) and the coordination numbers of Zn^{2+} with water molecules with the corresponding Zn^{2+} solvation structure in the PLCZ electrolytes. (c) The Zn^{2+} diffusion within the PLCZ electrolyte from the 3D snapshots of T =0 ns to 10 ns. (d) The digital photographs of the designed PLCZ electrolyte under initial state, kneading and recovering and the corresponding strain-stress test. SEM images of the PLCZ electrolyte on (e) the top view and (f) cross-sectional view.*

2) Fig. S4 and S5 weight is not given for strain-stress tests.

Author reply: Thank you very much for your comments. We have added the weight (686 g) in the figures, as shown in Fig. R20 and Fig. R21. We also wrote the weight in the figure caption.

Fig. R20 *The digital photograph of PLCZ without $ZnSO_4$ immersion after strain-stress test. The weight for strain-stress test is 686 g.*

Fig. R21 *The digital photograph of PLCZ with $ZnSO_4$ immersion after strain-stress test. The weight for strain-stress test is 686 g.*

Changes in supplementary information:

Supplementary Fig. S6 *The digital photograph of PLCZ without $ZnSO_4$ immersion after strain-stress test. The weight for strain-stress test is 686 g.*

Supplementary Fig. S7 *The digital photograph of PLCZ with $ZnSO_4$ immersion after strain-stress test. The weight for strain-stress test is 686 g.*

3) Fig. S7 displays the nucleation overpotential, not the potential.

Author reply: Thank you very much for your comments. The caption of Fig. S7 (in the revised manuscript, this figure is Fig. S9) has been updated to correctly describe the nucleation overpotential.

Changes in supplementary information:

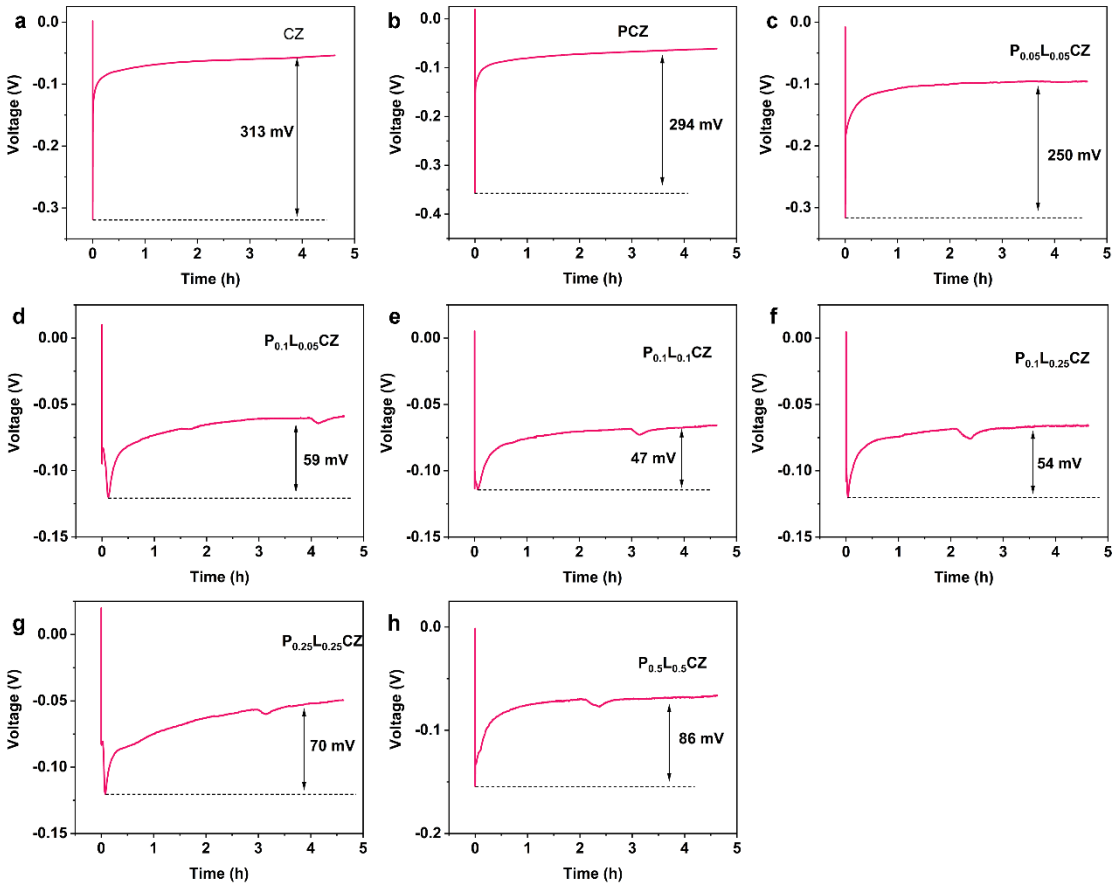

Supplementary Fig. S9 *The Zn nucleation overpotential of Zn^{2+} on Zn anodes with (a)*

CZ, (b) PCZ, (c) $P_{0.05}L_{0.05}$CZ, (d) $P_{0.1}L_{0.05}$CZ, (e) $P_{0.1}L_{0.1}$CZ, (f) $P_{0.1}L_{0.25}$CZ, (g) $P_{0.25}L_{0.25}$CZ and (h) $P_{0.5}L_{0.5}$CZ.

4) Why is in Fig 2a PAAs gel given as a reference for the lower wavenumber region but in Fig. 2b CZ for the higher wavenumber region? The reason for the choice of reference should be explained in the text/figure caption. Also 2c is the only one to not have a full frame around the axes.

Author reply: Thank you very much for your comments. In Fig. 2a, we mainly analyzed the asymmetric and symmetric -COO^- stretching vibrations. PAAS (sodium polyacrylate) gel, PCZ electrolyte and PLCZ electrolyte all contain -COO^- group in the polymer chain of PAAS molecules. The interaction between -COO^- and Zn^{2+} and LMS can be fully and profoundly analyzed by using the original PAAS gel compared with PCZ and PLCZ electrolytes. In detail, symmetric and asymmetric -COO^- stretching after ion exchange of the PCZ experience a notable blue shift, due to the metal coordination with Zn^{2+} ion with electrostatic forces (Fig. R22a). A further blue shift in -COO^- stretching of the PLCZ towards higher wavenumbers is also observed and stemmed from the electrostatic interactions between -COO^- and LMS. However, for CZ electrolyte, there is no any -COO^- stretching vibration signal detected in its FTIR spectrum. The FTIR spectrum of CZ electrolyte is almost same with that of CNF in the wavenumber range of 1300-1700 cm^{-1} (Fig. R23), because CZ is composed of CNF and $ZnSO_4$ solution that do not have any -COO^- groups (Fig. R24). Therefore, in Fig. 2a, only PAAS gel is chosen as a reference for the lower wavenumber region. Similarly, in the high wavenumber region of 2700-3700 cm^{-1}, we mainly focused on the O-H bonds in the water molecules and analyzed the effect of PAAS molecule and LMS on water. The CZ electrolyte shows a stretching vibration of the O-H bonds at 3245 cm^{-1} (Fig. R22b). The utilization of PAAS polymer and LMS causes the stretching vibration blue shifting to 3272 cm^{-1} of the PCZ and 3281 cm^{-1} of the PLCZ, suggesting an improved immobilization of water molecules through hydrogen bonding. Therefore, in the Fig. 2b for the high wavenumber region, we use CZ electrolyte as reference not PAAS gel. We also explain the reason for this choice in the figure caption.

For Fig. 2c, we have added full frame around the axes in the figures, as shown in Fig. R25.

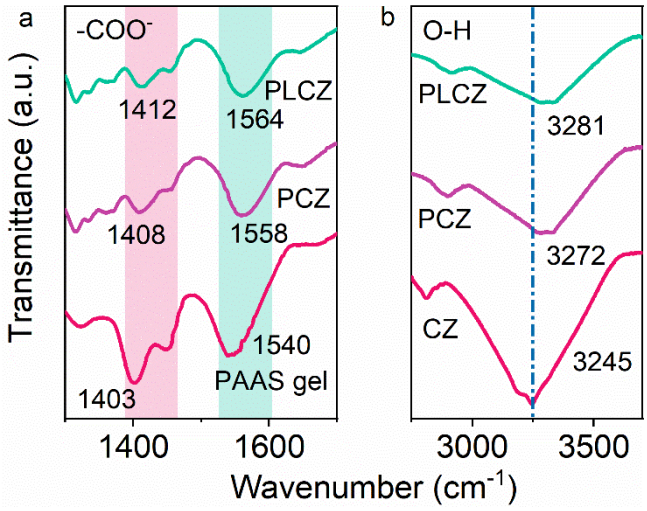

Fig. R22 *FTIR spectra focused on (a) the asymmetric and symmetric -COO⁻ stretching and (b) the stretching vibration of the O-H bonds. In the low wavenumber region, pure PAAS gel serves as the reference to assess the impact of Zn^{2+} and LMS on the -COO⁻ groups within the PAAS chain. In the high wavenumber region, CZ electrolyte is used as a benchmark for examining the influence of PAAS and LMS on water molecules.*

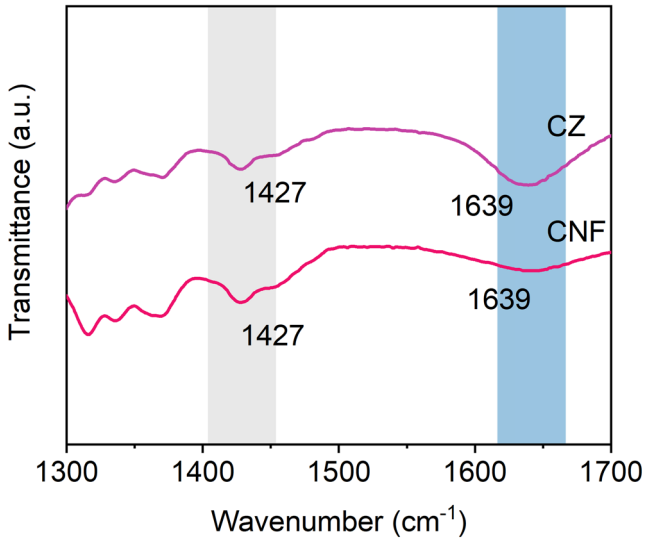

Fig. R23 *FTIR spectra of CNF and CZ electrolyte.*

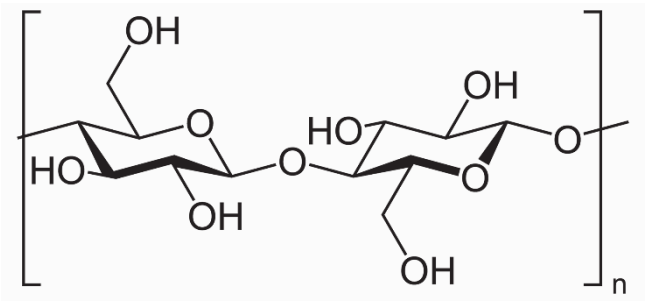

Fig. R24 *The molecule structure of cellulose.*

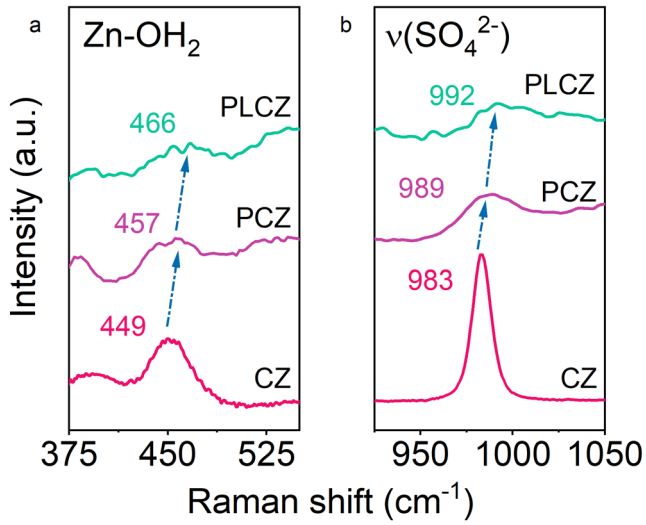

Fig. R25 *Raman spectra of (c) Zn-OH and (d) $v(SO_4)^{2-}$ vibrations of CZ, PCZ and PLCZ electrolytes.*

Changes in the manuscript (the highlighted part):

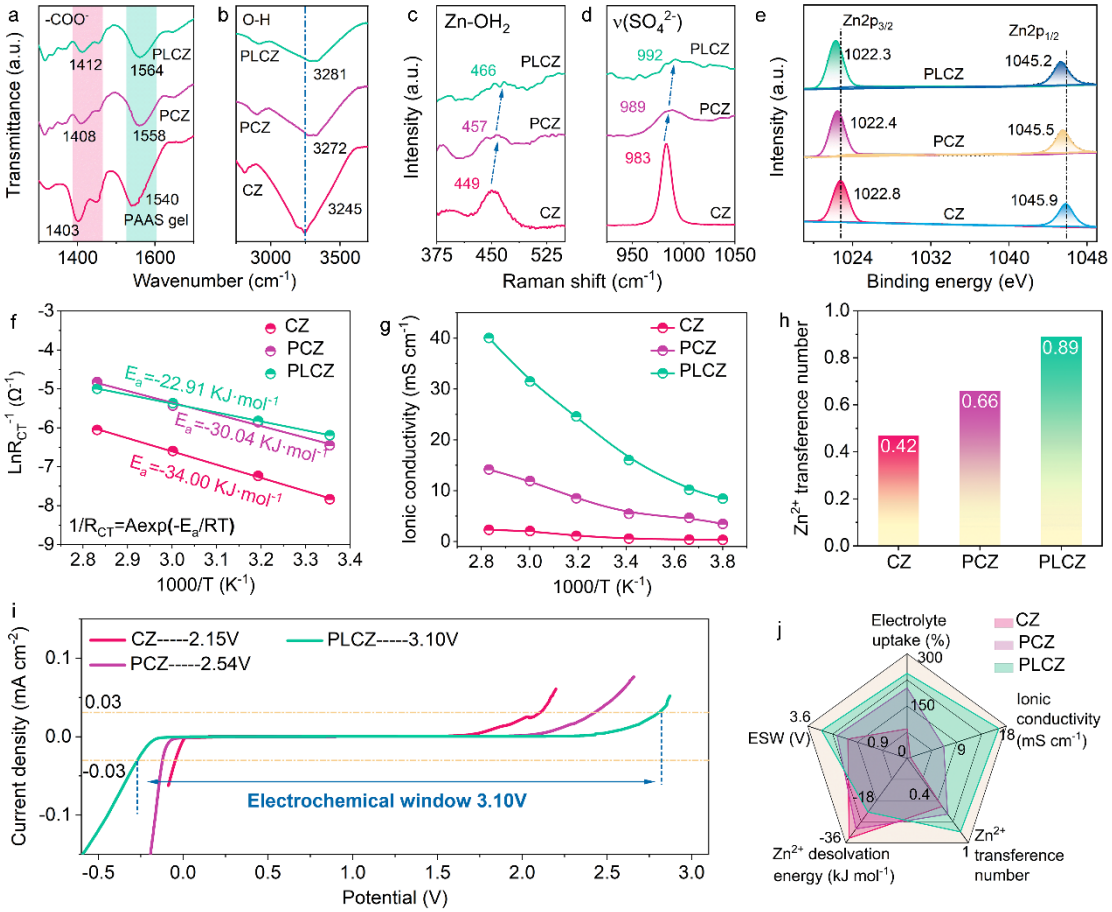

Fig. 2 *FTIR spectra focused on (a) the asymmetric and symmetric -COO- stretching and (b) the stretching vibration of the O-H bonds. In the low wavenumber region, pure PAAS gel serves as the reference to assess the impact of Zn^{2+} and LMS on the -COO- groups within the PAAS chain. In the high wavenumber region, CZ electrolyte is used as a benchmark for examining the influence of PAAS and LMS on water molecules. (c) Raman spectra of (c) Zn-OH and (d) $v(SO_4)^{2-}$ vibrations and (e) Zn 2p XPS spectra of CZ, PCZ and PLCZ electrolytes. The electrochemical characterizations of CZ, PCZ and PLCZ electrolytes. (f) The calculated activation energy (E_a), (g) ionic conductivity at different temperatures, (h) Zn^{2+} transference number and (i) ESW. (j) Radar diagram comparing the electrochemical performances of CZ, PCZ and PLCZ electrolytes.*

5) Fig. 2h y-axis label should be current density instead of current. At which current density was the ESW determined? This should be included.

Author reply: Thank you very much for your comments. The y-axis label has corrected to be current density, as shown in Fig. R26. The ESW was determined at the current density of 0.03 mA cm^{-2}, which was marked in the Fig. R26.

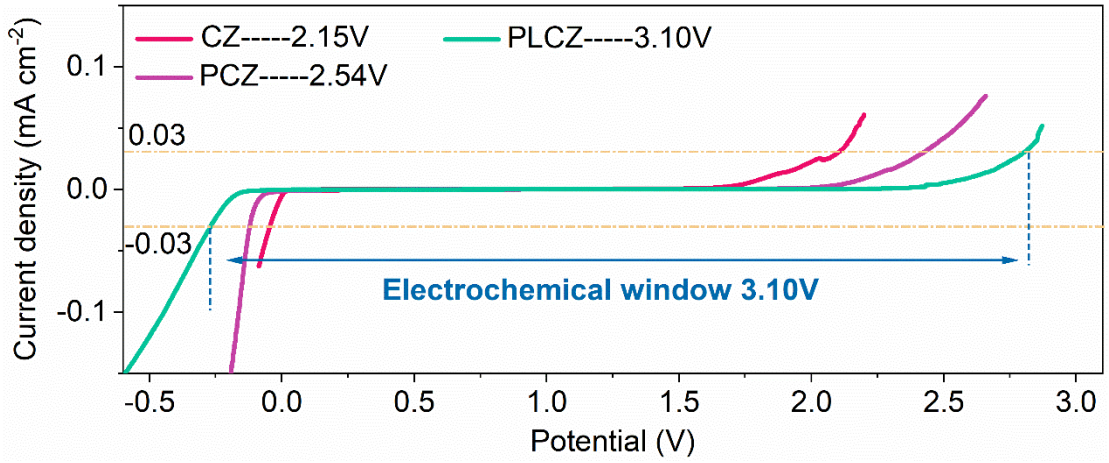

Fig. R26 *The tested ESW of CZ, PCZ and PLCZ electrolytes.*

Changes in the manuscript (the highlighted part):

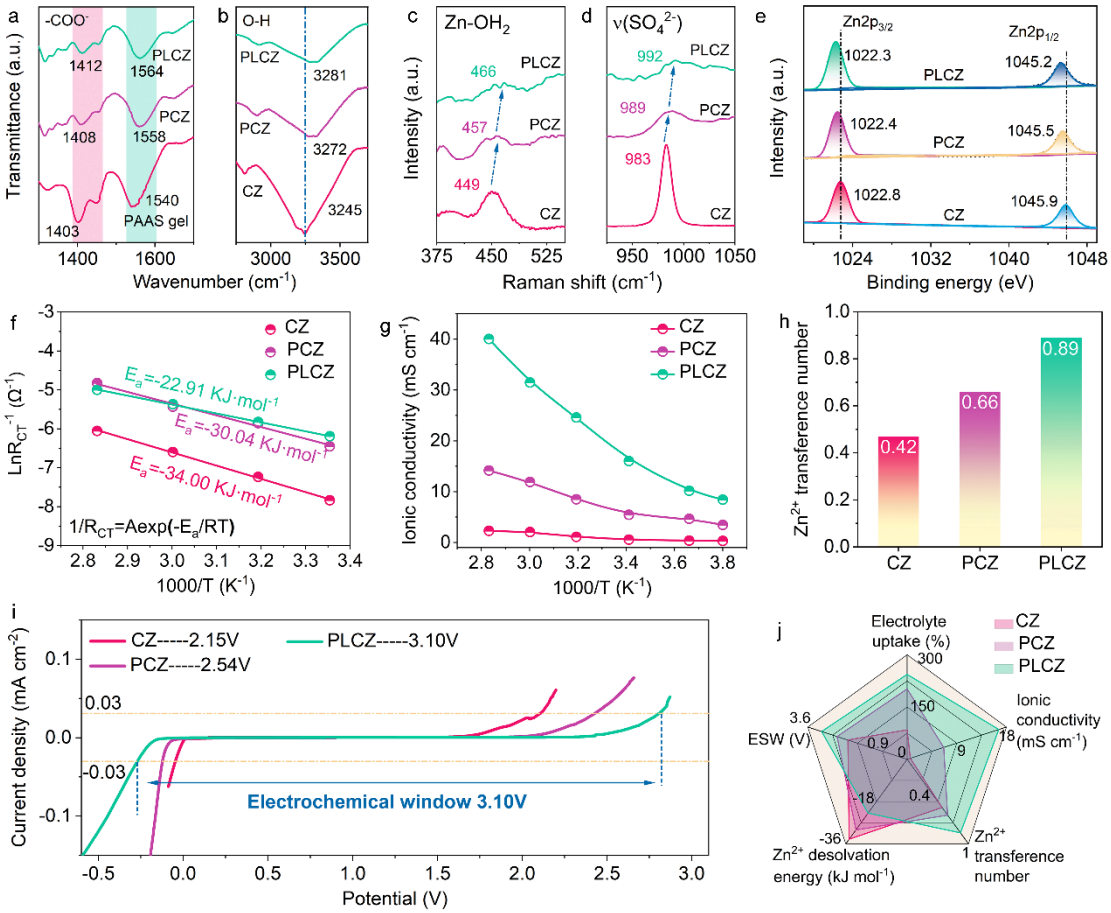

Fig. 2 *FTIR spectra focused on (a) the asymmetric and symmetric -COO- stretching and (b) the stretching vibration of the O-H bonds. In the low wavenumber region, pure PAAS gel serves as the reference to assess the impact of Zn^{2+} and LMS on the -COO- groups within the PAAS chain. In the high wavenumber region, CZ electrolyte is used as a benchmark for examining the influence of PAAS and LMS on water molecules. (c) Raman spectra of (c) Zn-OH and (d) $v(SO_4)^{2-}$ vibrations and (e) Zn 2p XPS spectra of*

CZ, PCZ and PLCZ electrolytes. The electrochemical characterizations of CZ, PCZ and PLCZ electrolytes. (f) The calculated activation energy (E_a), (g) ionic conductivity at different temperatures, (h) Zn^{2+} transference number and (i) ESW. (j) Radar diagram comparing the electrochemical performances of CZ, PCZ and PLCZ electrolytes.

6) Fig. 2i only for electrolyte uptake a value is given on the scale, whether values are used should be applied consistently across all axes.

Author reply: Thank you very much for your comments. The values on the scale are different for the axes of electrolyte uptake, ionic conductivity, Zn^{2+} transference number, Zn^{2+} desolvation energy and ESW, and we have set correct values to all axes, as shown in Fig. R27. We apologize for the cursoriness and mistake.

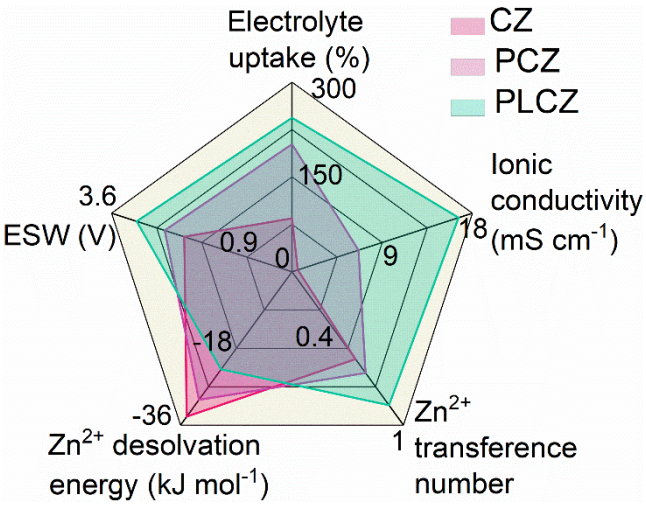

Fig. R27 *Radar diagram comparing the electrochemical performances of CZ, PCZ and PLCZ electrolytes.*

Changes in the manuscript (the highlighted part):

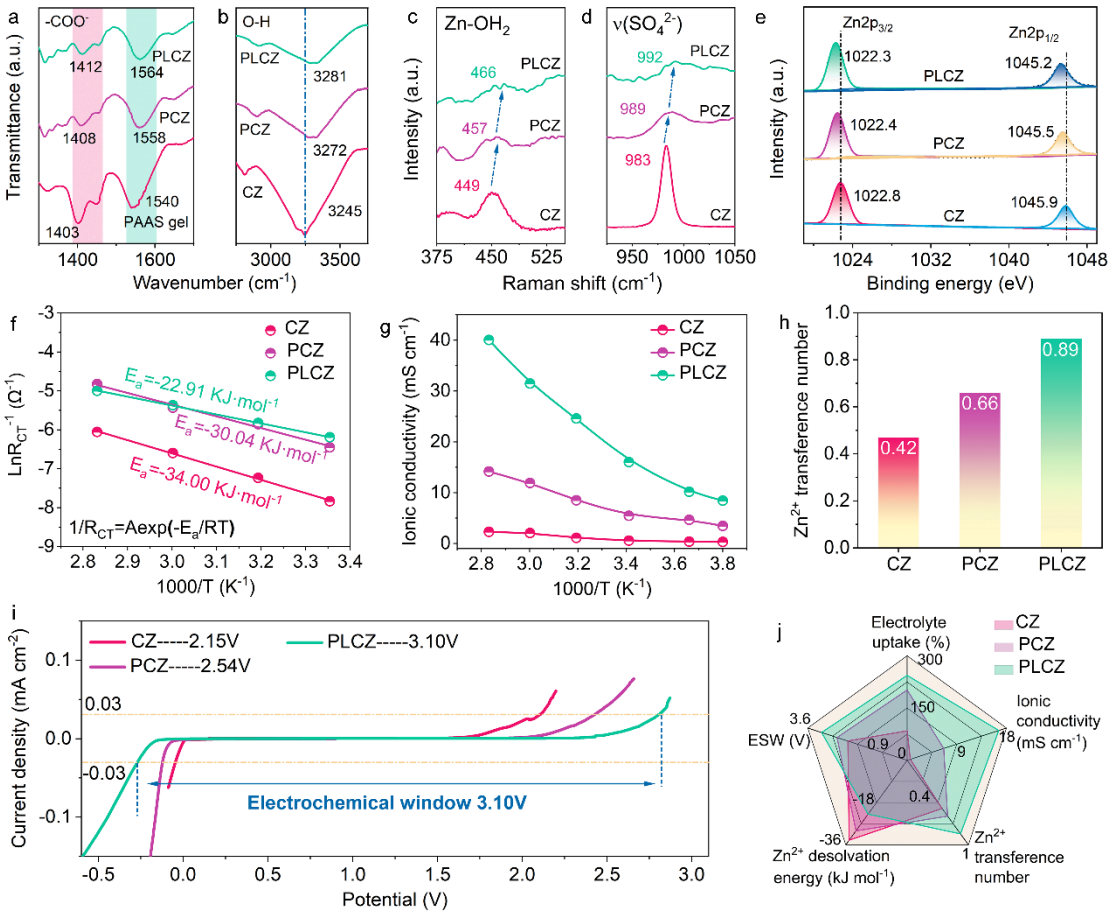

Fig. 2 *FTIR spectra focused on (a) the asymmetric and symmetric -COO⁻ stretching and (b) the stretching vibration of the O-H bonds. In the low wavenumber region, pure PAAS gel serves as the reference to assess the impact of Zn^{2+} and LMS on the -COO⁻ groups within the PAAS chain. In the high wavenumber region, CZ electrolyte is used as a benchmark for examining the influence of PAAS and LMS on water molecules. (c) Raman spectra of (c) Zn-OH and (d) $\nu(SO_4)^{2-}$ vibrations and (e) Zn 2p XPS spectra of CZ, PCZ and PLCZ electrolytes. The electrochemical characterizations of CZ, PCZ and PLCZ electrolytes. (f) The calculated activation energy (E_a), (g) ionic conductivity at different temperatures, (h) Zn^{2+} transference number and (i) ESW. (j) Radar diagram comparing the electrochemical performances of CZ, PCZ and PLCZ electrolytes.*

7) EIS spectra are not plotted using orthonormal scales making visual interpretation meaningless.

Author reply: Thank you very much for your comments. We fully understand the importance of visual clarity and have replotted all EIS spectra using orthonormal scales to ensure accurate and meaningful visual interpretation, as shown below.

Changes in supplementary information:

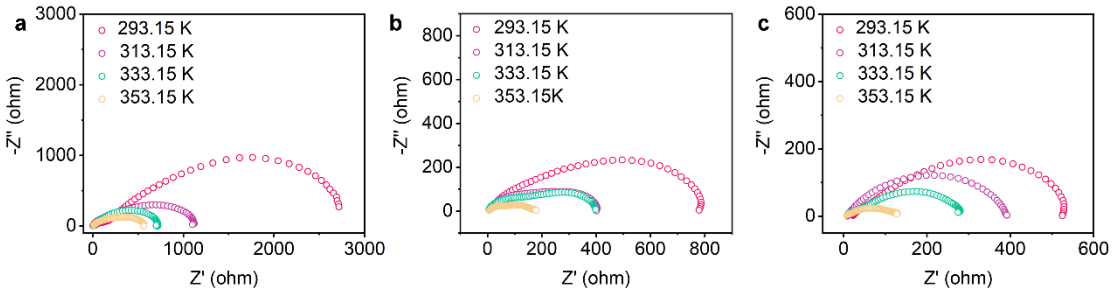

Supplementary Fig. S16 *EIS plots of Zn||Zn symmetric cells with (a) CZ, (b) PCZ and (c) PLCZ at different temperatures.*

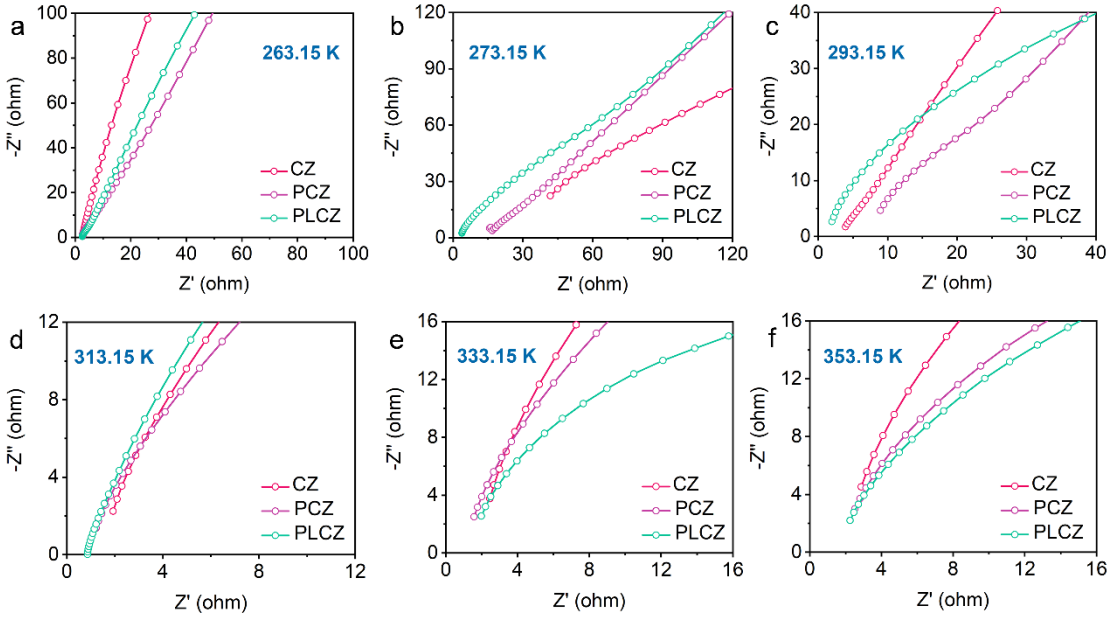

Supplementary Fig. S17 *EIS plots of CZ, PCZ and PLCZ at (a) 263.15 K, (b) 273.15 K, (c) 293.15 K, (d) 313.15 K, (e) 333.15 K, and (f) 353.15 K.*

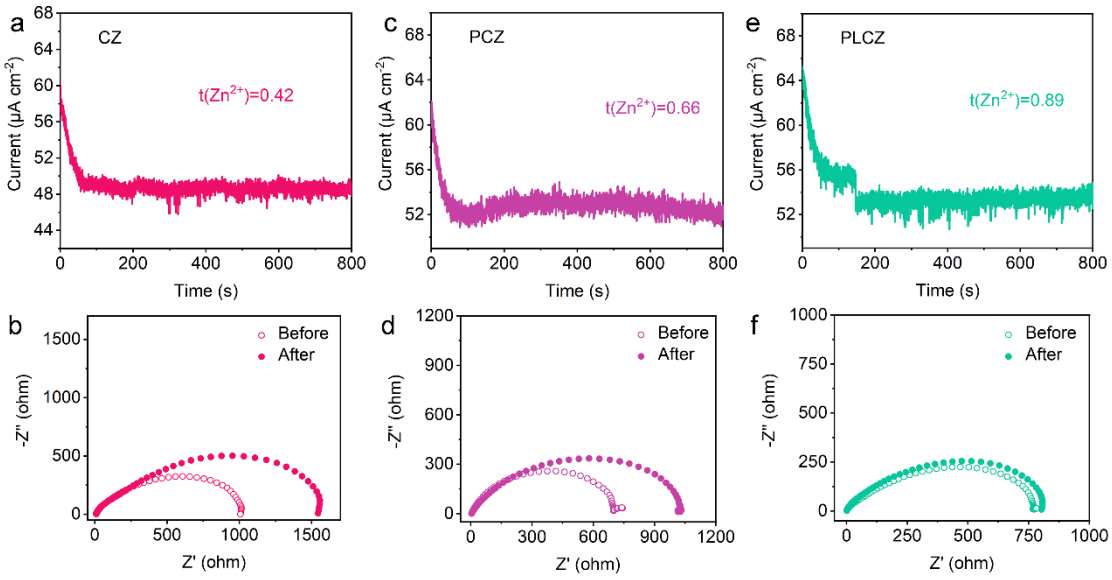

Supplementary Fig. S18 *CA curves and the corresponding EIS plots before and after CA of Zn||Zn symmetric cells. (a, b) CZ, (c, d) PCZ and (e, f) PLCZ.*

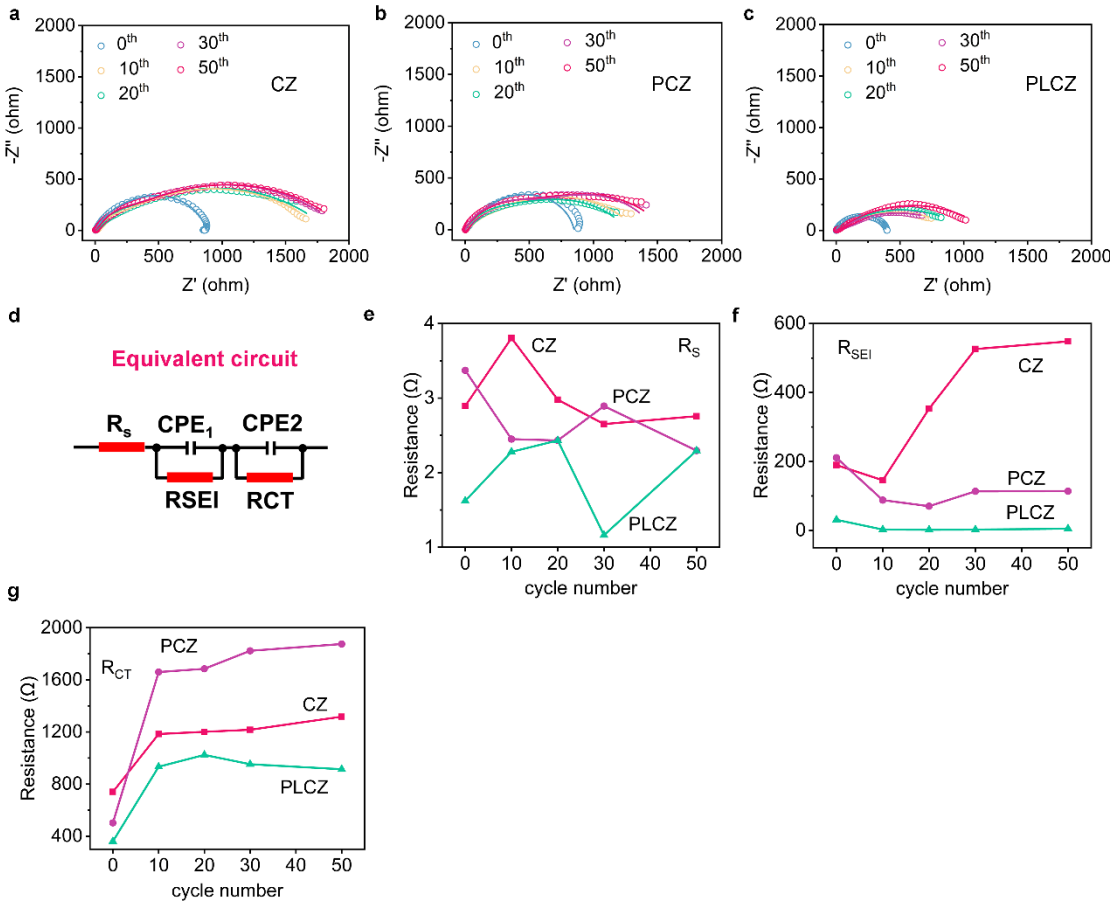

Supplementary Fig. S46 *EIS plots of Zn||Zn symmetric cells with (a) CZ, (b) PCZ and (c) PLCZ after cycling different times. The solid line represents the corresponding fitted EIS plots. (d) The equivalent circuit of EIS plots. The calculated resistances of (e) R_S, (f) R_{SEI} and (g) R_{CT}.*

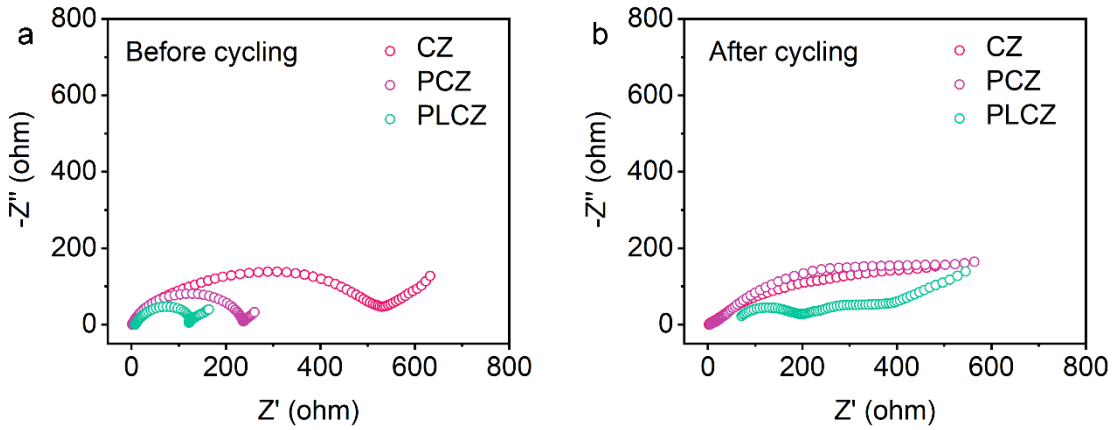

Supplementary Fig. S49 *EIS plots of Zn||V_2O_5 with CZ, PCZ and PLCZ electrolytes (a) before and (b) after cycling.*

8) At line 211 there is no reference to the technique used for activation energy

calculation.

*Author reply: Thank you very much for your comments. We apologize for the oversight. The calculation of the activation energy mentioned at line 211 utilized the Arrhenius equation. We have updated the manuscript to include a reference to this technique. The cited references are Nature Communications **14**, 6526 (2023) and ACS Energy Letters **8**, 2886-2896 (2023).*

Besides, the calculation of the Zn^{2+} activation energy was shown in the part of Electrochemical performance in the manuscript, as below.

*The Zn^{2+} desolvation energy was tested the resistance of Zn||Zn at various temperature and calculated via the Arrhenius equations (1) (cited reference: Nano-Micro Letters **13**, 69 (2021).):*

$$\frac{1}{R_{ct}} = A\exp(-\frac{E_a}{RT}) \qquad (1)$$

Where E_a, R_{CT}, R, T and A represent the activation energy, charge transfer resistance, molar gas constant, absolute temperature and Arrhenius constant, respectively.

Changes in the manuscript (the highlighted part):

The desolvation energy barrier of Zn at the interface between electrolyte and Zn anode was evaluated by calculating the Zn^{2+} activation energy (E_a)[27, 28].

9) In Fig. 3a parameters are given as 0.5 mA cm^{-2} 0.25 mAh cm^{-2}, whereas in the figure caption it is written 1 mA cm^{-2} 1 mAh cm^{-2}.

Author reply: Thank you very much for your comments. We apologize for this oversight. To address this issue, we have made the following corrections: 1 mA cm^{-2} 1 mAh cm^{-2} was changed to be 0.5 mA cm^{-2} 0.25 mAh cm^{-2}, as shown below.

Changes in the manuscript (the highlighted part):

***Fig. 3** Cycling performances of Zn||Zn symmetric cells with CZ, PCZ and PLCZ at (a) 0.5 mA cm^{-2}, 0.25 mAh cm^{-2} and (b) 2 mA cm^{-2}, 10 mAh cm^{-2}.*

10) After how many cycles were the SEM images taken in Fig. 3c-e? Why is the Zn foil in c not colored? The purpose or source of this color should be noted in the caption. Images/photographs are too small.

Author reply: Thank you very much for your comments. The SEM images of Zn anodes in Figs. 3c-e were taken after 200 cycles. Actually, in Fig. 3c, we wanted to make the Zn dendrite more visible and prominent (because the Zn dendrite is more important for the result discussion), so we only colored the Zn dendrite, not Zn foil. Also, in Fig. 3d and 3e, we wanted to distinguish different objects with different colors to make them clearer and stand out, including Zn foil, PCZ and PLCZ electrolytes. In the revised manuscript, we colored the Zn foil, Zn dendrite, PCZ and PLCZ with blue, red, pink and green colors, respectively, as shown in Fig. R28. And we added the purpose and

source of these colors in the figure caption. Besides, we enlarged the SEM images of the Zn anodes in the revise Fig. 3. In order to make the Fig. 3 more harmonious and beautiful, we moved the figure of OER and HER onset potentials (Fig. R29) to supplementary information.

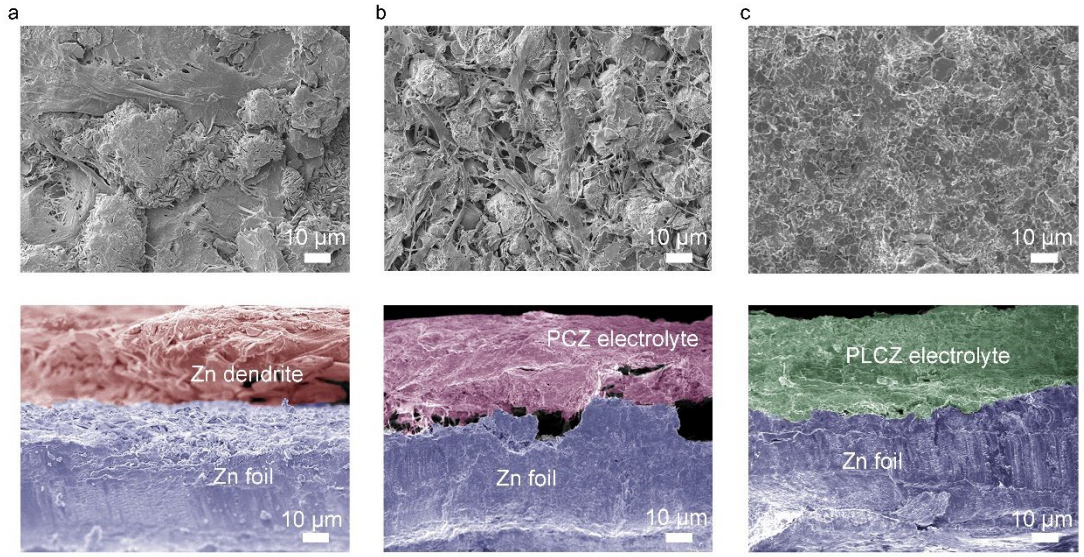

Fig. R28 *SEM images of the Zn anodes on the top view and side view of (a) CZ, (b) PCZ and (c) PLCZ after 200 cycles. For easy of result comparison and analysis, the Zn dendrite, Zn foil, PCZ electrolyte and PLCZ electrolyte are colored with red, blue, pink and green, respectively.*

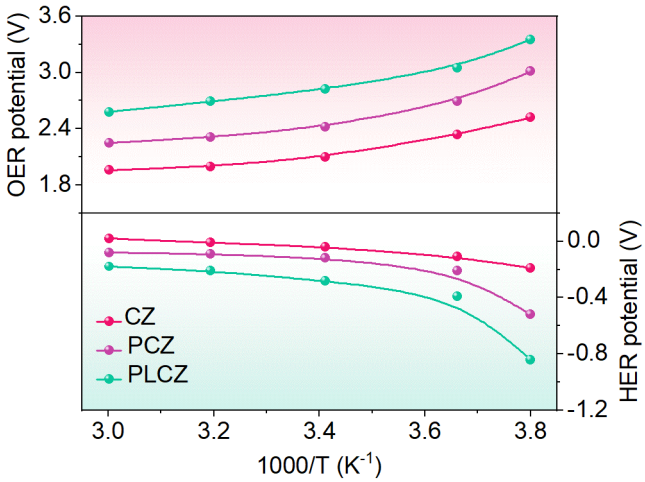

Fig. R29 *OER and HER onset potentials at different temperatures of CZ, PCZ and PLCZ.*

<u>Changes in the manuscript (the highlighted part):</u>

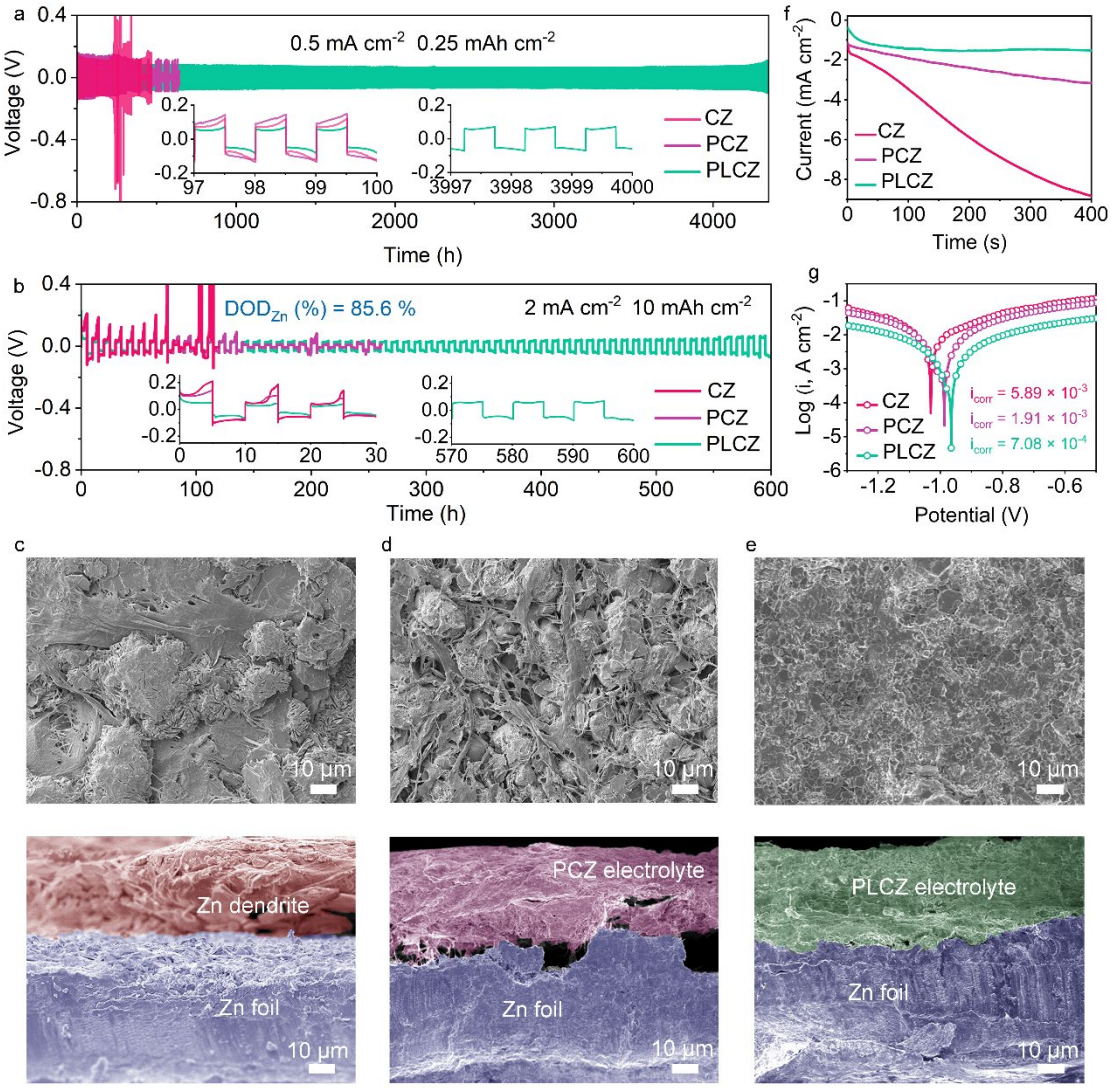

Fig. 3 *Cycling performances of Zn||Zn symmetric cells with the CZ, PCZ and PLCZ at (a) 0.5 mA cm^{-2}, 0.25 mAh cm^{-2} and (b) 2 mA cm^{-2}, 10 mAh cm^{-2}. When the thickness is 128 μm, the PLCZ obtains the best cycling lifespans. SEM images of the Zn anodes on the top view and side view of (c) CZ, (d) PCZ and (e) PLCZ after 200 cycles. For easy of result comparison and analysis, the Zn dendrite, Zn foil, PCZ electrolyte and PLCZ electrolyte are colored with red, blue, pink and green, respectively. (f) CA tests and (g) Tafel plots of the CZ, PCZ and PLCZ.*

Changes in supplementary information:

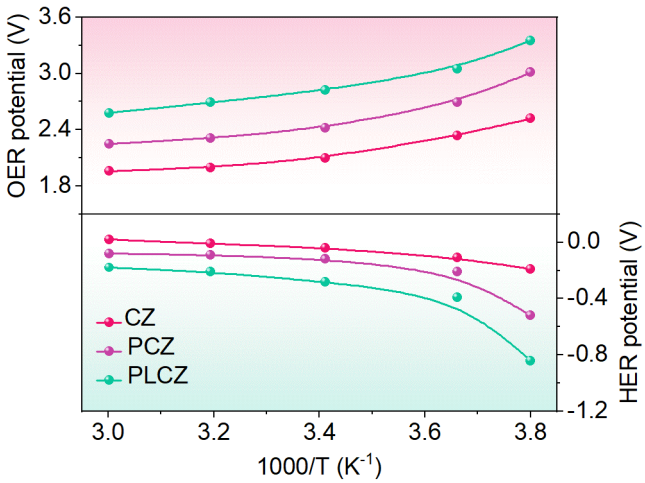

Supplementary Fig. S29 *OER and HER onset potentials at different temperatures of CZ, PCZ and PLCZ.*

11) In Fig. 3h it is confusing for the reader to give the x-axis in K^{-1}, when temperatures in the text are only described in C.

Author reply: Thank you very much for your comments. We understand the importance of clarity for our readers. We have changed all the unit of temperature to K in the manuscript and supplementary information as well in the figures.

Changes in the manuscript (the highlighted part):

1. Accordingly, by virtue of the enhanced dissociation capability of Zn^{2+}, the PLCZ demonstrates an excellent ionic conductivity across a temperature range from 263.15 to 353.15 K (Fig. 2g and Supplementary Fig. S17).

2. Consequently, symmetric cells with the PLCZ electrolyte all deliver superior cycling stability over 4200 h at 273.15 K, 1600 h at 313.15 K and 400 h at 333.15 K (Supplementary Fig. S30).

3. Moreover, $Zn||V_2O_5$ cells with the PLCZ were exposed to more challenging temperatures of 273.15, 313.15 and 333.15 K (Supplementary Fig. S52), which shows a more stable and reversible cycling capacity.

4. After that, the resultant PAAS-LMS-CNF solution was poured into Teflon petri dish and then dried at 348.15 K for 12h.

5. 10 g NH_4VO_3 was put into a crucible and heated at 673.15 K for 2 h with ramping rate of 10 K min^{-1}.

Changes in supplementary information:

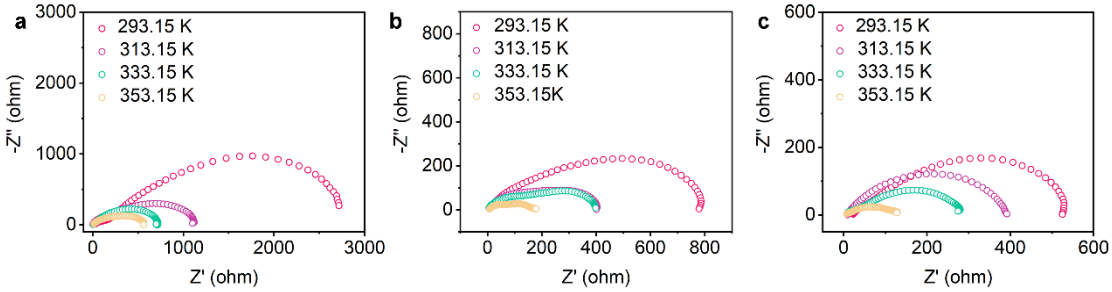

Supplementary Fig. S16 *EIS plots of Zn||Zn symmetric cells with (a) CZ, (b) PCZ and (c) PLCZ at different temperatures.*

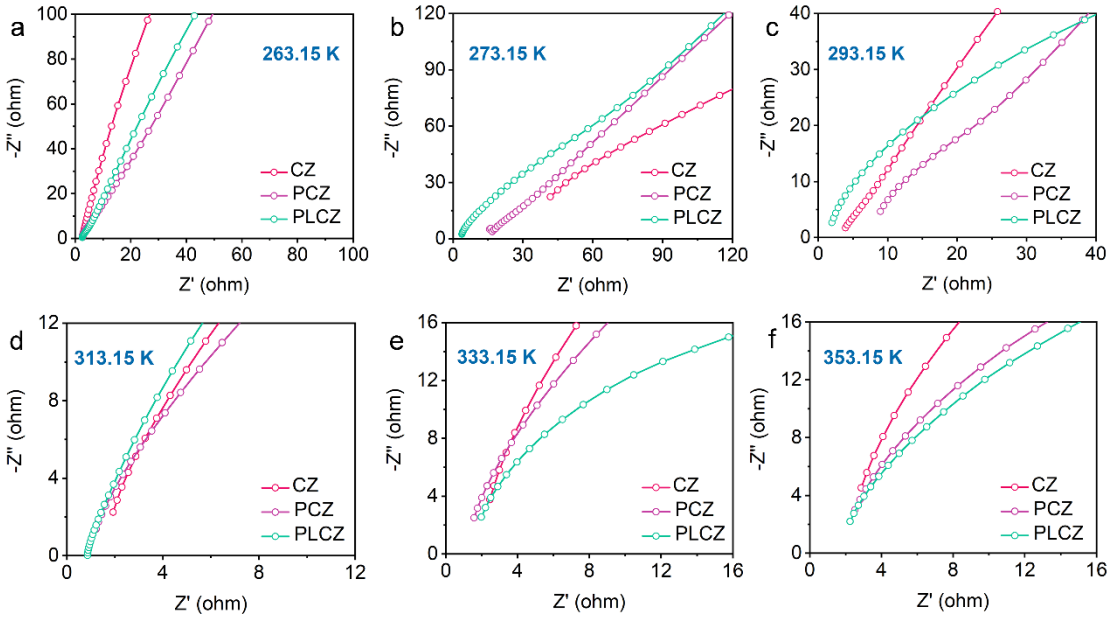

Supplementary Fig. S17 *EIS plots of CZ, PCZ and PLCZ at (a) 263.15 K, (b) 273.15 K, (c) 293.15 K, (d) 313.15 K, (e) 333.15 K, and (f) 353.15 K.*

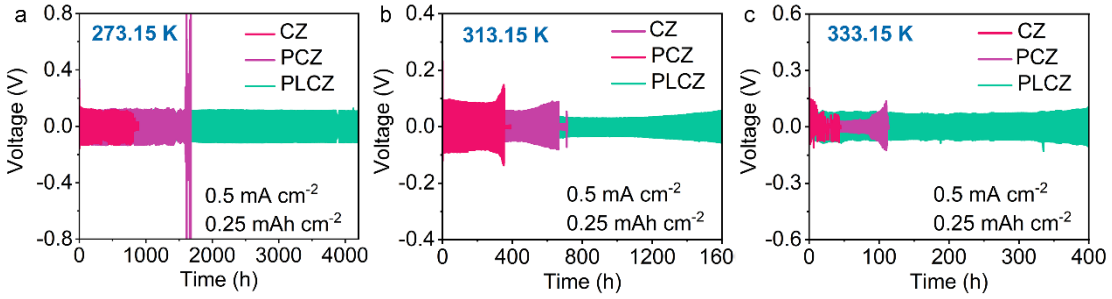

Supplementary Fig. S30 *Cycling stability of Zn||Zn cells with the electrolytes at (a) 273.15, (b) 313.15 and (c) 333.15 K.*

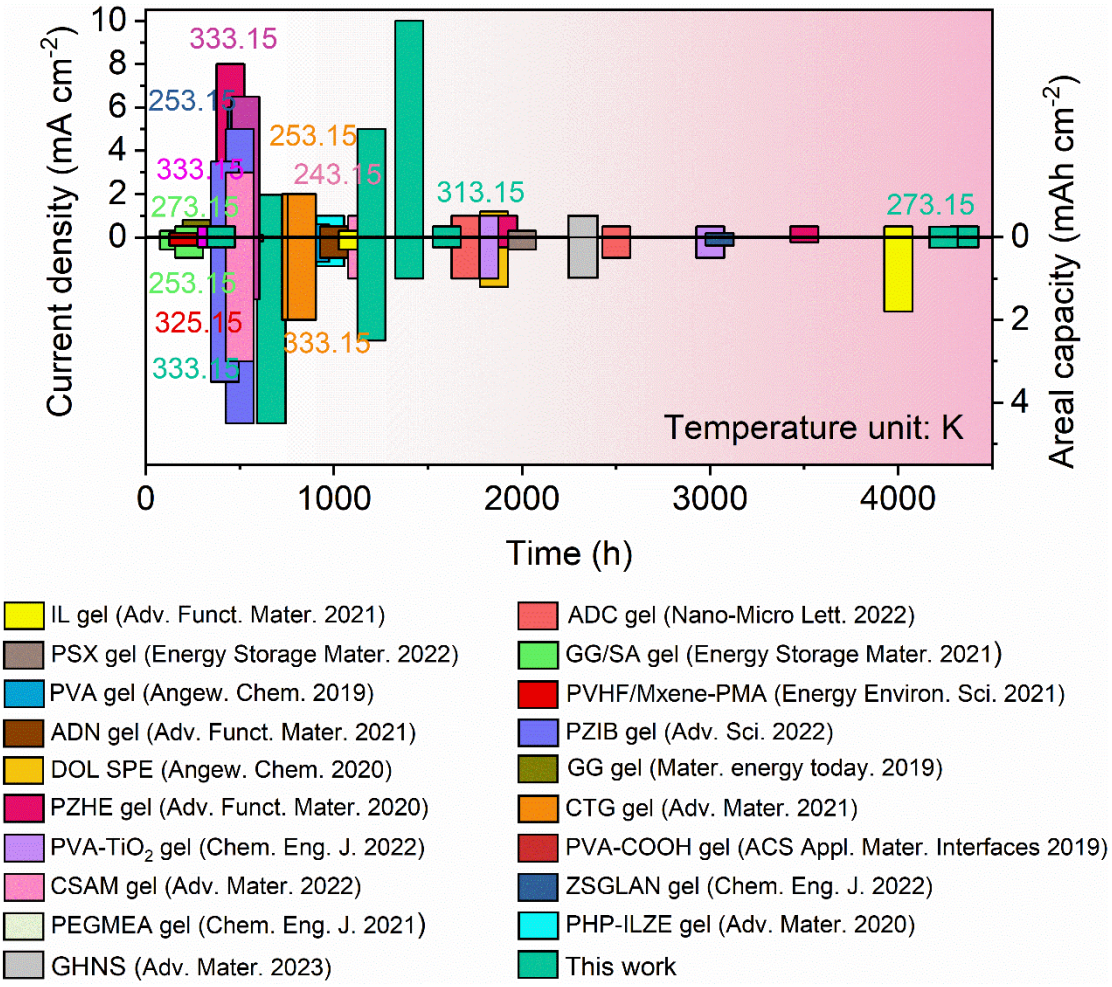

Supplementary Fig. S31 *The comparison of the cycling lifespan of the electrolytes.*

12) The figure caption in Fig. S24 is wrong. i, j, k instead of a, b, c.

Author reply: Thank you very much for your comments. We have corrected the figure caption in Fig. S24 (in the revised manuscript, this figure is Fig. S30) to accurately reflect the labels.

Changes in supplementary information:

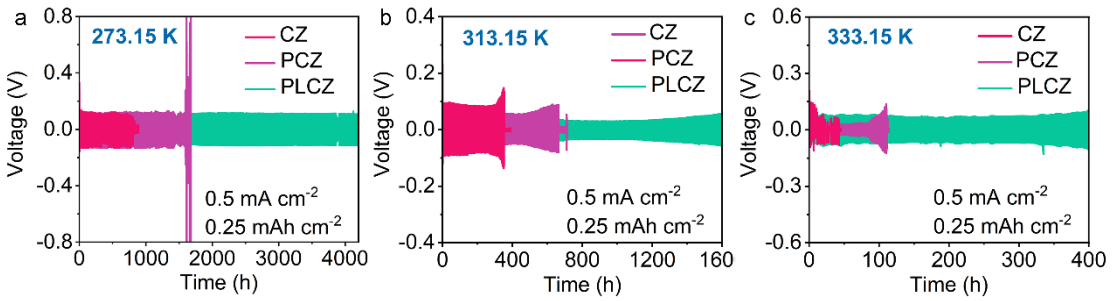

Supplementary Fig. S30 *Cycling stability of Zn||Zn cells with the electrolytes at (a) 273.15, (b) 313.15 and (c) 333.15 K.*

13) In Fig. 4 b-d the labelling is not visible very well. Furthermore, it is not explained what the colored regions in the SEM images represent. (Also Fig. S39 and mentioned above in Fig 3).

Author reply: Thank you very much for your comments. We have revised this problem and set the label in the blank area of the figure (only one label for the SEM images of Cu anodes of the CZ, PCZ and PLCZ), as show in Fig. R9. Additionally, we distinguished the object with color to make it more visible and stand out, using red color for the cellulose fiber. We also explained what the colored regions in the SEM images represent, including Fig. 3c-e, Fig. S23 and Fig. S39 (in the revised supplementary information, Fig. S23 and Fig. S39 were changed to be Fig. S28 and Fig. S51) in the figure caption. The revised Fig. 3c-e, Fig. S23 and Fig. S39 are shown as Fig. R28, Fig. R30 and Fig. R31, respectively.

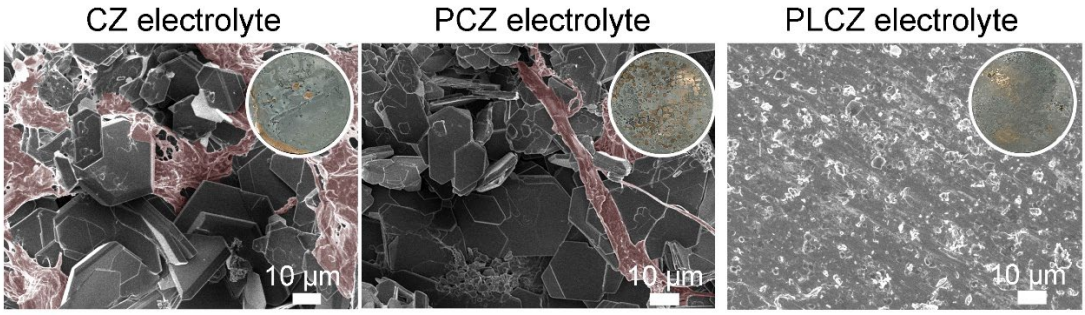

Fig. R9 *SEM images of Cu cathode of CZ, PCZ and PLCZ (insets: digital photographs of Cu electrodes). The red color in the SEM images represent the CNF fiber.*

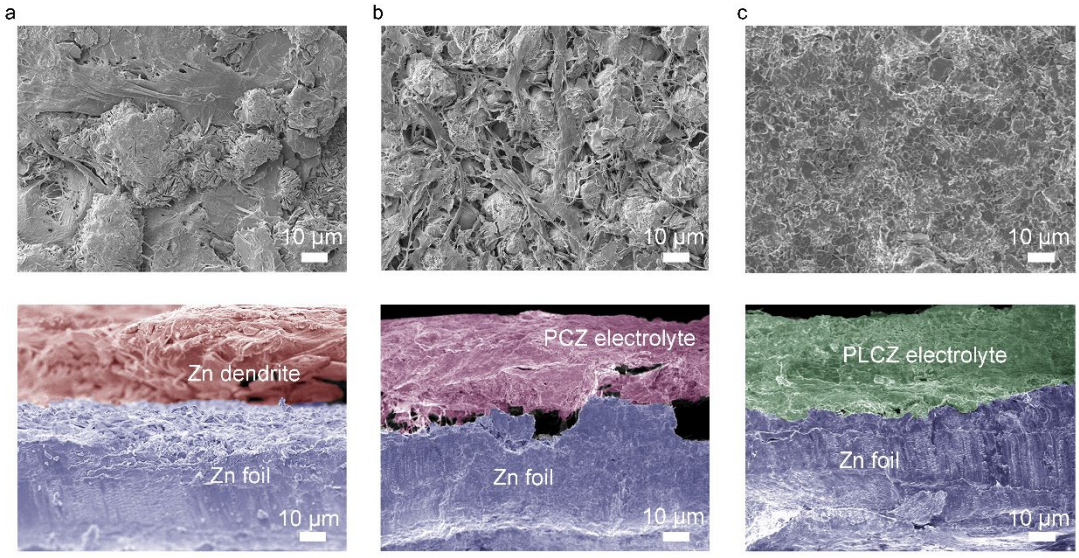

Fig. R28 *SEM images of the Zn anodes on the top view and side view of (a) CZ, (b) PCZ and (c) PLCZ after 200 cycles. For easy of result comparison and analysis, the Zn dendrite, Zn foil, PCZ electrolyte and PLCZ electrolyte are colored with red, blue, pink and green, respectively.*

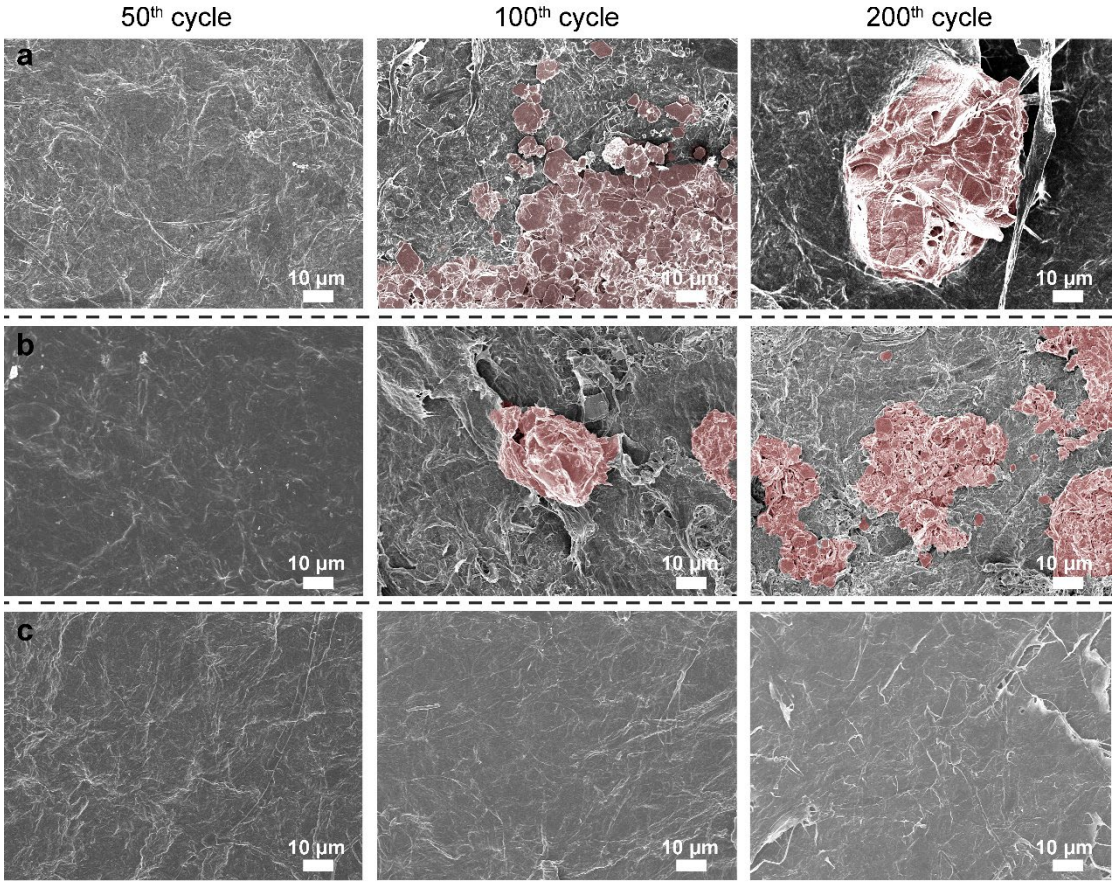

Fig. R30 *SEM images of (a) CZ, (b) PCZ and (c) PLCZ after cycling different cycles. The colored regions represent the formed Zn dendrites.*

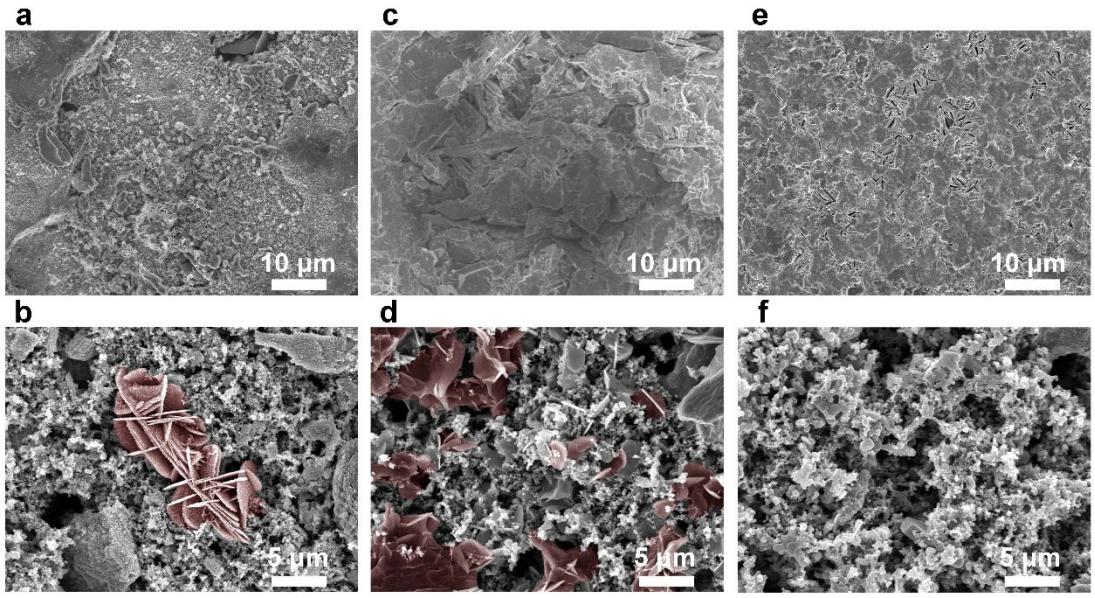

Fig. R31 *SEM images of Zn anode and V_2O_5 cathode after cycling with (a, b) CZ, (c, d) PCZ, and (e, f) PLCZ. The colored regions represent the formed Zn dendrites on the V_2O_5 cathode surface.*

Changes in the manuscript (the highlighted part):

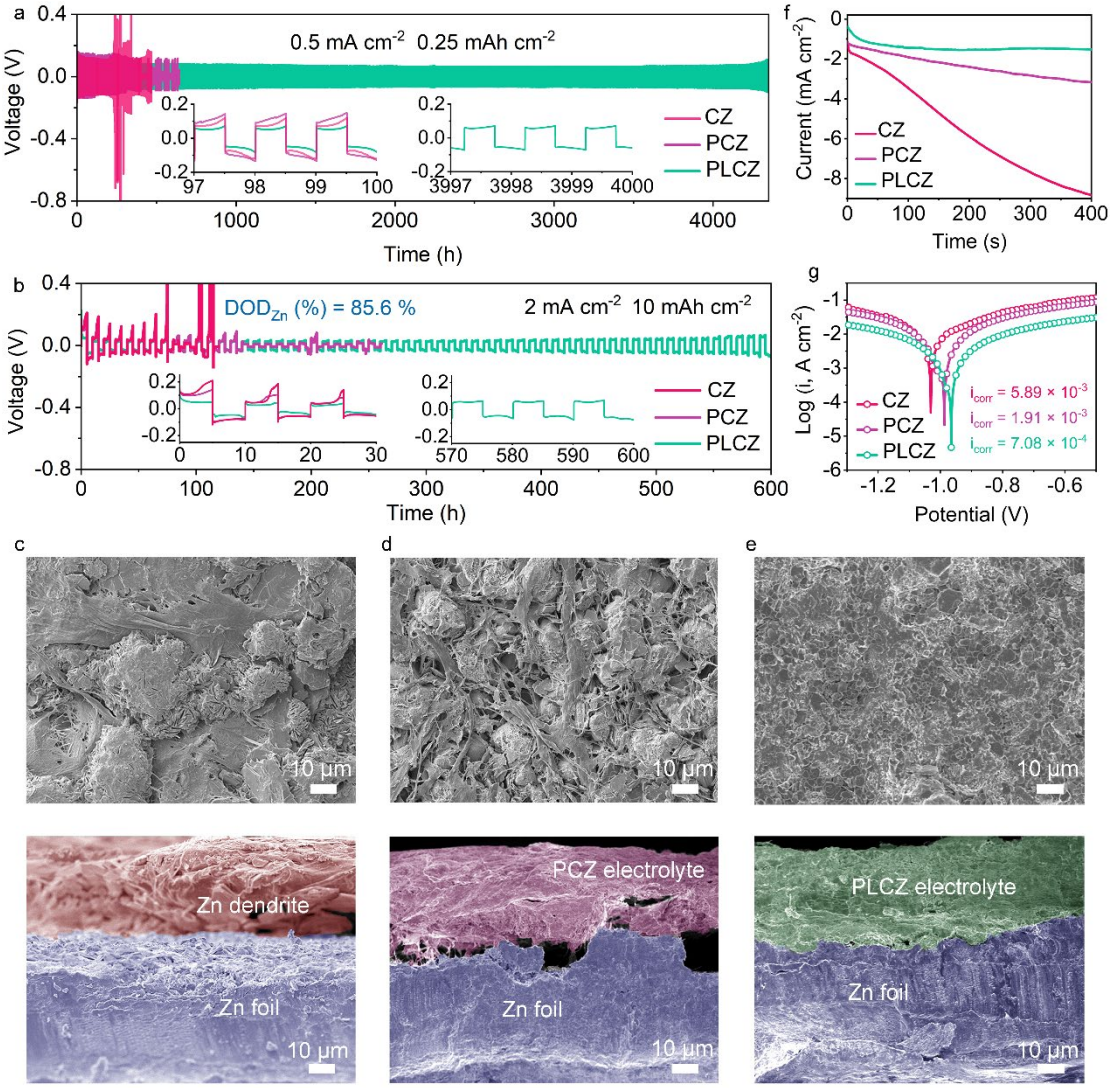

Fig. 3 *Cycling performances of Zn||Zn symmetric cells with the CZ, PCZ and PLCZ at (a) 0.5 mA cm^{-2}, 0.25 mAh cm^{-2} and (b) 2 mA cm^{-2}, 10 mAh cm^{-2}. When the thickness is 128 μm, the PLCZ obtains the best cycling lifespans. SEM images of the Zn anodes on the top view and side view of (c) CZ, (d) PCZ and (e) PLCZ after 200 cycles. For easy of result comparison and analysis, the Zn dendrite, Zn foil, PCZ electrolyte and PLCZ electrolyte are colored with red, blue, pink and green, respectively. (f) CA tests and (g) Tafel plots of the CZ, PCZ and PLCZ.*

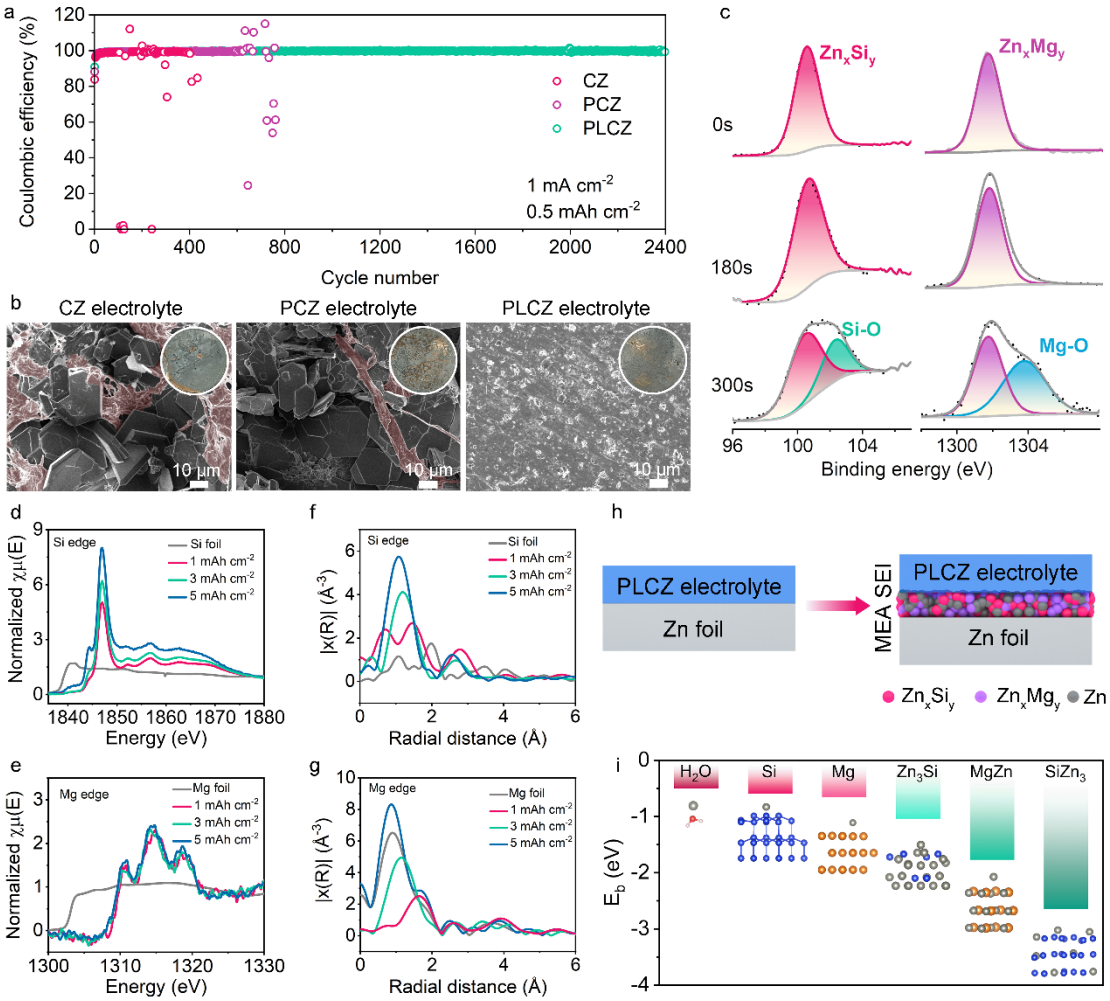

Fig. 4 *(a) Cycling performance of Zn||Cu asymmetric cells as well the corresponding (b) SEM images of Cu cathode of the CZ, PCZ and PLCZ (insets: digital photographs of Cu electrodes). The red color in the SEM images represent the CNF fiber. (c) Si 2p and Mg 1s XPS spectra of the cycled Zn anodes of PLCZ electrolyte. XANES spectra and the corresponding r-space date of (d, f) Si K-edge and (e, g) Mg K-edge of Zn anodes after deposited different Zn capacities with PLCZ electrolyte. (h) Schematically illustrating the formation of MEA SEI layer on Zn anode. (i) The calculated E_b of Zn on the alloy ingredients.*

Changes in supplementary information:

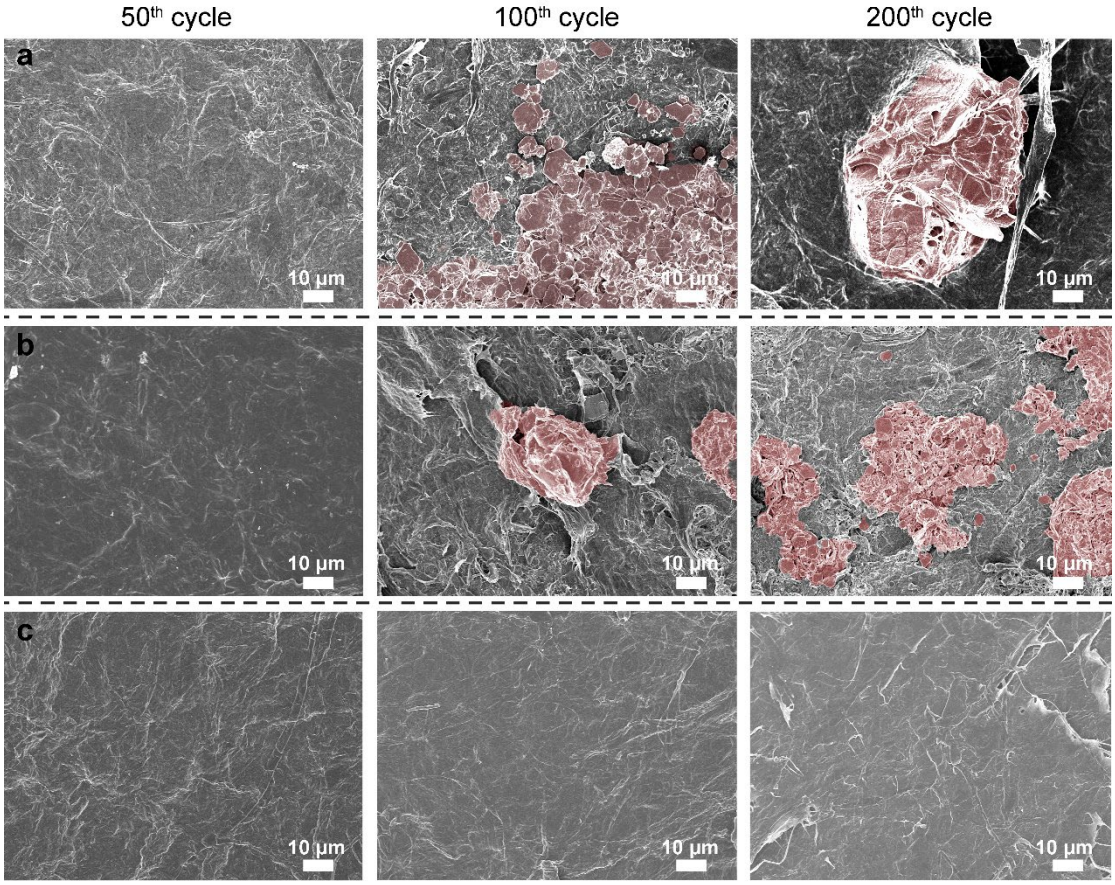

Supplementary Fig. S28 *SEM images of (a) CZ, (b) PCZ and (c) PLCZ after cycling different cycles. The colored regions represent the formed Zn dendrites.*

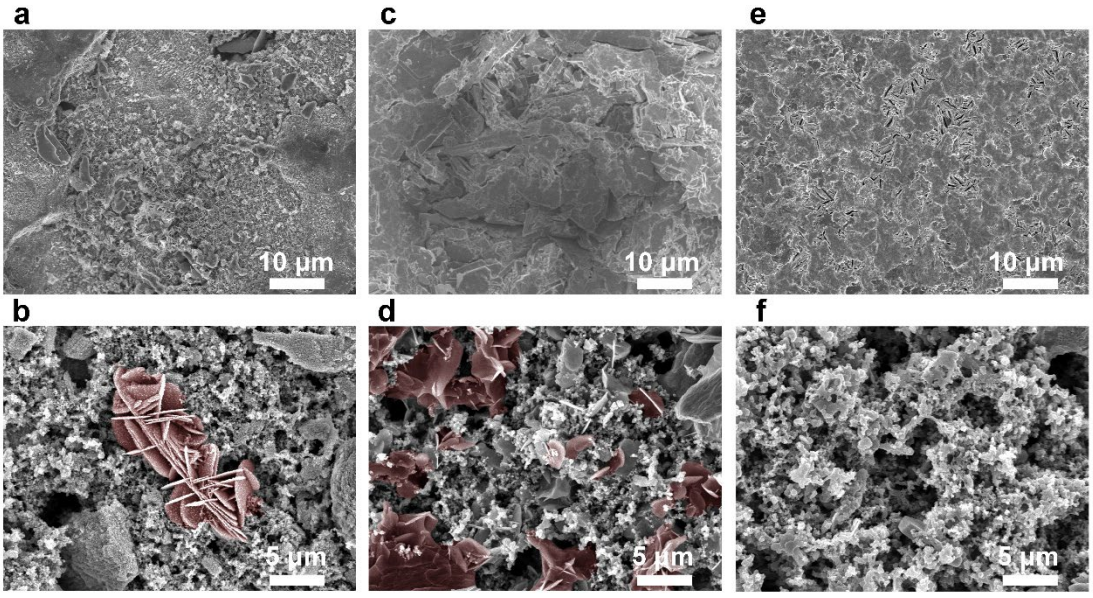

Supplementary Fig. S51 *SEM images of Zn anode and V_2O_5 cathode after cycling with (a, b) CZ, (c, d) PCZ, and (e, f) PLCZ. The colored regions represent the formed Zn dendrites on the V_2O_5 cathode surface.*

14) Plotting error in Fig. 4e. The area under the curve shouldn't be filled until the straight line but until the background.

Author reply: Thank you very much for your reminding and comments. We have revised this error, namely, the color only filled the area until the background, not the straight line. The revised figure is shown in Fig. R32.

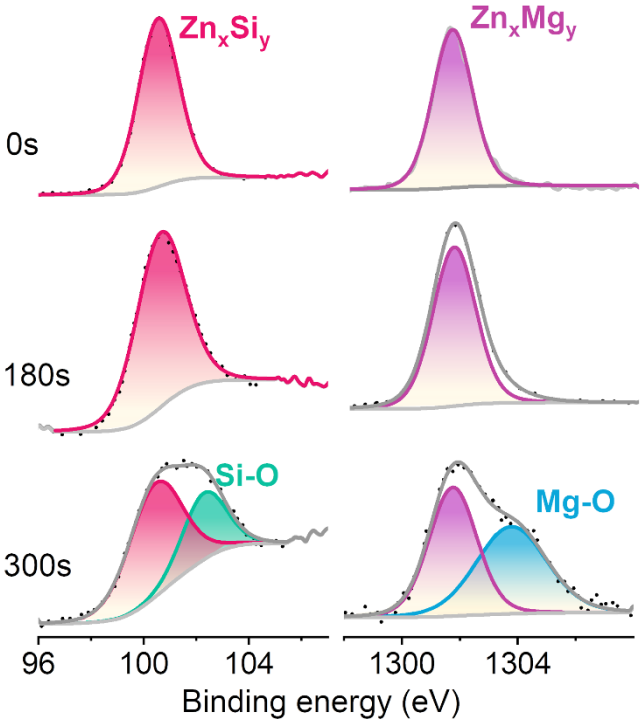

Fig. R32 *Si 2p and Mg 1s XPS spectra of the cycled Zn anodes of PLCZ electrolyte.*

Changes in the manuscript (the highlighted part):

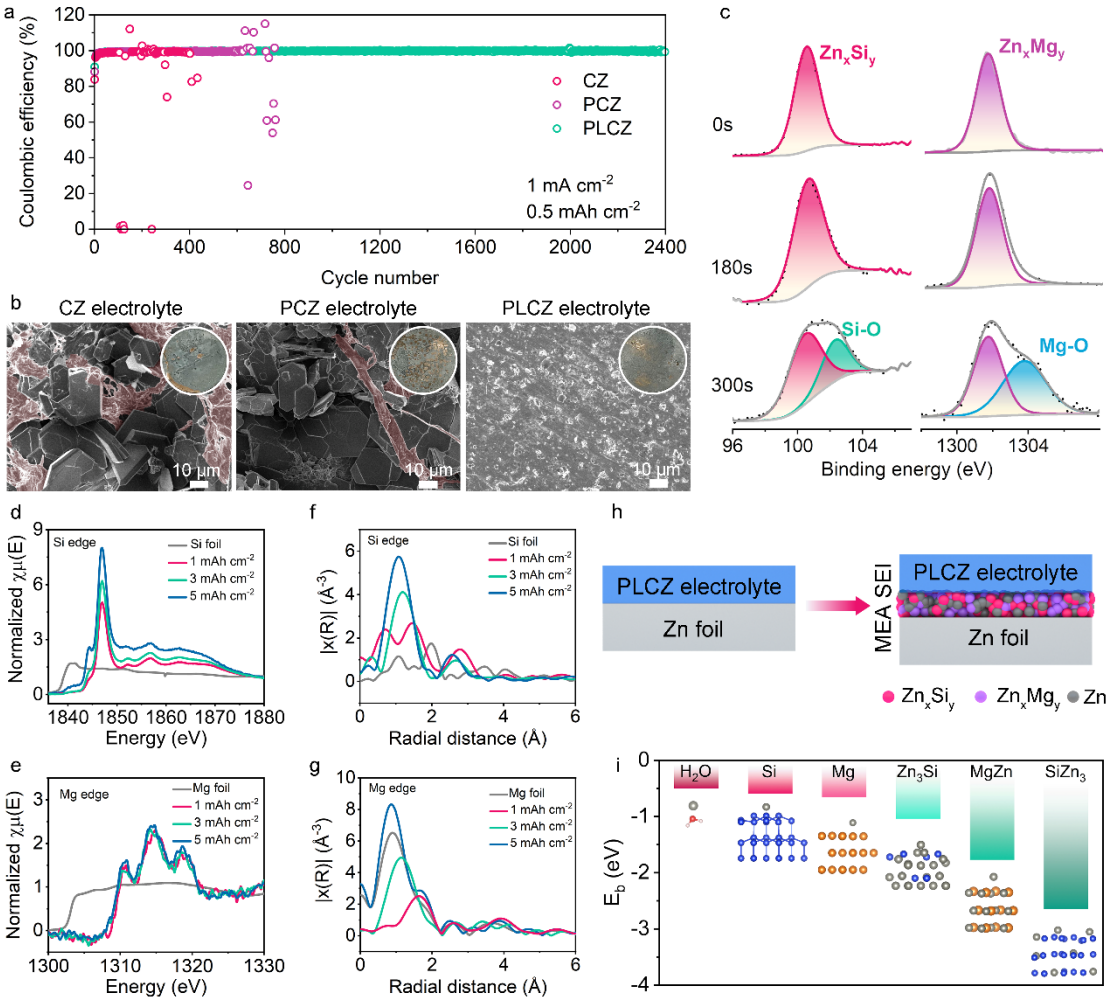

Fig. 4 *(a) Cycling performance of Zn||Cu asymmetric cells as well the corresponding (b) SEM images of Cu cathode of the CZ, PCZ and PLCZ (insets: digital photographs of Cu electrodes). The red color in the SEM images represent the CNF fiber. (c) Si 2p and Mg 1s XPS spectra of the cycled Zn anodes of PLCZ electrolyte. XANES spectra and the corresponding r-space date of (d, f) Si K-edge and (e, g) Mg K-edge of Zn anodes after deposited different Zn capacities with PLCZ electrolyte. (h) Schematically illustrating the formation of MEA SEI layer on Zn anode. (i) The calculated E_b of Zn on the alloy ingredients.*

15) How was the nucleation overpotential determined in Fig. S28?

Author reply: Thank you very much for your comments. As shown in Fig. R33, the nucleation overpotential in the cyclic voltammetry (CV) of Zn||Cu asymmetric cells is defined as the difference between the crossover point (point a, where the current density begins to increase from zero) and the onset point (point b) of Zn^{2+} ion reduction (Adv. Funct. Mater. 2022, 32, 2206695). And we have added this explanation in the figure caption. The CV curves reveal that compared to the CZ (105 mV) and PCZ (48 mV), the PLCZ electrolyte reduces the nucleation overpotential to a mere 23 mV while maintaining strong current density, indicating its ability to optimize reaction kinetics

for fast and uniform Zn deposition and dissolution.

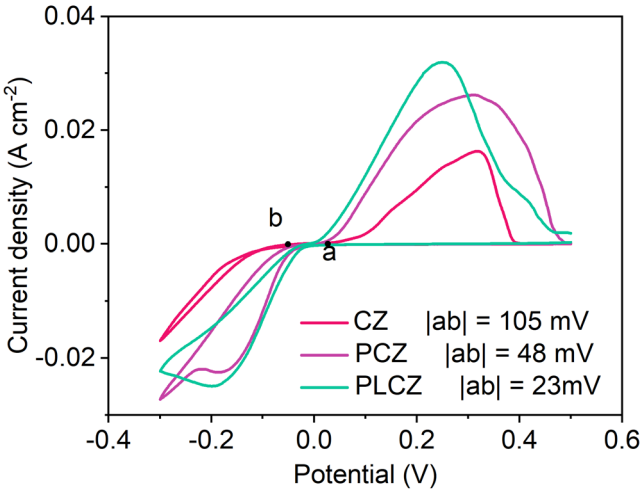

Fig. R33 *CV curves of Zn||Cu asymmetric cells with the CZ, PCZ and PLCZ. The nucleation overpotential in CV curves is defined as the difference between the crossover point (point a, where the current density begins to increase from zero) and the onset point (point b) of Zn^{2+} ion reduction.*

Changes in supplementary information:

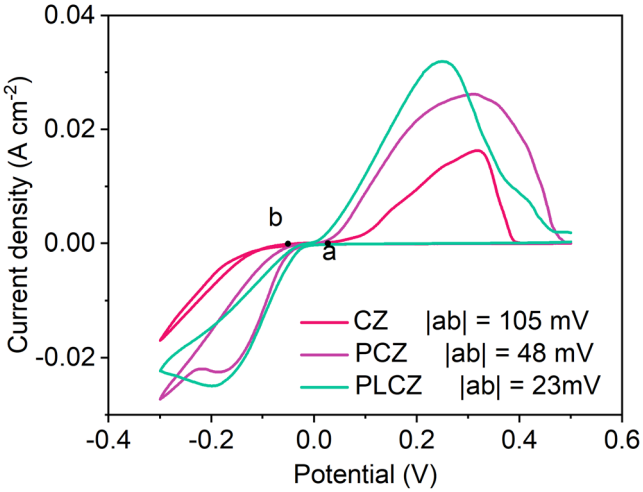

Supplementary Fig. S34 *CV curves of Zn||Cu asymmetric cells with CZ, PCZ and PLCZ. The nucleation overpotential in CV curves is defined as the difference between the crossover point (point a, where the current density begins to increase from zero) and the onset point (point b) of Zn^{2+} ion reduction.*

16) In Fig. 5 b-d, the color differences are difficult to see since they are quite small.
Author reply: Thank you very much for your comments. We consulted the instrument tester of micro-CT and asked for help to change the color. We have changed the color of in-situ micro-CT images of Zn||Zn cells with high color differences, as shown in Fig. R34. In order to make the color clearer, we enlarged the in-situ micro-CT images of Zn||Zn cells and move the micro-CT images of the cycled Zn electrodes (Fig. R35) to supplementary information. The symmetric cell configuration for assembly is shown in Fig. R36. In the in-situ Micro-CT images, materials of different densities are

represented by different colors, with the higher the density, the lighter the color, such as orange/yellow circle for cathode stainless steel case (material density: 7.9-8.0 g cm^{-3}), orange/yellow circle wafer for Zn metal electrode (material density: 7.14 g cm^{-3}, the density of Zn metal is similar with that of stainless steel, so they show same color but different shape), orange/yellow dot for Zn dendrite (same material density with Zn metal electrode), black/wine red for corrosion pit (surface corrosion and Zn loss on the Zn surface can decrease electrode thickness and density). The schematic illustration of Zn dendrite growth and surface corrosion on the Zn surface (cross-sectional view) and their corresponding micro-CT image (top view) is shown in Fig. R37. CZ and PCZ electrolytes are easy to produce Zn dendrite and surface corrosion (as proved by Tafel curves and SEM images after cycling), thus in the micro-CT images, the areas with Zn dendrite and surface corrosion exhibit chaotic and discontinuous color distribution. In contrast, PLCZ electrolyte effectively promotes homogeneous Zn deposition and suppresses surface corrosion, resulting in a uniform for Zn metal electrode.

We also explained what the different colors in micro-CT images represent in the figure caption and added the symmetric cell configuration for in-situ micro-CT test (Fig. S41) and the schematic illustration of micro-CT image (Fig. S42) into the file of supplementary information.

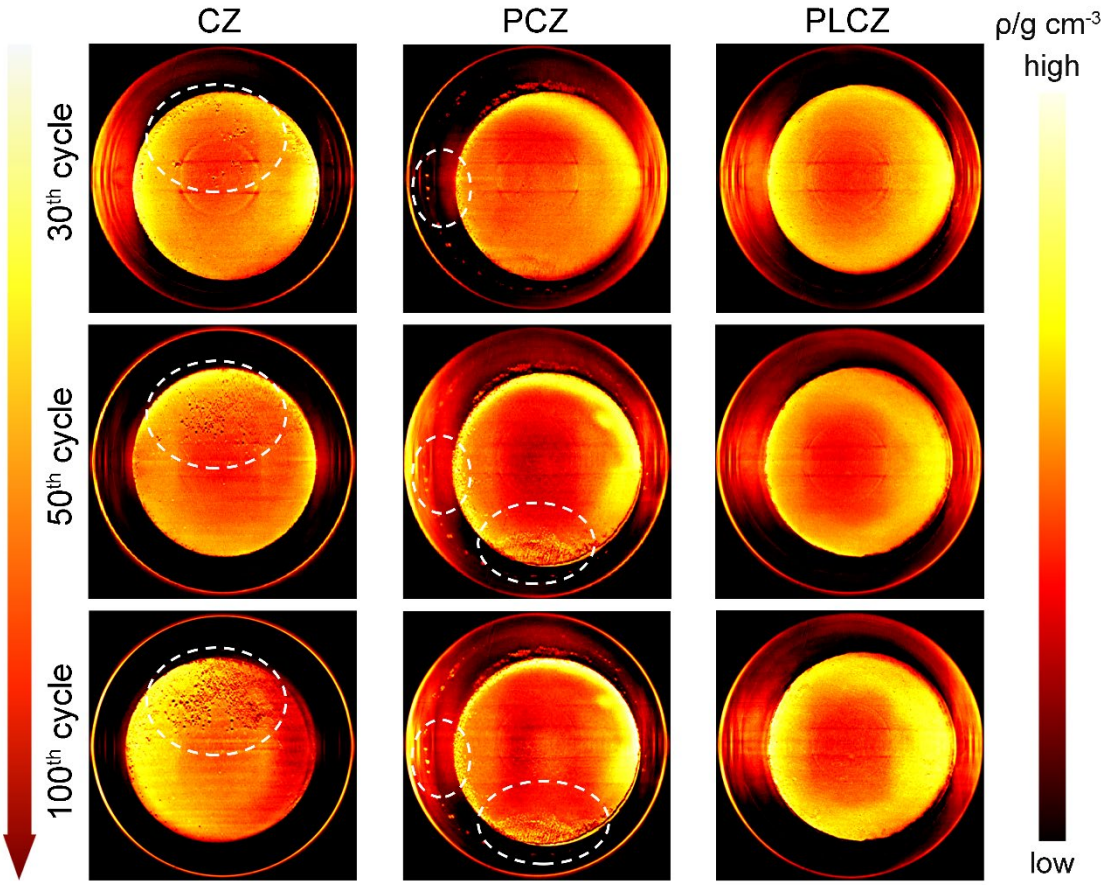

Fig. R34 *The micro-CT images of Zn||Zn cells at different cycles with CZ, PCZ and PLCZ electrolytes. Color representation: orange/yellow circle for cathode case, orange/yellow circle wafer for Zn electrode, orange/yellow dot for Zn dendrite, black/wine red dot for corrosion pit.*

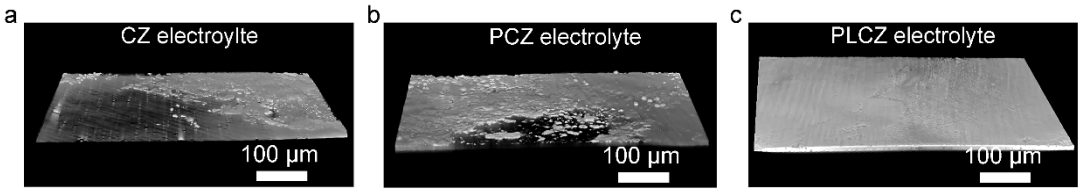

Fig. R35 *The micro-CT images of the cycled Zn anode with (a) CZ, (b) PCZ and (c) PLCZ electrolytes.*

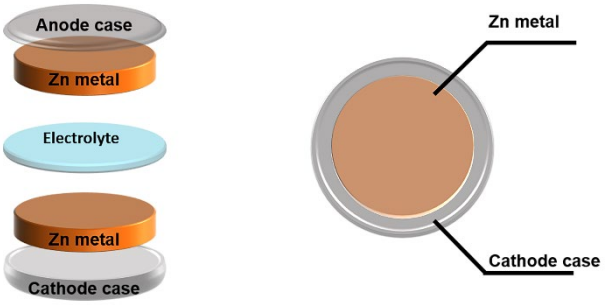

Fig. R36 *The Zn||Zn symmetric cell configuration for in-situ micro-CT test.*

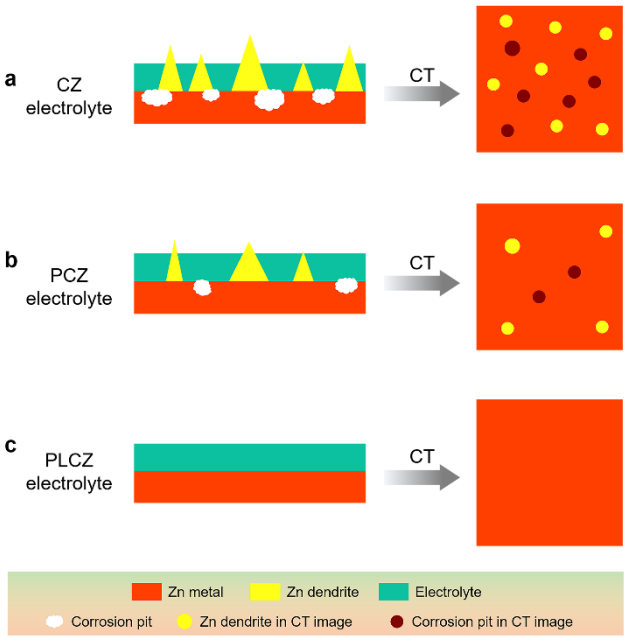

Fig. R37 *The schematic illustration of Zn dendrite growth and surface corrosion on the Zn surface (cross-sectional view) and their corresponding micro-CT image (top view). CZ and PCZ electrolytes easily produce Zn dendrite and surface corrosion, thus the areas with Zn dendrite and surface corrosion exhibit chaotic and discontinuous color distribution. In contrast, PLCZ electrolyte effectively promotes homogeneous Zn deposition and suppresses surface corrosion, resulting in a uniform color for Zn metal electrode.*

Changes in the manuscript (the highlighted part):

To track the evolution of Zn morphology over multiple cycles, in-situ micro-computed tomography (micro-CT) measurements were conducted on symmetric cells (Supplementary Fig. S41).

As illustrated in Fig. 5b and Supplementary Fig. S42, the CZ liquid electrolyte evidences dispersive dendrites and surface corrosions on the Zn surface at the 30^{th} cycle, which progressively worsened in subsequent cycles. Similarly, the PCZ electrolyte exhibits a comparable phenomenon that Zn electrode displays a rough surface at 50^{th} cycles and then deteriorates. In contrast, the Zn electrode with the PLCZ maintains a consistently smooth surface throughout the cycling process, illustrating a uniform and stable Zn^{2+} ion flux within the electrolyte.

Conspicuously, the Zn electrodes with the CZ and PCZ electrolytes exhibit a coarse morphology characterized by numerous humps and corrosion pits, whereas the PLCZ electrolyte facilitates the attainment of a glossy and unblemished Zn surface (Supplementary Fig. S43).

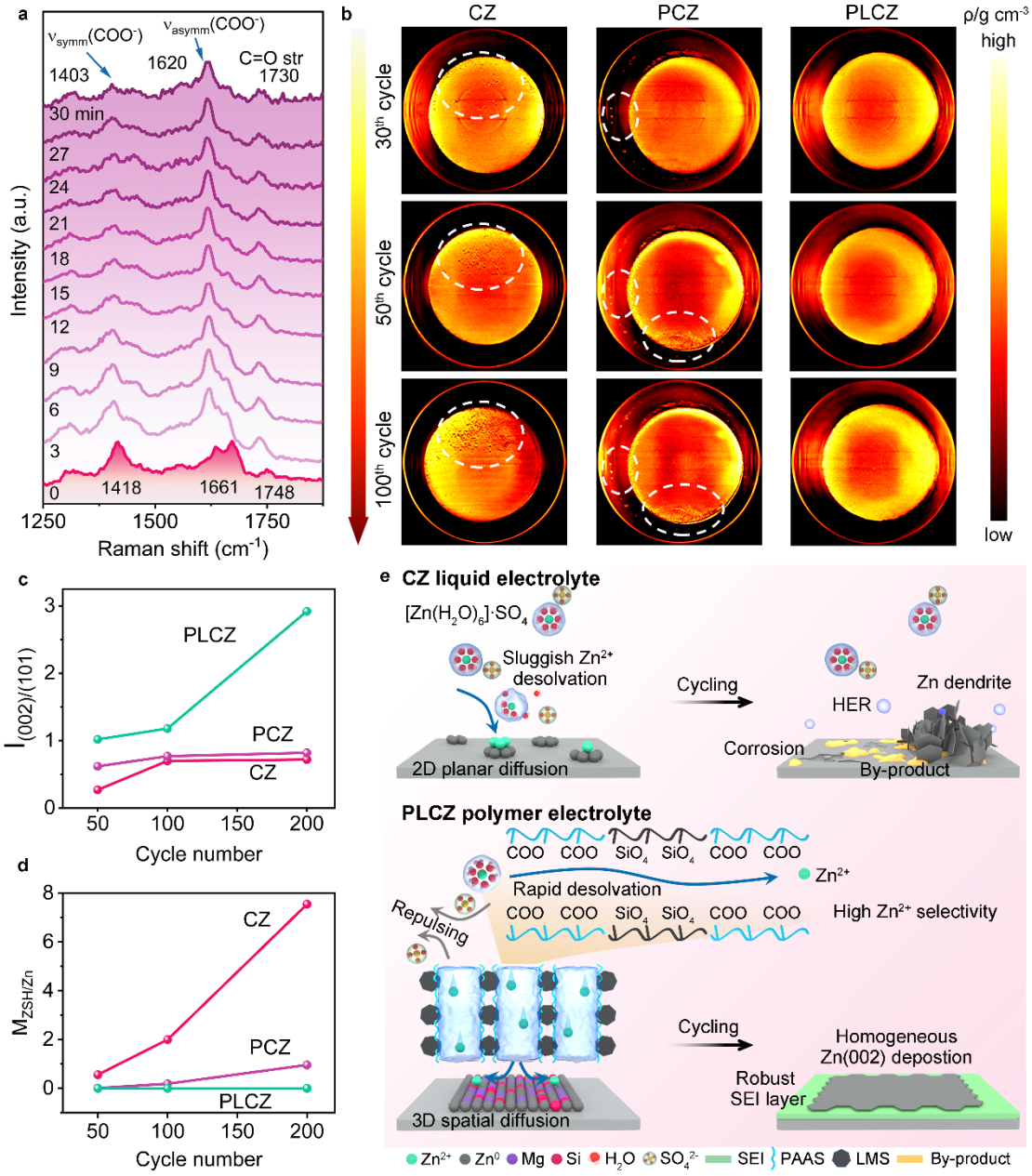

Fig. 5 *(a) The in-situ Raman spectra of Zn||Ag cell during deposition. (b) The micro-CT images of Zn||Zn cells at different cycles CZ, PCZ and PLCZ electrolytes. Color representation: orange/yellow circle for cathode case, orange/yellow circle wafer for Zn electrode, orange/yellow dot for Zn dendrite, black/wine red dot for corrosion pit. The calculated (c) $I_{(002)/(101)}$ and (d) $M_{ZSH/Zn}$ on Zn anodes based on XRD patterns. (e) Schematically illustrating the Zn deposition in CZ liquid and PLCZ electrolytes.*

Changes in supplementary information:

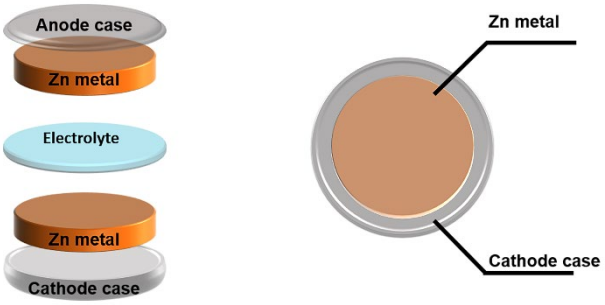

Supplementary Fig. S41 *The Zn||Zn symmetric cell configuration for in-situ micro-CT test.*

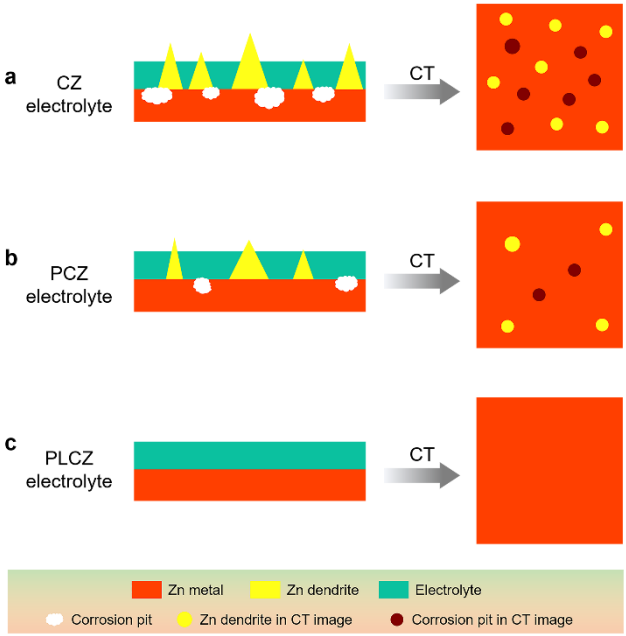

Supplementary Fig. S42 *The schematic illustration of Zn dendrite growth and surface corrosion on the Zn surface (cross-sectional view) and their corresponding micro-CT image (top view). CZ and PCZ electrolytes easily produce Zn dendrite and surface corrosion, thus the areas with Zn dendrite and surface corrosion exhibit chaotic and discontinuous color distribution. In contrast, PLCZ electrolyte effectively promotes homogeneous Zn deposition and suppresses surface corrosion, resulting in a uniform color for Zn metal electrode.*

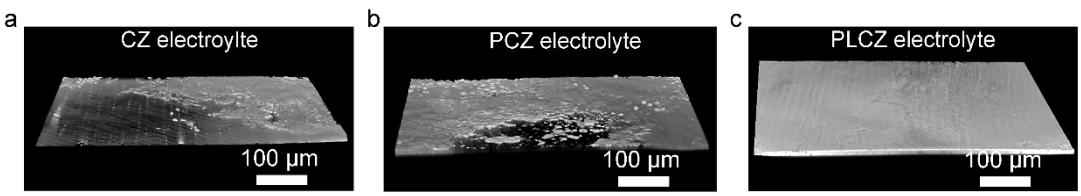

Supplementary Fig. S43 *The micro-CT images of the cycled Zn anode with (a) CZ, (b) PCZ and (c) PLCZ electrolytes.*

17) In Fig. S33, peak assignments (002) and (101) would be good for better understanding.

Author reply: Thank you very much for your reminding and comments. We have revised Fig. S33 to include the peak assignments (002) and (101), as shown in Fig. R38.

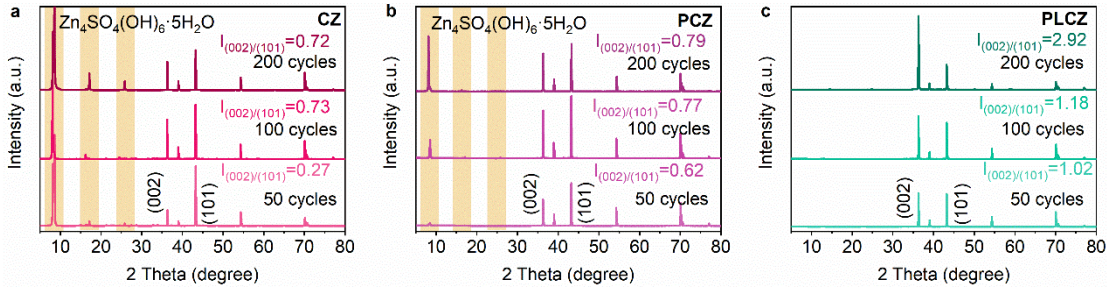

Fig. R38 *XRD patterns of Zn anodes in symmetric cells with (a) CZ, (b) PCZ and (c) PLCZ after cycling at 5 mA·cm^{-2}/2.5 mAh·cm^{-2}.*

Changes in supplementary information:

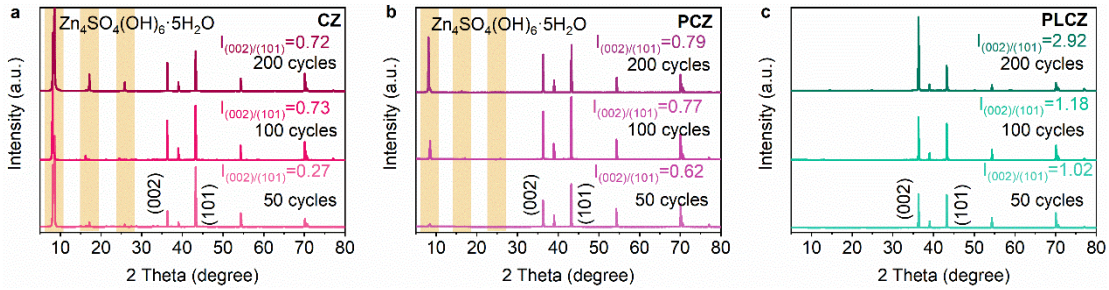

Supplementary Fig. S44 *XRD patterns of Zn anodes in symmetric cells with (a) CZ, (b) PCZ and (c) PLCZ after cycling at 5 mA·cm^{-2}/2.5 mAh·cm^{-2}.*

18) How were R_S, R_{SEI}, and R_{CT} determined in Fig. S34.

Author reply: Thank you very much for your comments. According to the shape of the electrochemical impedance spectra, we designed an equivalent circuit by selecting appropriate circuit elements (such as resistance, capacitance, etc.) to simulate or describe the dynamic response characteristics of the symmetric cells, as shown in Fig. R39. Then, we used the software of Zview to fit the EIS plots and calculate the electrolyte resistance (R_S), SEI resistance (R_{SEI}) and charge-transfer resistance (R_{CT}). The calculated values of Rs, R_{SEI} and R_{CT} of symmetric cells with the fitted error are listed in Table R4. The EIS plots with the corresponding fitted plots (solid line) are displayed in Fig. R40. Therefore, it can be seen that compared to the CZ and PCZ, the PLCZ obtains smaller and stable R_{SEI} and R_{CT} values, due to the highly conductive medium-entropy alloy (MEA) SEI and the suppressive byproducts.

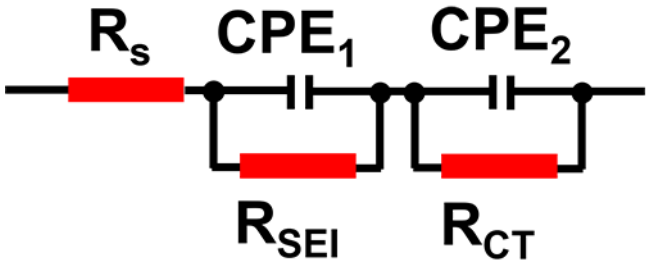

Fig. R39 *The equivalent circuit of EIS plots.*

Table R4 *The calculated values of Rs, RSEI and RCT of symmetric cells with the CZ, PCZ and PLCZ electrolytes.*

Electrolytes	***cycles***	***R_S***	***Error (R_s, %)***	***R_{SEI}***	***Error (R_{SEI}, %)***	***R_{CT}***	***Error (R_{CT}, %)***
CZ	*0*	*2.894*	*3.1*	*189.7*	*3.7*	*740.2*	*3.2*
	10	*3.805*	*1.4*	*145.5*	*2.0*	*1184*	*1.5*
	20	*2.978*	*1.9*	*352.9*	*2.3*	*1201.2*	*1.9*
	30	*2.652*	*2.2*	*526*	*1.5*	*1217*	*2.9*
	50	*2.757*	*1.9*	*548.2*	*4.0*	*1317.6*	*3.7*
PCZ	*0*	*3.372*	*1.6*	*210.8*	*0.8*	*502.2*	*4.0*
	10	*2.45*	*3.1*	*87.89*	*7.7*	*1660*	*1.9*
	20	*2.432*	*3.7*	*70.33*	*3.7*	*1685*	*1.2*
	30	*2.893*	*2.6*	*113.5*	*4.1*	*1823*	*1.5*
	50	*2.295*	*3.2*	*113.8*	*4.2*	*1875*	*1.6*
PLCZ	*0*	*1.621*	*2.5*	*30.94*	*5.5*	*359.9*	*2.1*
	10	*2.279*	*3.3*	*2.617*	*8.2*	*933*	*1.1*
	20	*2.432*	*4.4*	*1.978*	*4.0*	*1024*	*1.5*
	30	*1.162*	*3.8*	*2.45*	*3.1*	*952.2*	*1.8*
	50	*2.295*	*4.0*	*5.173*	*2.8*	*914*	*1.0*

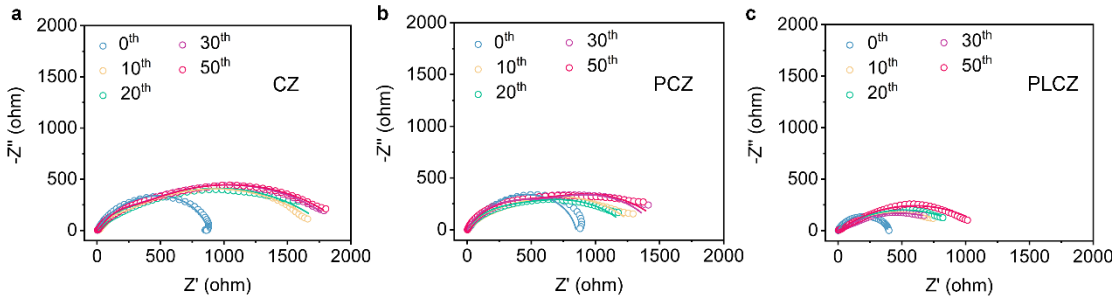

Fig. R40 *EIS plots of Zn||Zn symmetric cells with (a) CZ, (b) PCZ and (c) PLCZ after cycling different times. The solid line represents the corresponding fitted EIS plots.*

<u>Changes in supplementary information:</u>

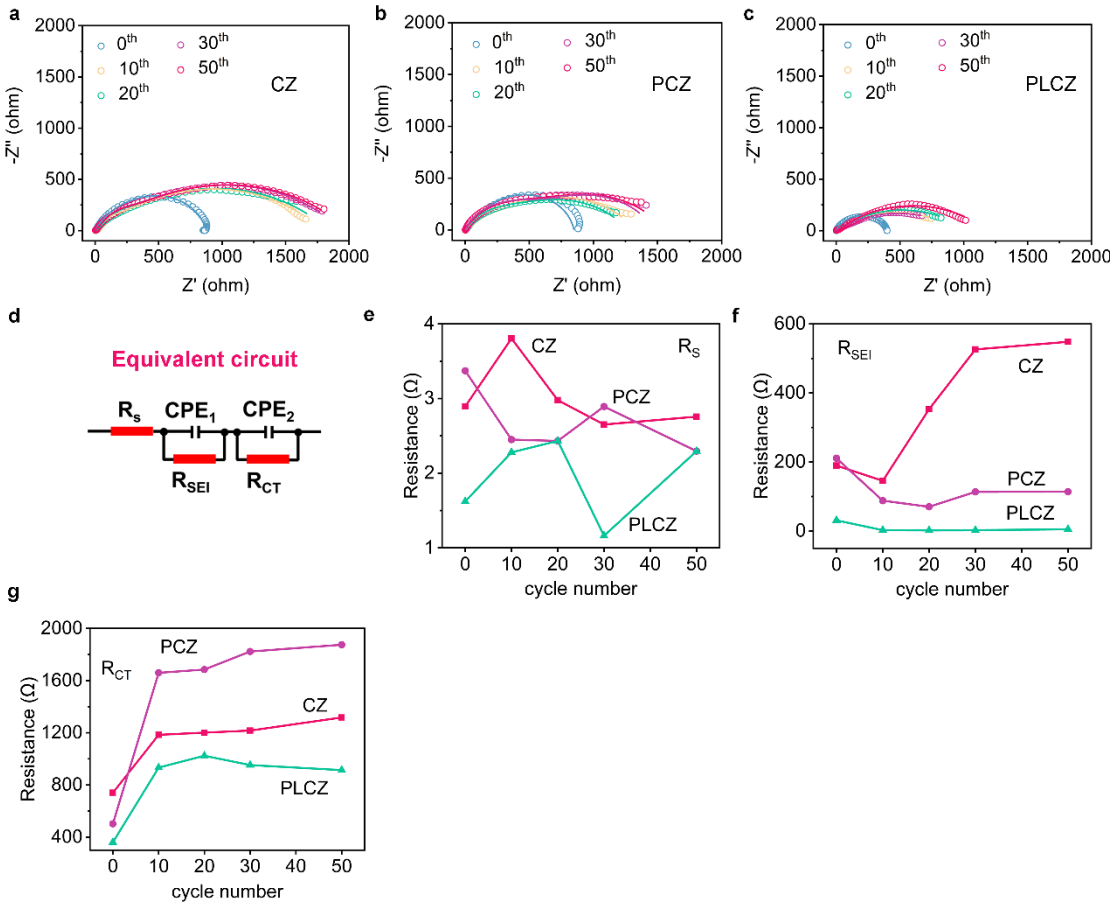

Supplementary Fig. S46 *EIS plots of Zn||Zn symmetric cells with (a) CZ, (b) PCZ and (c) PLCZ after cycling different times. The solid line represents the corresponding fitted EIS plots. (d) The equivalent circuit of EIS plots. The calculated resistances of (e) R_s, (f) R_{SEI} and (g) R_{CT}.*

19) In Fig 6 d and e no clear assignment of the data to the left and right y-axis is visible.

Author reply: Thank you very much for your comments. We have added the arrows to the left and right y-axis in these two figures, as shown in Fig. R41. Besides, we also have added the arrows to the figures of the cycling performances of Zn||V_2O_5 cells at various temperatures of 273.15, 313.15 and 333.15 K (0, 40 and 60 ℃), as shown in Fig. R42.

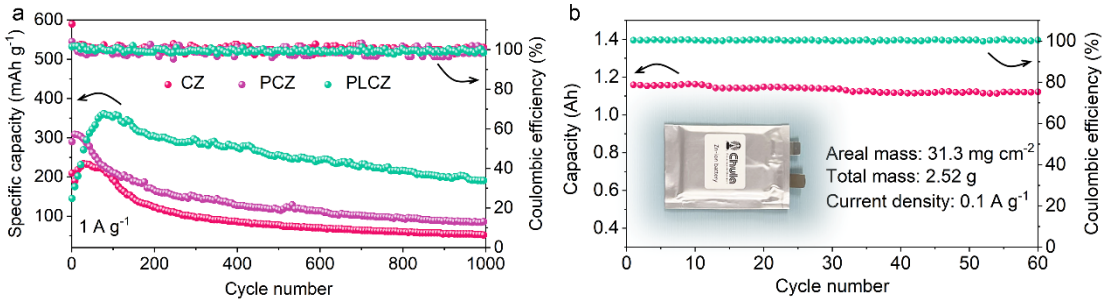

Fig. R41 *(a) Long-term cycling performances of full cells. (b) Cycling performance of pouch cell with PLCZ.*

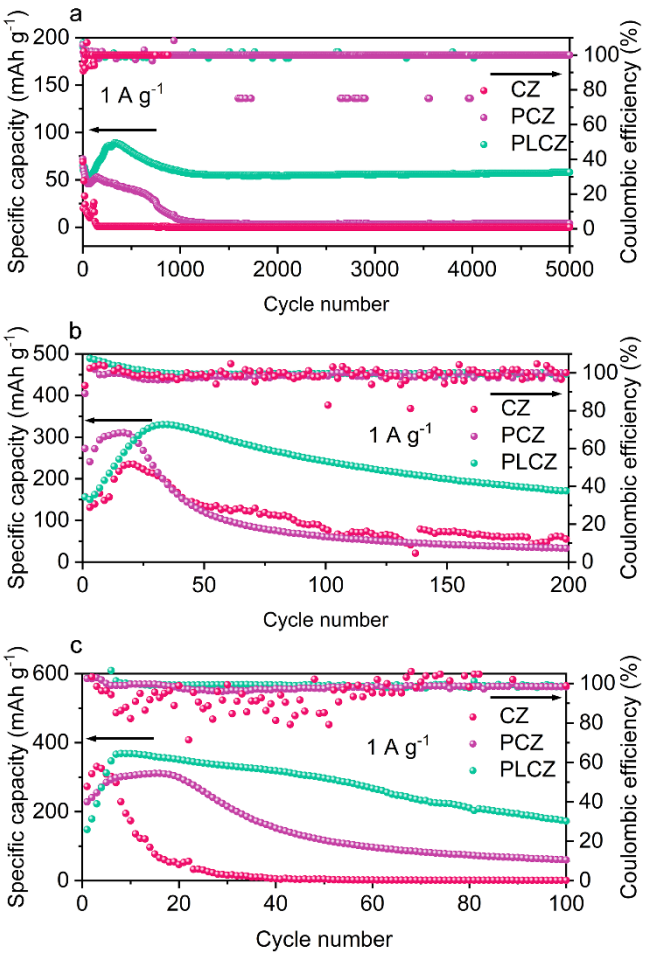

Fig. R42 *The discharge-charge cycling performances of Zn||V_2O_5 cells with different electrolytes at various temperatures of (a) 273.15, (b) 313.15 and (c) 333.15 K.*

Changes in the manuscript (the highlighted part):

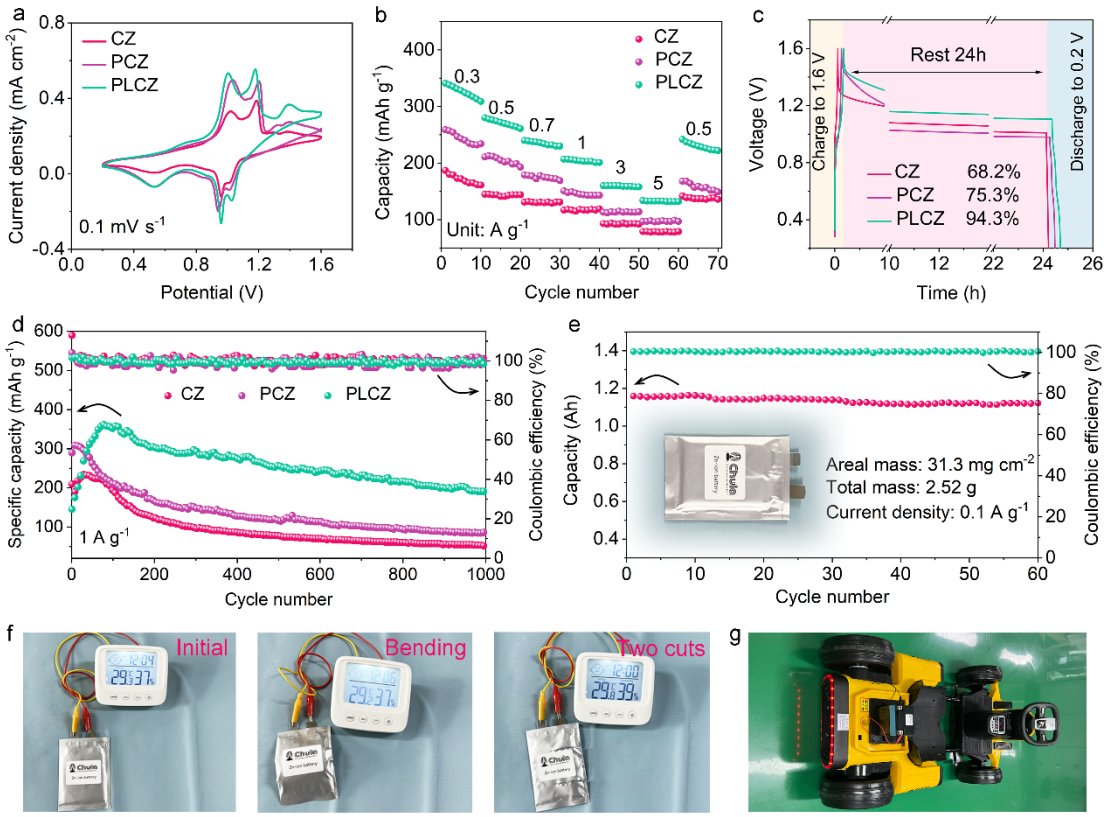

Fig. 6 *(a) CV curves Zn||V_2O_5 cells with CZ, PCZ and PLCZ. The electrode area is 1.54 cm^{-2}. (b) rate performances of Zn||V_2O_5 cells with CZ, PCZ and PLCZ. (c) Capacity retention test after charging to1.6 V, resting 24 h and discharging to 0.2 V. (d) Long-term cycling performances of full cells. (e) Cycling performance of pouch cell with PLCZ. The digital photographs of pouch cell (f) supporting electronic device under initial state, bending and cutting and (g) running a toy car.*

Changes in supplementary information:

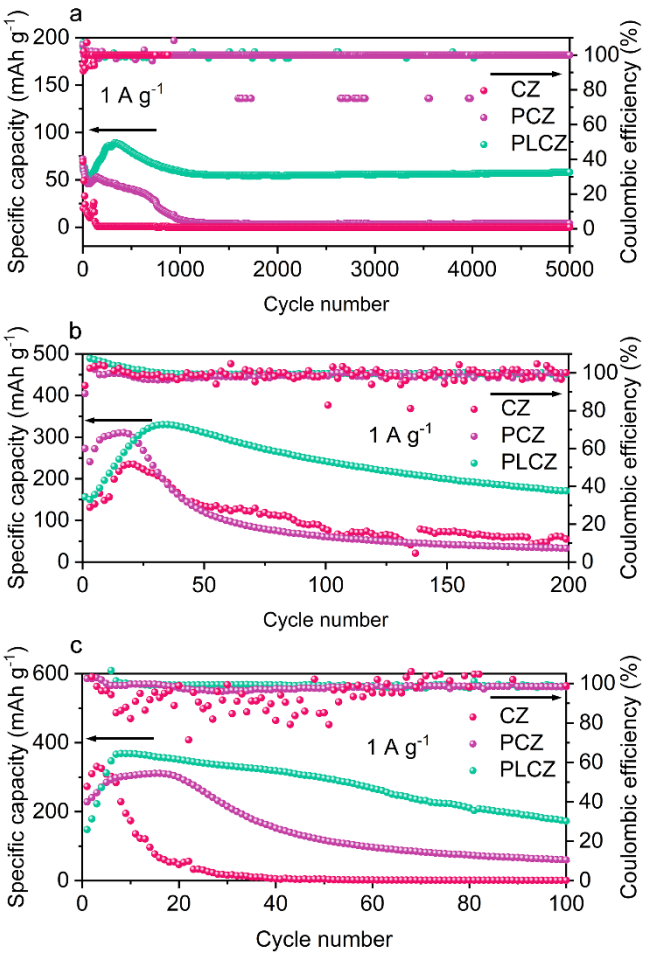

Supplementary Fig. S52 *The discharge-charge cycling performances of Zn||V_2O_5 cells with different electrolytes at various temperatures of (a) 273.15, (b) 313.15 and (c) 333.15 K.*

20) Fig 6 g images with digital thermometers are very small, difficult to read.

Author reply: Thank you very much for your comments. We apologize for any inconvenience caused by the small size of the images with digital thermometers, making them difficult to read. We have enlarged these images that have digital thermometers to improve visibility and readability of the digital thermometers, as shown in Fig. R43. On the other hand, in order to make the Fig. 6 look elegant and clean, we moved the capacity-voltage curves of pouch cell at different cycles (Fig. R44) to the file of Supplementary information.

Fig. R43 *The digital photographs of pouch cell (a) supporting electronic device under initial state, bending and cutting and (b) running a toy car.*

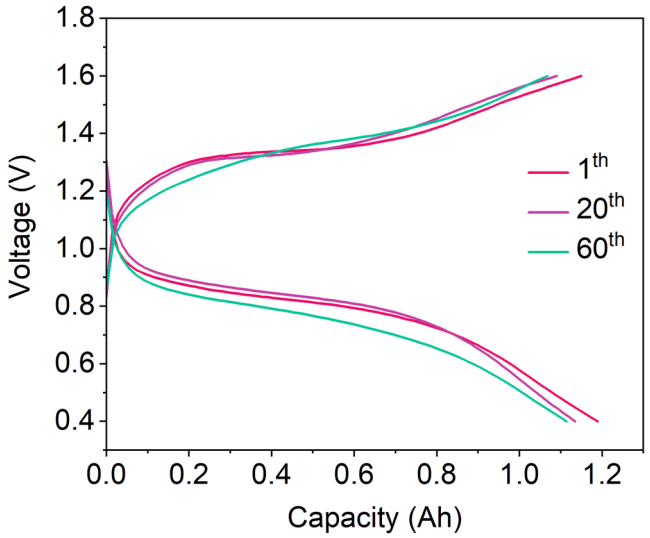

Fig. R44 *Comparison of cycling performance of pouch cell at different cycles.*

Changes in the manuscript (the highlighted part):

And the pouch cell shows similar capacity-voltage curves at different cycles (Supplementary Fig. S54).

Changes in supplementary information:

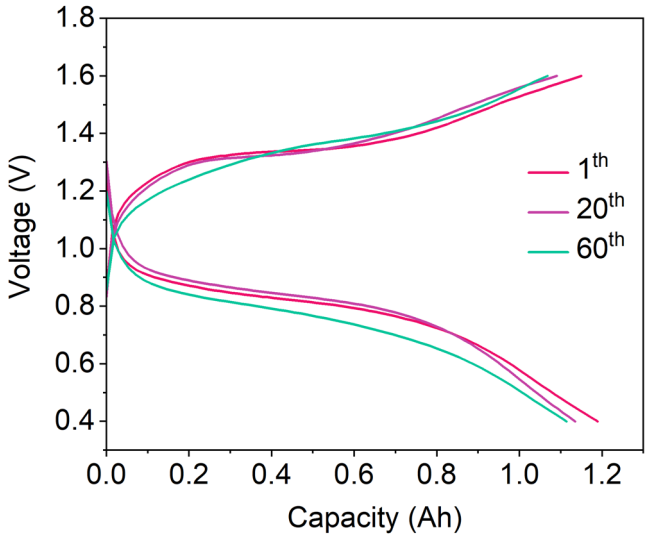

Supplementary Fig. S54 *Comparison of cycling performance of pouch cell at different cycles.*

Reviewer #4:

I co-reviewed this manuscript with one of the reviewers who provided the listed reports. This is part of the Nature Communications initiative to facilitate training in peer review and to provide appropriate recognition for Early Career Researchers who co-review

manuscripts.

Author reply: Thanks for your positive comments and we are glad that you find our work of interest and importance. We have revised the manuscript point-by-point according to your comments. Please see the answer to the above comments.

REVIEWERS' COMMENTS

Reviewer #1 (Remarks to the Author):

The authors have carefully addressed the reviewers' comments and thoroughly reviewed the revised manuscript. We agree to its publication in its current form.

Reviewer #2 (Remarks to the Author):

Most of the concern raised by the reviewers has been addressed. The manuscript can be accepted for its publication.

Reviewer #3 (Remarks to the Author):

The authors have addressed the vast majority of of our concerns well and therefore the manuscript has improved. The methods are now more thoroughly described and the conclusions better supported. The paper should now be ready for publication. There are just two small comments that could be addressed during the editing process. 1) In the latest edits the caption of Fig. 6 has a typo saying area is cm-2 whereas it should be cm2. 2) In addition to visualising the variation in Young's modulus graphically, it would also be useful to provide the standard error or the standard deviation on the mean.

Reviewer #4 (Remarks to the Author):

I co-reviewed this manuscript with one of the reviewers who provided the listed reports. This is part of the Nature Communications initiative to facilitate training in peer review and to provide appropriate recognition for Early Career Researchers who co-review manuscripts.

Response letter to reviewers

We are very grateful to the reviewers for their professional and insightful comments. These comments have greatly improved the quality of our manuscript and will be of great help to our future work. We have carefully revised the manuscript according to these comments. A detailed point-by-point response to comments is attached as below and the revised parts in the manuscript are highlighted.

Reviewer #1 (Remarks to the Author):

The authors have carefully addressed the reviewers' comments and thoroughly reviewed the revised manuscript. We agree to its publication in its current form.

Author reply: Thanks for your positive comments and we are glad that you find our work of interest and importance. We appreciate your recommendation of our work for publication in Nature Communications.

Reviewer #2 (Remarks to the Author):

Most of the concern raised by the reviewers has been addressed. The manuscript can be accepted for its publication.

Author reply: Thanks for your positive comments and we are glad that you find our work of interest and importance. We appreciate your recommendation of our work for publication in Nature Communications.

Reviewer #3 (Remarks to the Author):

The authors have addressed the vast majority of our concerns well and therefore the manuscript has improved. The methods are now more thoroughly described and the conclusions better supported. The paper should now be ready for publication. There are just two small comments that could be addressed during the editing process. 1) In the latest edits the caption of Fig. 6 has a typo saying area is cm^{-2} whereas it should be cm^2. 2) In addition to visualising the variation in Young's modulus graphically, it would also be useful to provide the standard error or the standard deviation on the mean.

Author reply: Thanks for your positive comments and we are glad that you find our work of interest and importance. We have revised the manuscript point-by-point according to your comments.

1) In the latest edits the caption of Fig. 6 has a typo saying area is cm^{-2} whereas it should be cm^2.

Author reply: Thank you very much for your comments. We have revised this error, shown as below.

Changes in the manuscript (the highlighted part):

Fig. 6 Electrochemical performance and application of Zn||V_2O_5 full cells. *(a) CV curves Zn||V_2O_5 cells with CZ, PCZ and PLCZ. The electrode area is 1.54 cm^2. (b) rate performances of Zn||V_2O_5 cells with CZ, PCZ and PLCZ. (c) Capacity retention test after charging to 1.6 V, resting 24 h and discharging to 0.2 V.*

2) In addition to visualising the variation in Young's modulus graphically, it would also be useful to provide the standard error or the standard deviation on the mean.

Author reply: Thank you very much for your comments. We have calculated the standard error by the equation:

$$S=\sqrt{\frac{(x_1-x)^2+(x_2-x)^2+\cdots+(x_n-x)^2}{n-1}}$$

Where x_n is the values of Young's modulus; x is the average value of Young's modulus; n is the total number of Young's modulus (n=64 in this work); S is the standard error.

The calculated standard errors of the CZ, PCZ and PLCZ electrolytes are 2.07, 2.28 and 1.90 GPa, respectively. The PLCZ obtains a lower standard error, indicating a more uniform distribution of Young's modulus.

Changes in supplementary information:

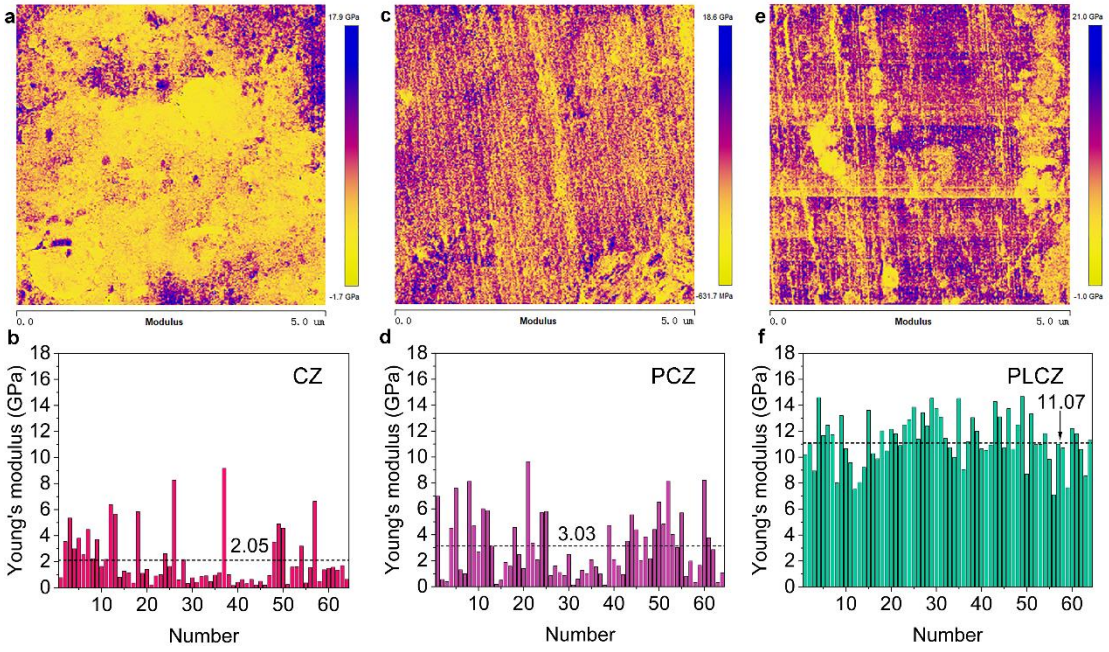

Supplementary Fig. S38 *The distributions of Young' modulus with the measured values on the Zn electrodes with (a, b) CZ, (c, d) PCZ and (e, f) PLCZ. The standard error is calculated by the equation:*

$$S=\sqrt{\frac{(x_1-x)^2+(x_2-x)^2+\cdots+(x_n-x)^2}{n-1}}$$

Where x_n is the value of Young's modulus; x is the average value of Young's modulus; n is the total number of Young's modulus (n=64 in this work); S is the standard error.

The calculated standard errors of the CZ, PCZ and PLCZ electrolytes are 2.07, 2.28 and

1.90 GPa, respectively. The PLCZ obtains a lower standard error, indicating a more uniform distribution of Young's modulus.

Reviewer #4 (Remarks to the Author):

I co-reviewed this manuscript with one of the reviewers who provided the listed reports. This is part of the Nature Communications initiative to facilitate training in peer review and to provide appropriate recognition for Early Career Researchers who co-review manuscripts.

Author reply: Thanks for your positive comments and we are glad that you find our work of interest and importance. We have revised the manuscript point-by-point according to your comments. Please see the answer to the above comments.